INFORMATION TO USERS

NOTE TO USERS

The original manuscript received by UMI contains pages with indistinct print.   Pages were microfilmed as received.

This reproduction is the best copy available

UMI

University of Alberta

Development of A Bone Modeling Model

by

Haoran Yang ©

A thesis submitted to the Faculty of Graduate Studies and Research in partial fulfillment of the requirements for the degree of Master of Science

Department of Mechanical Engineering

Edmonton, Alberta

Fall 1998

University of Alberta

Library Release Form

Name of Author: Haoran Yang

Title of Thesis: Development of A Bone Modeling Model

Degree: Master of Science

Year this Degree Granted: 1998

Permission is hereby granted to the University of Alberta Library to reproduce single copies of this thesis and to lend or sell such copies for private, scholarly, or scientific research purposes only.

The author reserves all other publication and other rights in association with the copyright in the thesis, and except as hereinbefore provided, neither the thesis nor any substantial portion thereof may be printed or otherwise reproduced in any material form without the author's prior written permission.

Haoran Yang
6076 Michener Park
Edmonton, Alberta, Canada
T6H 5A1

Date: _Oct. 2, 1998_
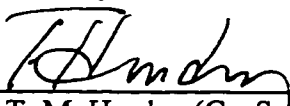
University of Alberta

Faculty of Graduate Studies and Research

The undersigned certify that they have read, and recommend to the Faculty of Graduate Studies and Research for acceptance, a thesis entitled **Development of A Bone Modeling Model** submitted by **Haoran Yang** in partial fulfillment of the requirements for the degree of Master of Science

Dr. M.G. Faulkner (Supervisor)

Dr. T. M. Hrudey (Co-Supervisor)

Dr. A.W. Lipsett

Dr. H. Uludag

Date: Oct. 2, 1998

Abstract

A new bone modeling model is developed. The new modeling model is based on Cowin's external modeling and adopts the weighting factors to reflect the different effects of different strain components on the bone modeling. The new theory overcomes the flaw in Cowin's external remodeling theory and is approved to have flexibility over the existing modeling theories. The new theory also reflects biological factors in the model which are not considered by the existing theories.

By association of the new model with various numerical techniques, several computer simulations are presented to validate model and simulate some interesting idealized clinical problems. All example problems show an excellent agreement to the analytical solution or qualitatively to the experimental facts.

The results obtained in those examples are very close to the real bone modeling situation and provide very promising information on the method to simulate the bone modeling in the real clinical practice.

To my parents, wife and son…

— 微献给我的父母，妻子及杨漾

Acknowledgments

Content

List of tables

List of figures

Glossary

Cancellous bone -- the sponge bone which predominates in the metaphyses and epiphyses.

Cement line -- a line 1 to 5 μm thick around Haverisan bone which separates the osteon as a structural unit from extraosteonal bone matrix.

Cortical bone -- the compact bone which comprises the diaphysis of long bones and thin shell that surrounds the metaphyses.

Diaphysis -- the shaft of a long bone which is a hollow tube.

Endosteum -- a thin layer of reticular cells, lining the walls of the bone marrow cavities and of the haversian canals of compact bone and convering trabeculae of cancellous bone.

Epiphyses -- the part that surmount the metaphysis and is united to its metaphysis by a cartilaginous growth plate.

Haversian systems or osteons -- an irregularly cylindrical and branching structure, with thick walls and a narrow lumen.

Metaphysis -- the expansion at the end of a long bone.

Ostectomy -- removal of a section of a long bone.

Periosteum -- the connective tissue surrounding bone.

Chapter 1

Introduction

Functional adaptation is the term used to describe the ability of organisms to increase their capacity to accomplish their function with the increased demand and to decrease their capacity with lesser demand. It has long been recognized that bone could sense its mechanical environment and in certain situations adapt to it - collectively termed as "Modeling/Remodeling" or "Adaptation" of bone. For example, it has been well known that bed rest and weightlessness as in space flight, lead to a reduction in bone size and reduced growth rate of bone while intensive loading of a bone can result in an increase in bone mass. For example, arm bones of professional tennis players are larger on the racket-holding side than on the other side.

The concept of bone adaptation is attributed to Julius Wolff, a nineteenth century physician, and his original statement about the response of bone to mechanical usage is called Wolff's law. In fact, Wolff's law is a series of descriptions of the remodeling/modeling phenomenon. The translation of Wolff's law (Treharne, 1981) published in German back in 1892 is as follows:

> "Every change in the ...function of a bone...is followed by certain definite changes in ... internal architecture and external conformation in accordance with mathematical laws."

According to Wolff's law, bone's adaptation to its mechanical environment includes two aspects: changing its internal structures (internal remodeling or remodeling) and changing its external shape (external remodeling or modeling). The former is achieved by osteonal remodeling and the latter by adding or removing bone from the bone surface.

There are two phases of adaptation. One is the embryonic phase during which biological factors such as regulatory genes and chemical morphogenes

1

play an important role on the bone growth. The pure biological influences gradually disappear over time and the mechanical factors become more and more dominant on the bone adaptation throughout the adult life. Wolff's law actually addresses the latter case.

Since Woff's law was first proposed, the adaptive phenomenon of bone has received considerable attention. The study of this phenomenon generally falls into two broad classes: mathematical and biological. Biologists try to deal with the problem microscopically and with mathematical simplicity. On the other hand, mechanical engineers prefer to use more rigorous mathematical tools to set up the model and neglect the details of how bone's microstructure and material constituents change.

The two approaches each have their advantages and shortcomings. The biological one links bone cell activities and biomechanical conditions, thus providing a useful framework for discussing experimental results. But its attributing the experimental findings to some simple mechanical signal limits its capacity to explain the problem locally and not globally. As for the mechanical approaches, their comprehensive considerations of only the mechanical environment and rigorous mathematical formulation provide them with the potential capacity to globally predict the clinical results although at present it seems to lack a good biological basis.

All adaptation theories are closely associated with the design of bone implants and the explanation of experimental results. Procedures such as total joint replacement are performed in large numbers and at significant cost each year. Over 300,000 total hip and knee replacements occur annually in the U.S. alone. Although orthopedic implants are designed to last for the life time, the results are not satisfactory due to the fact that the implants often lose contact with the bone, and undermine the mechanical stability of the implant leading to implant failure. The explanation is that the 'stress shielding' plays an important role in this problem. 'Stress shielding' implies that a load, originally carried by bone itself, is now shared with an implant and as a result the bone stress decreases and bone resorbs according to Wolff's law.

The clinical importance of long term stability of implants, along with the large number and high cost of the surgical procedures, indicates that computer based simulation could be used to investigate the biomechanical behavior of a

bone-implant system and predict the adaptive change of the bone around prostheses. The objective of computer simulation is to predict the shape changes as well as bone adaptation around the implant surface and thus simulate the effects of the implant on the bone after years in the body thus assisting implant designers in the refinement of the prostheses design.

Compared with the animal experiments, which have been traditionally used to investigate bone response to implants, computer simulation is inexpensive and fast (Cowin, 1993). According to Cowin, although computer models can not take place of animal experiments, they have the potential to reduce the number of animal experiments by focusing on experimental designs.

The objective of the current study is to develop a numerical bone external remodeling simulation. The work can be divided into three phases: (1) comparison and evaluation of the existing remodeling theories; (2) based on those evaluations, development of an improved new remodeling/modeling model; (3) and development of numerical techniques to validate this new model by comparing the "outputs" with other theoretical and experimental results.

The current study focuses on the mathematical approaches but attempts to consider the connection of biology and mechanics. In the remainder of this chapter, the physiology and the mechanical properties of bone are briefly discussed so that the mechanisms of bone adaptation can be discussed later.

1.1 Physiology of bone

Bone is a structure as well as metabolic tissue which is a highly specialized form of connective tissue, composed of branching cells in an intercellular substance and forming the skeleton or framework of the body of most vertebrates.

As a structural material, bone is very different compared to engineering structural materials since it is self-repairing and can alter its properties and geometry in response to changes in mechanical demand. As a tissue, it has certain characteristics that differentiate it from other forms of connective tissue. The most striking one is that it is relatively hard which results from deposition,

within a soft organic matrix (collagen fiber), of a complex mineral substance (composed chiefly of calcium, phosphate etc.). Bone has its own specialized forms of cells derived from those common to connective tissue.

The function of bone is to protect vital internal organs and provide a mechanical framework that allows the skeleton to execute motions that are necessary for survival. In many cases, bone microstructure will reflect the varied and diverse mechanical needs of the particular organism. In addition to strength and stiffness, it possesses a mechanism to avoid fatigue fracture.

While the shapes of whole bones are marvelously varied a large proportion of them fall into three groups.

- Tubular bone (long bones): consisting of a shaft (diaphysis) with an expansion (metaphysis) at each end. It includes most of the long bones and ribs;
- Tabular bone (flat bones): one dimension is much less than the other two such as scapula, the pelvis and etc.;
- Short bones: roughly the same size in all directions.

1.1.1 Structures of bone

To appreciate the behaviour of bone, it is necessary to consider its structure from different views.

Bone is composed of cells and mineralized extracellular substance. This interstitial substance includes the organic framework or matrix and the inorganic parts of the mineral of bone and water.

Bone cells can be divided into three types which are associated with specific functions: osteoblasts with the formation of bone; osteocytes with the maintenance of bone as a living tissue, and osteoclasts with the resorption of bone.

Osteoblast is generally found as a continuous layer on the bone surface where active bone formation takes place. These may be periosteum-covered external bone surfaces or the internal (endosteal) surfaces. It is actively engaged in the production of an extracellular matrix and has the characteristic morphology of protein-secreting cells. Osteocyte is actually the remnants of osteoblast that have secreted bone around themselves and serve to maintain an extensive network of contacts of adjacent cells. It is the only type of bone cell that are encased in the mineralized bone matrix (the other two are located on all available extracellular matrix surfaces).

Osteoclasts are usually found on the surfaces of bone (that, at different times, are occupied by osteoblasts), in close relationship to areas of resorption. Osteoclasts are responsible for major bone tissue removal, following the initiation of this process by osteoblasts. Developmentally and functionally, they are totally different from the osteoblasts and osteocytes which are connected by gap junctions (intercellular contacts, which permit electric coupling of cells, as well as free movement of a common pool of small metabolites and ions) of the cell processes, forming a connected cellular network that allows direct cell-to-cell communication. No gap junction contacts between osteoclasts and the other bone cells have been reported.

In general, bone microstructure can be divided into three categories: woven bone, primary bone and secondary bone.

• **Woven Bone**

Woven bone is a poorly organized, randomly oriented tissue. It is associated with periods of rapid formation such as that of active growth or in fracture repair. Woven bone can be deposited without any previous hard tissue. The function of woven bone is primarily mechanical, rapidly providing both temporary strength and scaffolding upon which lamellar bone may be deposited.

• **Primary Bone**

Unlike woven bone, primary bone must be deposited on a preexisting substrate. This substrate may be a cartilaginous anlage (base), calcified or uncalcified or may be preexisting bone.

Primary bone can be divided two types--primary lamellar, and primary osteons.

Fibrous layer of periosteum
Osteogenic layer of periosteum
Outer circumferential lamellae
Lacunae containing osteocytes
Canaliculi
Cementing line
Compact bone
Interstitial lamellae
Haversian system
Inner circumferential lamellae
Blood vessel and endosteal lining of haversian canal
Volkmann's canals
Blood vessels into marrow
Endosteum
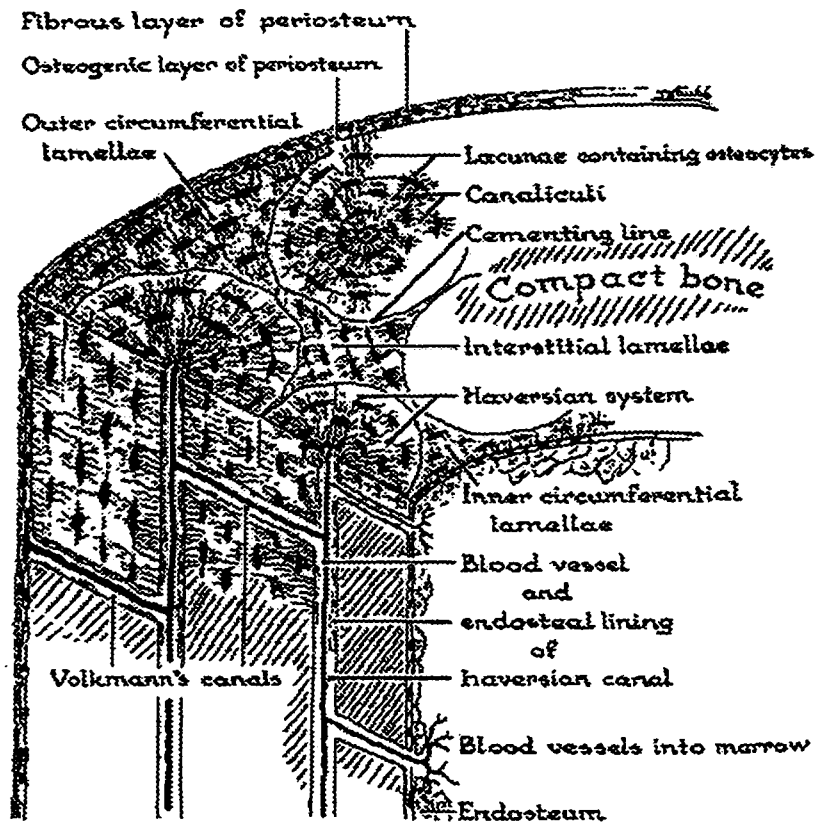
Figure 1.1   The basic structure of compact bone (Fung 1993)

- **Secondary Bone**

Primary bone is a new bone made in a space where bone has not existed before. When bone is the product of resorption of previously existing bone tissue and the deposition of new bone in its space, it is called secondary bone.

In cortical bone, the replacement of preexisting bone by secondary bone is initiated by resorption of whole bone by osteoclasts. The result of osteoclastic resorption and subsequent formation by osteoblasts is a secondary osteon (Haversian system). The two major distinguishing features of Haversian system are the organization of lamellae around the central canal (Haversian canal) and the presence of a cement line 1 to 5 μm thick separating the osteon as a structure unit of bone from the extraosteonal bone matrix (Figure 1.1).

The structure of secondary osteons is quite similar to primary osteons. The main distinction is that primary osteons do not have the cement.

Bone consists of compact and sponge regions of hard-matter which are called *cortical bone* and *cancellous* or *trabecular* bone respectively. Cortical bone comprises the diaphysis of long bones and the thin shell that surrounds the metaphyses. Cancellous bone predominates in the metaphyses and epiphyses which is continuous with the inner surface of the metaphyseal shell and exists as a three dimensional, interconnected network of trabecular rods and plates (the short struts of trabecular bone are called trabeculae). Short bones tend to have very thin cortices and to be mostly filled with cancellous bone. Figure 1.2 shows cortical bone and cancellous bone in the proximal femur.

1.1.2 Summary

Bone is composed of cells and mineralized extracellular matrix. The extracellular matrix has two principal ingredients: fibrous collagen and an inorganic mineral phase mainly composed of calcium phosphate. At the macroscopic level, bone can be divided two major forms: compact bone (cortical) and spongy bone (trabecular or cancellous bone). At the microstructural level bone exits in three distinct forms: woven bone, primary bone and secondary bone. Woven bone is poorly arranged and associated with periods of rapid formation such as that of active growth or in fracture repair. Primary and secondary bone are in the forms of lamellae. The trabeculae (short struts) of spongy bone are generally composed of a collection of more or less parallel lamellae. In compact bone, the lamellae may be arranged either in a parallel fashion (circumferential lamellae) or concentrically in quasi-cylindrically shaped structure called osteons (primary osteons and secondary osteons or Haversian system, Figure 1.1). Control of primary bone apposition to periosteal

Figure 1.2 A longitudinal section at the proximal femur reveals the cortical bone at the diaphysis. At the femur head shows a thin shell of cortical bone with the trabecular network (Hastings et al 1984)

(outer) or endosteal (inner) bone surfaces is different from that replacing preexisting bone by secondary bone . The former is associated with modeling process whereas the latter is controlled by remodeling process.

Bone cells are responsible for the modeling and remodeling processes. These cells form a continuous cellular layer that covers all the available extracellular matrix surface. Among them, osteoblasts, associated with bone formation and osteoclast, the bone resorbing cells are always located on bone surfaces where active bone formation or resorption takes places. Osteocytes are the only type of bone cells that are encased in the mineralized bone matrix (in small spaces or lacunae). They are responsible for bone maintenance and continue to maintain contacts with other osteocytes and osteoblasts via a system of cell processes located in canaliculi (tiny tubes, project from all surfaces of a lacuna, Figure 1.1) which functions as a single functional osteocyte network. This connected cellular network is the primary candidate for the communication system by which bone modeling and remodeling signals are transmitted.

It is believed that bone cells are capable of responding to mechanical stimuli and they do so in a predictable fashion (Wolff's law). This is the basis of modeling and remodeling theories.

1.2 The Mechanical properties of bone

The mechanical properties of bone have been extensively studied. From a mechanical theory perspective, bone is both anisotropic and heterogeneous. In addition, the degree of anisotropy of bone can vary with position so that the material properties of bone are functions of anatomical position. Due to these features, the traditional engineering methods for material property determination are difficult to apply to bone. As a result other techniques, such as ultrasonic methods have become more common.

It was noted before that bone structurally can be divided into two general types, i.e., cortical bone and cancellous bone. Because of their very different structures, their mechanical properties are also different. As a result their mechanical properties will be presented separately.

1.2.1 The Mechanical properties of cortical bone

Figure 1.1 illustrates schematically the microcomponents of a cortical bone. It consists of five parts. (1) periosteal bone having a lamellar structure following the outer curvature of the cortex; (2) endosteal bone, also lamellar but with the radius of the lamellae corresponding to the inner radius of the cortex; (3) primary osteons; (4) secondary osteons (Haversian system); (5) interstitial bone (the remodeled remains of primary or secondary bone lamellae).

The determination of the material symmetry of amorphous material such as bone is more difficult than for a crystalline material. According to Cowin's (Cowin and Mehrabadi, 1989a) definition, the elastic symmetry of bone falls into the category of textural symmetry which is in contrast to crystallographic symmetry. The latter is easily determined by the chemical constituents of the material but textural symmetry can only generally be identified by experiment.

Based on the pioneering work of Katz and others (Yoon and Katz, 1976a,b, 1979, Katz, 1980, Ashman et al., 1984, Buskirk and Ashman, 1981a, b) as well as the identification methods given by Cowin et al. (Cowin and Mehrabadi, 1989a) for the elastic symmetry of bone, it is generally accepted that cortical bone can be considered as an *orthotropic material.*

As the degree of textured anisotropy of bone can vary with anatomic site (and from individual to individual), some cortical bone tissue may be transversely isotropic or even isotropic. For example, the work on microstructure shows that cortical Haversian bone is transversely isotropic if it has a hexagonal packing, and as Ashman and Van Buskirk (Ashman and Van Buskirk, 1987) reported, mandibular bone is essentially transversely isotopic.

The choice of material symmetry for an elastic model of bone depends to a large extent on the intended application. Huiskes (1982) indicates that the stress analysis of a human femur is adequately served with a transversely isotropic elastic model. This is also justified by the data provided by Ashman and Van Buskirk (1981) which showed that the percentage difference between the orthotropic elastic constant values and the transversely isotropic constant values are quite small, and are therefore unlikely to have a significant effect on the stress analysis of a bone.

Bone is basically a viscoelastic material, however, previous work (Cowin, 1986, chpt. 6) has shown it is reasonable to consider the bone as *a linear elastic material.*

Several studies have been done to determine the elastic properties of cortical bone. Due to the different testing methods and approaches, the results varied even for the same kind of cortical bone. This reflects the complexity of determination of mechanical properties of bone that are functions of age, sex, and anatomical site.

A typical result is given in Table 1.1 (Ashman et al. 1984) where cortical bone is assumed to be an orthotropic material, and directions X_1, X_2, X_3 indicate radial, circumferential and longitudinal directions respectively.

The data in Table 1.1 are all related to long bones. There is little information about cortical bone in other positions where the shape of bone is less regular such as the craniofacial area. Although some general data may be available, more precise values are still needed.

1.2.2 The Mechanical properties of cancellous bone

The microstructural features of trabecular bone have received considerably less attention than those of cortical bone. Individual trabecular plate and rods are composed primarily from interstitial bone of varying composition, although on occasion lamellar trabecular plates and osteonal trabecular rods are found.

The architectural feature of cancellous bone are remarkably similar to porous foams (Figure 1.3). Macroscopically its mechanical properties can be studied as a whole or as individual trabeculae (i.e. a single strut taken from cancellous bone). By doing both some confusion about the difference between cortical bone and cancellous bone can be understood.

Depending upon whether the pores are connected or not, the theoretical models for the mechanical properties of high porosity materials are generally classified as open cell or closed cell models. The microstructure of cancellous

Table 1.1 AVERAGE TECHNICAL CONSTANTS FOR FEMORAL BONE

	Human	Canine
E1(GPa)	12.0	2.8
E2(GPa)	13.4	15.6
E3(GPa)	20.0	20.1
G12(GPa)	4.53	4.68
G13(GPa)	5.61	5.68
G23(GPa)	6.23	6.67
v12	0.376	0.282
v13	0.222	0.289
v23	0.235	0.265
v21	0.422	0.366
v31	0.371	0.454
v32	0.350	0.341
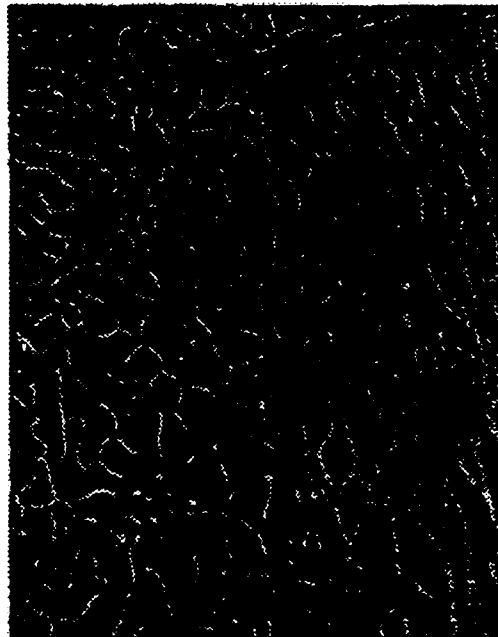
Figure 1.3 The porous strcuture of cancellous bone (Cowin et al 1989a)

bone does not exactly match either of these idealized models as it falls between these two but is closest to the open celled case.

The studies of closed cell and open cell models suggest that both (all models are assumed as isotropic) Young's modulus E and the shear modulus G are proportional to the square of structural density for open cell material, and to the cube of structural density for closed cell material (Note that the structural density is the mass per unit bulk volume of porous bone tissue).

Although the cancellous bone is not an isotropic material and its cell size is not uniform, the above discussion suggests that both the Young's and shear modulus as well as strength of cancellous tissue should depend on the square of the structural density (i.e. the open cell model).

There are several studies to determine the relationship between structural density and Young's modulus for cancellous bone.

Carter and Hayes (1977) gave the following empirical relationship for the dependence of the longitudinal Young's modulus upon structural density:

$$E = 3790(\frac{d\varepsilon}{dt})^{0.06}\rho^3 \tag{1-1}$$

where E is in MPa, ρ is in g/cm^3 (10^{-3} kg/m^3), and $\frac{d\varepsilon}{dt}$ is the strain rate in (1/s).

This relationship is called the combined data relationship because it is derived from the data which included both bovine and human cancellous and cortical bone data.

However this result is not consistent with that of Rice (Rice et al., 1988). The latter analysis made the distinction between bovine and human bone and the data for cortical bone were not included. Rice concluded that the axial Young's modulus was proportional to the square rather than the cube of the structural density and that the constants of proportionality between Young's

modulus and structural density differ between human and bovine cancellous bone.

Rice's results seem to be justified by the theoretical model mentioned above (open cell model). Rice also used statistical methods to analyze several sets of data from a number of previous experiments. It was concluded that differences in the data are due to species, direction and stress rather than to properties of particular bone or laboratory conditions. The empirical relationship for human bone by Rice is given in Table 1.2.

Table 1.2 Realtionship betwee Young's modulus and structural density for cancellous bone

ORIENTATION OF SPECIMEN	AXIAL STRESS CONDITION	E
longitudinal	compression	$0.06+0.9\rho^2$
longitudinal	tension	$0.06+1.65\rho^2$
transverse	tension	$0.06+0.6\rho^2$

where E is in GPa and ρ is in g/cm^3 (10^{-3} kg/m^3) at strain rate $0.01s^{-1}$.

1.2.3 Discussion

- **Cortical Bone and Titanium**

Most of implants are made from Titanium. The Young's modulus of titanium is about 103.4GPa. Compared with that of cortical bone which is approximately 12 GPa, titanium is a much more stiff material than bone. This big difference of two Young's modulus explains that phenomenon of "stress shielding".

- **Material modulus of single trabecular**

In 1892, Wolff suggested that cortical bone was simply more dense cancellous bone. However, several investigators pointed out this assumption is inaccurate when only the mechanical properties of these two tissues are considered. The reasons for disputing Wolff's hypothesis include:

(1) the Young's modulus of individual trabeculae was significantly less than that of cortical bone;

(2) the Young's modulus of cortical bone could not be extrapolated from the relationship between density and Young's modulus of cancellous bone;

(3) the Young's modulus of trabecular material (not a single trabeculae) could be extrapolated from that of cancellous bone by using a quadratic relation.

These conclusions suggests that when considered mechanically, cortical and cancellous bones are not the same material.

1.3 Thesis Outline

Chapter 2 describes some of existing remodeling/modeling theories including both biological and mechanical ones. For each theory, its characteristics, basic assumptions, equations, as well as its advantages and shortcomings are discussed. As well, these mechanical theories are evaluated by applying them to some simple problems. In this chapter, the relationship between biological and mechanical theories are also discussed and why Cowin's external remodeling theory is chosen as the base model is explained.

Chapter 3 presents the development of new modeling model. The difficulties with Cowin's remodeling theories is presented and the background of introducing weighting factors into the new model is discussed. Also, the details of the new model is provided and its flexibility of conversion to other existing modeling theories is described. This chapter also discusses the limitation of weighting factors as a result of the tensor transformation rule.

In chapter 4, the new model is used to investigate a variety of simple bone modeling problems. The bone cross section is modeled as simple or double connected which are assumed as a cylinder with a circle or elliptical section, and loading varies from axial tension and compression, radial tension and compression, and axial eccentric tension and compression. The numerical techniques associated with those different problems are introduced and all results are presented.

Chapter 5 associates the new modeling model with the finite element methods. The new model is used to investigate the simple modeling problems again but by using the finite element method as the numerical approach. The numerical results of those problems are presented. Finally the FEM model results and a real implant case are compared. The difficulties with a lack of experimental data on bone modeling is discussed at the end of this chapter.

Chapter 6 summarizes the results of the current study on bone modeling. The difficulties with this study is also discussed. The advantages and shortcomings of new model are presented. As well, the future work in this area is discussed.

Chapter 2

Discussion & Evaluation of Remodeling Theories

Bone is able to adapt its internal and external structure to its mechanical environment. This is so called Wolff's law. Wolff's original statement didn't contain any quantitative or mechanical information. How bone's external shape and internal structure responds to the mechanical demand has captured the interest of biologists and mechanical engineers for a long time. However, the basic questions as to what triggers the adaptive response, what stops it, how quickly the bone response to a change in mechanical demand and how completely it responds etc. are still unanswered. It was noted before that there exist two kinds of bone remodeling and modeling theories: biological and mechanical. The big difference between these two methods is that biological ones explain the problem in a qualitative way while mechanical ones attempt to predict modeling and remodeling results in a quantitative way. Thus far, both kinds of theories are mostly phenomenological in nature.

The term remodeling was previously used to describe any adaptive change in bone and included both internal and external remodeling. But the distinction between modeling and remodeling in recent bone biology literature has been generally accepted. As was stated before, the secondary osteon (Haversian system) is very special from a histological point of view as its formation follows well-defined phases which always begin with activation (A), followed by resorption (R), and followed by formation (F). Remodeling is thus defined as any A-R-F sequence while modeling is referred as a process which only involves formation or resorption independently.

Thus, bone adaptation could be accomplished by: (1) remodeling, an A-R-F process; (2) modeling, adding or removing lamellar bone from the bone

surface; (3) a response in which woven bone is formed as a result of modeling or repair response to damage.

Generally speaking, remodeling is related more to secondary osteons and internal remodeling whereas modeling is an external process in which only primary bone (circumferential lamellar bone and primary osteon) or woven bone are involved. In modeling processes, resorption and formation of bone are achieved by activation of osteoclast and osteoblast respectively, however, in remodeling process, the secondary osteons are formed by activation of a group of cells functioning as organized units called *basic multicellular units* (BMUs).

According to Wolff's law, bone has the ability to adapt its structure to its mechanical environment. This implies that bone has internal sensors that enable it to react to an actual state of deformation and to translate mechanical signals to biomechanical ones that activate bone cells to cause a modeling or remodeling process.

The question of which of stress or strain is this internal sensor has triggered considerable discussion. This question is intrinsically difficult to answer because stress and strain are related. However, as bone is a nonhomogeneous and anisotropic material, the relationship between stress and strain is quite complicated.

Based on the results of experiments employing *in vivo* strain gauge techniques, it has been generally accepted that strain rather than stress is more likely the candidate as this internal sensor. The main reasons behind this conclusion are summarized as follows:

(1) Stress is an entity that can not be measured directly which means that nothing could sense the stress, in other word, no stress receptor exists in nature.

(2) The fact that measured peak strains are nearly constant in different bones and in different animals while the corresponding stresses vary widely suggests that adaptation occurs in response to factors in the strain environment.

(3) Electrical phenomena in bone are closely related to strain gradients. It has been shown that bone cells have stretch and voltage receptors.

All these arguments suggest strain as a primary mechanical sensor. In fact, most of contemporary modeling and remodeling theories take strain or some function of strain (such as strain energy density) as the mechanical signal sensor.

Most modeling and remodeling theories consider the adaptive process as a feedback system. They assume there exists an adaptive equilibrium environment. When this equilibrium is disturbed by changes in the mechanical environment, the mechanical signal sensor triggers bone cells to encourage modeling and remodeling until the adaptive equilibrium is again regained. This equilibrium status is thus referred as the *objective* of bone modeling or remodeling.

For different theories, the adaptive objectives are different. Biological theories tend to use simple forms while mathematical theories prefer to take complicated forms. These will be addressed below.

2.1 Biologically based theories

In this section, the remodeling/modeling theories developed by Frost, who has a rich clinical experience as an orthopedic surgeon, will be introduced, and some biological observations as well as various important concepts related to bone adaptation will be discussed.

2.1.1 FNT theory

Frost's flexural neutralization theory (FNT) was proposed in 1963 (Frost 1963) and in fact was one of the first mathematical formulations of bone modeling and remodeling as a function of mechanical variables.

FNT was triggered by the observation that fractures that heal in a bent configuration tend to straighten themselves. In light of this model, if the bent bone is to be straightened, bone must be removed from the convex side and apposition must occur on the concave side. The objective of FNT is that a

curved bone subjected to intermittent bending will drift actively towards the load induced concavity until both cortices are arranged so as to neutralize the bending and be subjected to overall compression. It predicts :

--Increased surface convexity (positive strain gradient)--> osteoclast activity--> bone resorption;

--Decreased surface convexity (negative strain gradient)--> osteoblast activity--> bone apposition.

In this instance, positive surface strain gradient is defined as that the strains become more tensile nearer the surface as shown in Figure 2.1.
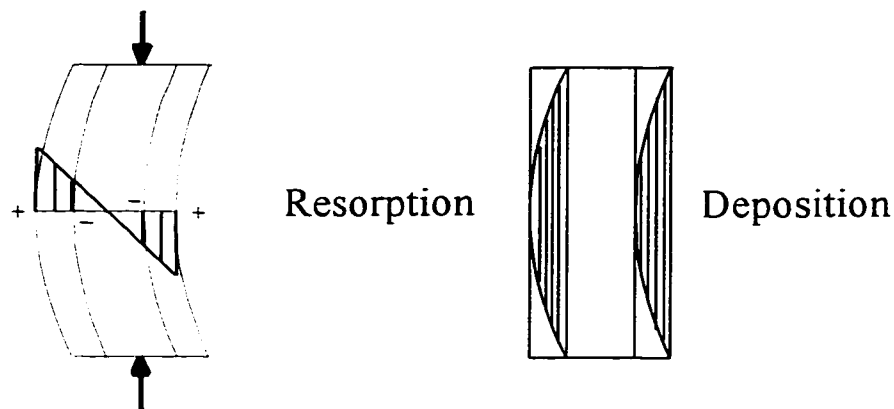
Figure 2.1 A segment of a curved long bone.

FNT theory applies to both modeling and remodeling. In modeling, only osteoclasts are activated on the convex surface and only osteoblasts are activated on the concave surface. In remodeling, BMUs are activated on both surfaces.

It is noteworthy that the FNT coincides well with observed electrical phenomena in bone. It was found that the streaming potentials rather than piezoelectricity are possible primary sources of strain generated electrical potentials on the surface of bones. Streaming potentials occur when ionized

liquids are made to flow through channels in a solid that has charged surfaces. In the case the surface charge is negative, the positive ions in the liquid will be attracted to the surface where the velocity of liquid is slower (dynamic slip plane) while the ions far from the surface will be negative and move faster at the center of the channel, constituting a flow of current through the channel. This current causes a potential difference to be developed along the channel. This potential difference is called the streaming potential.

Figure 2.2 schematically shows the streaming potential produced when a bone is bent. In a bent bone, the internal channels will be distorted so as to cause flow from the compressed side to the tensile side. As the potential difference of bone is normally negative, so the tensile surface will be positive relative to the compressive surfaces.
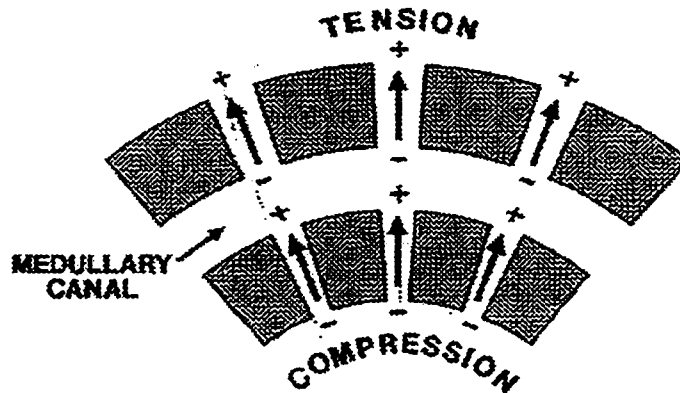
Figure 2.2 Schematic diagram showing that the streaming potential produced when a bone is bent (Martin et al. 1989).

It happens that positive potentials produced in the bone are associated with positive strain gradient and negative potential with a negative strain gradient. Because experiments concluded that bone formation is stimulated near a cathode and resorption is stimulated near an anode, it is reasonable to postulate that streaming potentials are caused by the strain gradients and cellular activities are promoted by streaming potentials. It seems that streaming

potentials play the role of a transducer that translates the mechanical signal to a biochemical one.

Since the FNT was proposed, several experiments have been conducted to verify it. However up to now, these studies have not resolved the controversy over Frost's theory. More recently, Frost (1986) proposed another theory which is called *the Mechanostat theory*.

2.1.2 Mechanostat theory

The Mechanostat theory differs from the FNT in that it seeks to predict when and at what condition the modeling or remodeling will occur in response to increased or decreased strain magnitudes whereas the FNT describes how the modeling or remodeling will proceed (resorption or formation).

This theory suggests that there is a range of strain values (Minimum Effective Strain, MES) that will evoke no adaptive response -- this is termed modeling or remodeling equilibrium. Strain above this range will evoke a positive adaptive response (increased bone) and strains below this range will cause a negative adaptive response (loss of bone). Frost suggests that for the equilibrium range the upper strain is 2,500 microstrain in compression and 1,500 microstrain in tension , the low limit is 200 microstrain for both tension and compression.(See Figure 2.3) The objective of modeling/remodeling is to keep strain within or below the threshold strain range.

POL	OL modeling	PL equil.	TL remodelling	PL equil.	OL modeling	POL
	-3000	-2500	-200	200	1500	?
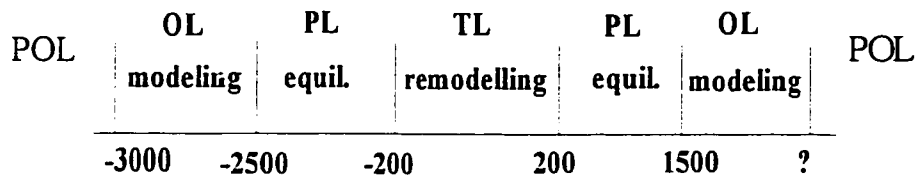
Figure 2.3 A diagram showing the relationship between average peak strain and adaptive response. Where PL: physiological loading zone in which bone is in equilibrium; OL: overload zone in which modeling is stimulated; TL: trivial loading zone in which remodeling is stimulated; POL: pathological zone in which woven bone is formed.

Mechanostat theory suggests that on the compression side modeling is stimulated at strain magnitudes above 2,500 microstrain whereas remodeling is stimulated when strain magnitudes fall below 200 microstrain. Because modeling and remodeling are stimulated within different strain ranges , they are not stimulated at the same time, on the same surface and do not work at cross purposes (Table 2.1).

Table 2.1 Effects of strain on skeletal

Effects on skeletal envelopes	Modeling	Remodeling
Increased Strain	**Activated**	**Inhibited**
Periosteal	Expansion	Expansion??
Endosteal	Loss retarded	Loss retarded
Trabecular	Loss retarded	Loss retarded
Intracortical	No effect	Activation retarded
----------------- bone increases mass----------------		
DECREASED STRAIN	**Inhibited**	**Activated**
Periosteal	Apposition retarded??	Apposition retarded??
Endosteal	Loss accelerated	Loss accelerated
Trabecular	Loss accelerated	Loss accelerated
Intracortical	No effect	Activation stimulated
----------------- bone decreases mass----------------		

Although Mechanostat theory can explain some experimental results with respect to disuse or overuse of bone in animals, it still fails to explain other phenomena. Experiment evidence has supported some essential features of the Mechanostat theory including (Martin et al. 1989):

- an upper strain threshold does exist;
- strains on the high side of this threshold inhibiting activation of new BMUs, depressing formation of new osteons and initiating loss of bone from endosteal surfaces;

- strains on the low side of the threshold enable activation of new BMUs, increasing the number of new osteons and permitting endosteal resorption.

2.1.3 Reparative response to bone microdamage

In Frost's mechanostat theory, the strain range can be divided into four zones: (1) physiologic loading zone (PL), in which bone strains are tolerable with no adaptive response; (2) trivial loading zone (TL) with strain magnitude below those for PL, and in which the remodeling is initiated; (3) overload zone (OL) with strain magnitude above those for PL, and in which the modeling occur; (4) pathologic overload zone (POL) (Figure 2.3).

From Figure 2.3, we can see that the pathologic overload zone is above the overload zone. In this zone, the adaptive response occurs by woven bone formation because normal lamellar bone formation is too slow. Experimental results show that woven bone is generally associated with fracture repair and could also be found in rapidly growing children, so an occurrence of massive proliferation of woven bone could be considered as a modeling response as well as repair reaction to the microdamage caused by surgery or overload.

Generally speaking, adaptive response can be in four types: (1) normal modeling; (2) remodeling; (3) a pathophysiologic modeling in which woven bone is produced; (4) a reparative response to surgical intervention or bone microdamage.

In addition to woven bone, it is also suggested that microdamage could cause bone remodeling (osteons). Biologists (see Martin and Burr, 1989, 1992) believe that the unique microstructural arrangement of the various components of Haversian bone is adapted to prevent crack growth, and extend fatigue life. Osteonal bone is specially designed so that microdamage itself initiates the reparative remodeling process.

As a result it is conjectured that if the applied load is too high, the microdamage in the bone caused by this load will initiate formation of woven

bone and secondary osteons. This is confirmed to some degree by experiments (Hoshaw et al. 1992, Lanyon et al. 1982).

2.1.4 Bone adaptation signal sensors

As already noted, strain is considered by most researchers as a mechanical signal sensor. However, as strain is a tensor, then what aspects of strain, in addition to its magnitude, are important enough to affect the modeling and remodeling of bone? Putting the question another way, what will be taken as the sensor, the strain magnitude itself, or combination of the magnitude with other factors ?

There are several such factors that are associated with strain such as (1) strain mode, tension, compression or shear; (2) strain direction; (3) strain distribution -- the pattern of strain magnitude across a section of bone; (4) strain energy density. These factors will be examined below.

(1) Strain mode

Before Frost's FNT, it was once simply believed that tension caused bone resorption and the compression caused apposition. Although this conclusion is too simplistic to be accepted, it is still felt that tension and compression result in different adaptive responses. However, the work dealing with the trajectory of trabeculae suggested that both compression and tension could be osteogenic because predominant orientations of trabeculae coincide with the principal compressive and tensile strain directions.

Experiments show the greatest density of osteons often appears within the compression cortex and not within the tension cortex. But because the compression cortex is also where the largest strains are generated, it is not clear at all that large tensile strains are achieved in bone.

Experimental results have continued to show conflicting conclusions, and this uncertainty about the effect on the modeling and remodeling of strain

mode maybe indicates that knowledge of only strain mode (tension or compression) can not predict the adaptation result. In other words, it is not the key factor to be taken as an independent mechanical sensor. It should however be considered when considering the adaptive behavior of bone.

(2) Strain direction

From Wolff's law, it is known that the axes of the trabeculae coincide with the directions of principal stress and principal strain (Cowin 1985). Although this observation is made for the trabecular bone, there is a similar phenomenon for the cortical bone. Corresponding to the trabeculae, which are the basic unit of trabecular bone, osteons can be considered as the basic components of cortical bone. It is generally considered beneficial for osteons to be aligned with principal loading direction, and experiments (Lanyon and Boun, 1979) have shown that for long bones, secondary osteons are orientated close to the principal strain direction (loading direction).

In vivo tests of single osteons also indicate that they are weak in longitudinal shear which could be justified by the assumption that osteons align with the principal strain direction in which the shear strain is zero. The approximate alignment of osteons with the principal strain direction reduces the shear strain developed in the cement line, and may reduce fatigue damage during normal loading events (avoiding cracks caused by fatigue damage to extend to the outside of the cement line).

From the fact that the principal strain direction is associated with the basic material units in both cortical bone and cancellous bone, and the fact that the secondary osteon is the result of the remodeling, as well as the fact that the trajectory of trabeculae is the important characteristic of modeling and remodeling equilibrium, it appears that the strain direction is a vital factor affecting the bone modeling and remodeling. Both the strain direction and the strain magnitude should be considered as mechanical sensors .

(3) Strain distribution

In the field of orthopedics, it is believed that the transfer of load from the prosthesis to the bone thus causing unnatural stress/strain will lead to the adaptive modeling or remodeling of bone. The unnatural stress or unnatural strain include both stress/strain patterns and their magnitude. This fact implies that the strain pattern is also a very important factor regarding the bone's adaptation.

Experiments (Rubin and Lanyon, 1984) also showed that adaptive responses were more easily generated by a variety of different loading conditions than by repetition of the normal pattern of loading. In this experiment, ulna preparation of roosters received a load regime with the magnitude similar to the intact ulna bone but the distribution of strain was different. It was found that physiological levels of strain imposed with an abnormal distribution could produce an osteogenic stimulus that was capable of increasing bone mass and the maximum osteogenic response was produced by a relatively few strain reversals, occupying a very short time (thirty-six cycles in seventy-two seconds a day). It is suggested that the strain required to elicit an adaptive response may be lower if the manner of loading is markedly different from the usual pattern (Martin and Burr, 1989).

This in fact suggests that the bone adaptive behavior is position sensitive, i.e., every point of bone material can sense its own signal. If the pattern of loading changes, the stress or strain at one point is therefore changed, which results the modeling or remodeling of bone.

(4) Strain energy density

While several authors have used strain energy density as the overall sensor, it contains less information than the strain. For example, the fact that it is a scalar and is always positive does not allow a distinction in the direction of loading. As discussed above, bone adaptation is sensitive to both strain magnitude and strain direction. Strain energy has obviously no characteristic of direction, so it is not a good candidate as a mechanical signal sensor. In fact,

there is little experimental evidence that relates adaptive changes to strain energy density.

2.1.5 Discussion

We have discussed Frost's FNT and Mechanostat theories and found that they are straightforward, and relatively easy to be tested and compared to experiments. This has meant that his theories are used by biologists and researchers involved in experimental work. In fact, much of the research aimed at studying bone's ability to adapt to its mechanical environment was promoted by Frost's theories. However, the validation of these theories is still being challenged as they are difficult to apply in a global sense. Some of these shortcomings are illustrated in two examples below.

According to FNT, the process of "flexure drift" would ensure that each bone cortex is subjected to overall compression. But Lanyon and Baggott (1976) reported that the sheep's radius was bent during locomotion and that the strain was consistently larger and of a different sign on the caudal than on the cranial surface. If the controlling processes were those suggested by FNT, then one would have expected this state to be unstable and accompanied by hypertrophy of the caudal cortex or drift of the whole bone towards the caudal facing concavity. However the experiment conducted by Lanyon and Boggott showed that although the strains on the compressed cortex of the sheep radius were nearly twice the magnitude of those on the tensile cortex, there was no difference in the thickness of the two cortices.

As a second example, it was also observed (Uhthoff and Jaworski, 1978) that disuse osteopenia (high degree of porosity) in young adult dogs is characterized by failure of the periosteal surface to expand. This is consistent with disuse inhibition of periosteal expansion by modeling according to Frost's Mechanostat theory (refer to Table 2.1), but the theory also predicts that the endosteal surface should be remodeling, and one would have expected endosteal expansion to be promoted by disuse. However, this was not the case.

It has been already noted that an adaptive theory should have two basic features, one is the mechanical sensor, and the other is the objective of

adaptation. Frost's theories are not completely successful regarding the former aspect.

As discussed above, several factors associated with strain play an important role in the adaptive behavior of bone. The mechanical sensor should consider all these factors (strain magnitude, strain direction, strain distribution). However the FNT uses only the strain gradient (in a scalar sense, defined in the section 2.1.1) as the sensor, and the Mechanostat theory takes the strain magnitude as the sensor. Their lack of full considerations of the mechanical signal could be one of reasons for their failure to explain certain experiments.

Moreover, FNT can only be applied to long bones and Mechanostat theory does not specify the strain ranges for certain type (long, short or flat) of bone in which modeling or remodeling is activated.

As these two theories have been developed for simple loading conditions, for complicated cases such as the interaction between bone and an implant, they can not be readily applied. There is need for a more general theory which attempts to address these issues.

2.2 Mathematically based theories

It has been noted that the structure of bone can be divided into three levels. At the molecular level, bone can be considered to be a composite material consisting of a fibrous protein, collagen, stiffened by an extremely dense filling of calcium phosphate; at the microscopic level, bone exists in three distinct forms, woven bone, primary bone (lamellar bone and osteons), and secondary bone (Haversian Systems). At the macroscopic level, there is an extremely important mechanical distinction between compact and cancellous bone which was described above. Unlike the biological remodeling theories and experimental work which focuses on the bone at the molecular and microscopic levels, mathematical theories study bone at the macroscopic level. In all these theories, bone materials, both cortical bone and cancellous bone are assumed to obey Hooke's law, which means the classical linear elasticity theory can be applied to bone. Bone is modeled as either an isotropic or anisotropic (orthotropic or transversely isotropic) material depending on the application.

Another characteristic of mathematical theories is the computational feature of their application. As the objectives of these theories are closely associated with the design of bone implants or bone morphology investigations, some numerical methods such as the finite element and the boundary element method have to be employed to perform the stress analysis for the complicated stress/strain environment caused by the shape of implant and bone. These numerical methods are generally combined with an time stepping algorithm.

The application of elasticity theory to bone has a limit. This limit comes from the continuum assumption. Because the bone is not a really a continuous material, there exists a length scale below which the continuum model is no longer applicable. For cortical bone, this is not a big problem, however, when it is applied to the trabecular bone, special care must be taken with the lack of existence of solution theorems as most of the existence of solution theorems in elasticity do not extend to inhomogeneous materials such as trabecular bone.

In addition to the elasticity, each mathematical theory is characterized by their special remodeling rate equations which relate the rate of bone tissue deposition and resorption to some measure of mechanical loading on the bone (mechanical stimulus or sensor). Generally speaking, a remodeling theory is formed from the set of equations consisting of remodeling and the equations of linear elasticity.

As mentioned in the last section, most of the remodeling theories consider bone to operate as a simple closed loop feedback control system. They assume there exists a remodeling equilibrium (RE) state under which there is no net deposition or resorption of bone tissue. The control system is shown in Figure 2.4.

When the RE is disturbed, the mechanical signal sensor, which is measured in some way from the strain field, deviates from its corresponding value at RE. The error signal stimulates bone remodeling cells and their action results in the modeling or remodeling of bone which changes its structure or shape, and in turn, the strains.

Loads———► Build of bone◄——— remodelling

▼

Strains(signals)   Osteoblast-clast

▼

Comparison———————► Error Signal
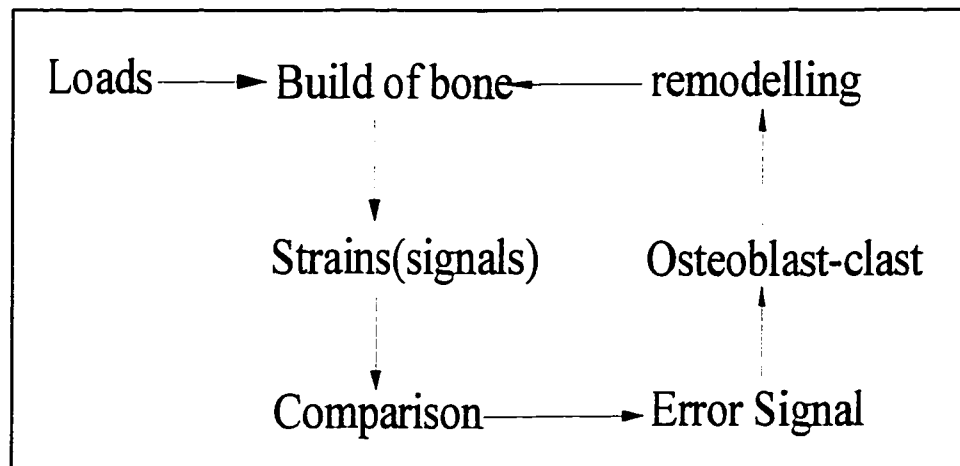
Figure 2.4 The schematic representation of remodeling control system

Different theories adopt different methods to deal with the problem of remodeling equilibrium and employ different aspects of strain as the mechanical signal sensor (stimulus). It has been already noted that there are several factors to account for in choosing a candidate as the mechanical sensor. The theories will be evaluated by examining these factors. Different theories are also associated with different discrete-time computational algorithms. The convergence and the stability of an algorithm are also crucial to the success of the theory. Finally, there exist two different opinions considering the difference between cortical and cancellous bone materials. One, which originates directly from Wolff's law, is that cortical bone is simply more dense cancellous bone. Another opinion suggests that cortical bone is a different material from cancellous bone (this argument was highlighted in the section 1.2.3). The different considerations of cortical and cancellous bone are reflected in the different theories.

Consideration will be given to three prevailing mathematical remodeling theories. Among them, Carter and Fyhre's theory (Carter et al. 1987) focuses on the morphology of bone, in other words, their theory tries to predict bone material properties of remodeling equilibrium under daily loading conditions. Huiskes' theory (Huiskes 1982) is a special form of Cowin's (Cowin el al. 1976, 1979) theory, but its main thrust is in the application of the theory to orthopedics. Cowin's theory is based on continuum mechanics and can be

considered as the most rigorous formulation among the existing theories. Recently a method of predicting bone adaptation using damage accumulation has been provided by Prendergast and Taylor (Prendergast and Taylor, 1994). They consider the adaptation behavior of bone from a fracture mechanics point of view.

In the following sections, Carter and Fyhre's theory will be first discussed , followed by Huiskes' and Cowin's theories. Finally Prendergast and Taylor's theory along with several other miscellaneous interesting problems will be mentioned. In the following discussion, only remodeling rate equations are presented while the equations from the elasticity theory will be omitted.

2.2.1 Carter and Fhyre's theory

2.2.1.1 Hypothesis and objective

Carter and Fyhre's theory assumes there exists a relatively stable (homeostatic) situation between bone stress and local bone density --remodeling equilibrium. Its objective is to predict at this homeostatic condition the relationship between the current trabecular bone apparent density and the normal loading environment.

In their theory, cortical bone is considered as "densified" trabecular bone, so that these two tissues are basically the same, differing only in their porosity.

They argued that during daily activities, bone is repeatedly loaded under many different loading conditions with a widely varying number of loading cycles. They chose one day as the characteristic time period over which they summarized the relevant loading history. In a homeostatic situation, they assume that the daily stimulus to maintain a certain bone mass is related by a linear superposition of the stimuli created by each loading condition.

2.2.1.2 Formulation

They postulate that bone tissue is a self-optimizing material with the objective of aligning trabecular architecture with principal stress orientation (trajectory hypothesis from Wolff's law) and adapting its apparent density to an "effective stress" which is determined from the strain energy density principle. Based on the strain optimization criteria (use the least amount of bone to maximize the bone's structural integrity), for multiple loading conditions, Carter and Fhyre's theory assumes the local apparent density of cancellous bone can be approximated by:

$$\rho = k(\sum_{i=1}^{c} n_i \sigma_{i,eff}^m)^{(\frac{1}{2m})}$$
(2-1)

where the daily loading history has been summarized as c discrete loading conditions, n_i the number of loading cycles, ρ is the bone apparent density, k and m are constants, the cyclic peak effective stress $\sigma_{i,eff}$ is defined as:

$$\sigma_{i,eff} = \sqrt{2EU_i}$$
(2-2)

where U is the strain energy density, E the elastic modulus which is calculated from the relationship between the structural density and Young's modulus. For quasi-static loading condition, they use

$$E = 3790\rho^3$$
(2-3)

2.2.1.3 Convergence of computational algorithm

Carter and Fyhre (Fyhre etc. 1986) applied their approach to calculate the apparent density in a two-dimensional representation of the proximal adult femur. Two loading conditions, which represent single-loading direction solutions and multiple-loading direction solutions were assumed.

Their results showed that by using their computational algorithm, the density distributions calculated for about the first three time steps were reasonable but the distributions calculated for the seventh time step were not. This indicates the solution does not appear to approach a reasonable limit. The method employed appeared to be converging toward a condition in which most of the bone elements will either be saturated with a density 1.8 g cm^{-3} which represents the fact that the bone become cortical or be completely resorbed.

Weinans and Huiskes (Weinans et al., 1992) have used a modified form (Eqn. 2-6, 2-7 below) of Carter and Fyhre's method to investigate the same problem. They found that the solution obtained is generally a discontinuous patchwork although the cortical and cancellous bone were described as continuous material. They concluded that the discontinuous end configuration was dictated by the nature of the differential equations describing the remodeling process. The evolution of their method can be considered as a nonlinear dynamic system with many degrees of freedom, which diverged from the objective, leading to many possible solutions.

Cowin et al.(1993) also showed that the discrete time computational algorithm employed by Weinans and Huiskes (1992) or Carter et al. (1986) has a well-known chaos mechanism. They note the existence of an overshooting calculation step in this discrete-time computational algorithm, which, when coupled with the input from an inhomogeneous stress field, could deflect the algorithm from a path prescribed by the bone-density stress adaptation model.

2.2.1.4 Discussion

The studies of Weinans et al. (1992) and Cowin et al. (1993) showed that the mechanism of computational internal remodeling model based on Carter

and Fyhre's theory can not be well understood and suggest caution in the conclusions obtained from such models. The goal of Carter and Fyhre's theory is to predict the bone apparent density at remodeling equilibrium rather than to predict the remodeling process due to the disturbance of the load environment. As a result no process of remodeling is involved in their theory although it can be modified as was done by Weinans and Huiskes (1992).

Carter and Fyhre's theory assumes that the actual material of cancellous bone is the same as that of cortical bone. As mentioned above, it is possible that from the perspective of mechanical properties, this assumption is not appropriate. The mechanical signal sensor or stimulus in their theory is strain energy density. As discussed previously, strain energy density is a scalar containing less information than the strain tensor and thus is not a good candidate for a signal sensor.

2.2.2 Huiskes' theory

2.2.2.1 Hypothesis and objective

The goal of Huiskes' theory (1982) was to investigate the "stress shielding" phenomenon in orthopaedics. This idea indicates that after implantation of the prothesis, the surrounding bone is partially "shielded" from load carrying and starts to resorb. This theory primarily attempts to describe the adaptive behaviour of bone from one loading configuration to another. For this purpose, it is assumed that bone tissue has a site-specific natural or homeostatic remodeling equilibrium state and that the mechanical signal sensor is the strain energy density. Change of load, or in fact, an abnormal strain energy density will stimulate the bone tissue to adapt its mass in such a way that the equilibrium strain energy density is again obtained. In this theory, internal and external remodeling are separated (according to the definition above, internal remodeling refers to remodeling whereas external remodeling refers to modeling). Like Carter and Fyhre's theory, Huiskes' theory assumes that cortical bone is the same material as the cancellous bone at a different density.

2.2.2.2 Formulation

(1) Modeling

According to the Mechanostat theory, modeling and remodeling are stimulated within different strain ranges. They are not stimulated at the same time on the same surfaces and do not work at cross purpose. As a result theories about modeling and remodeling can be separated. In the theory of surface remodeling, the chemical reactions occur only on the external surfaces of bone and mass is added to or removed by changing the external shape of bone. Huiskes' theory postulates a causal relationship between the rate of surface deposition or resorption and the strain energy density in the surface of bone. This relationship can be expressed as:

$$\frac{dX}{dt} = C_x(U - U_n) \qquad (2\text{-}4)$$

where x is the location of surface point, and $\frac{dX}{dt}$ is the moving rate of x point perpendicular to the surface, and C_x is the modeling coefficient. U is the actual strain energy density (SED), U_n is the site-specific homeostatic equilibrium SED.

(2) Remodeling

The theory of internal remodeling acknowledges the orthopaedic principle that states the prolonged or strenuous straining of bone tends to make the bone stiffer and more dense while prolonged bed rest or inactivity will tend to make the bone less stiff and less dense. The theory postulates a causal relationship between the rate of deposition or resorption of bone matrix at any point and the strain energy at that point in the bone matrix. This relationship is:

$$\frac{dE}{dt} = C_e(U - U_n)$$ (2-5)

where U is the actual strain energy density (SED), U_n is the site-specific homeostatic equilibrium SED, E is the modulus, and C_e is the coefficient of remodeling.

2.2.2.3 Convergence of computational algorithm

Huiskes' theory was applied to investigate the relationship between "stress shielding" and adaptive cortical bone remodeling around an intramedullary prothesis. The intramedullary fixation was simulated by an axisymmetric straight stem (Figure 2.5).
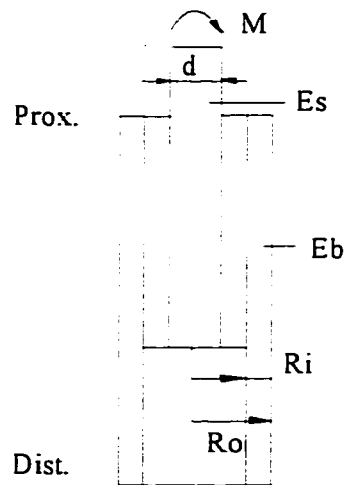
Figure 2.5 The simplified, general model of intra-medullary fixation applied in the remodeling/modeling analysis.

In the calculations, modeling and remodeling were simulated separately. The results showed that for modeling, the loss of bone increased with the

increase of the thickness of stem in which case the degree of stress shielding is much higher due to higher stem rigidity, and in most cases, the modeling equilibrium strain energy density couldn't be obtained. This meant that the computational process didn't converge. On the other hand, in the case in which internal remodeling of the elastic modulus was simulated, the results turned out to be much less effective. Because of their first unsatisfactory model, Huiskes and his coworkers adopted another candidate as the feed-back variable (signal sensor), which, in fact, is modified from Carter and Fyhre's theory. The formulation is as follows:

Remodeling $\qquad\qquad \dfrac{d\rho}{dt} = B_c (\dfrac{U}{\rho} - K_c)$ $\qquad\qquad$ (2-6)

Modeling $\qquad\qquad \dfrac{dX}{dt} = B_x (\dfrac{U}{\rho} - K_x)$ $\qquad\qquad$ (2-7)

where ρ is the apparent density, U is the stain energy density, B_c, B_x are the remodeling and modeling coefficients respectively, K_c, K_x are the remodeling and modeling equilibrium sensors.

It was previously mentioned the application of this new model to the proximal femur showed an interesting paradox because, in spite of the underlying assumption of continuity, the discontinuous density distribution predicted by their model appears to replicate the observed density distribution in real bone. However the solution obtained by their computational algorithm was unstable.

2.2.2.4 Discussion

In addition to what has been mentioned, the choice of SED as the feed-back control variable in Huiskes' theory has other drawbacks. As an example,

for the two changes in loading shown in Figure 2-6, no modeling or remodeling would happen according to Huiskes's theory as the SED is the same. This may be unrealistic.
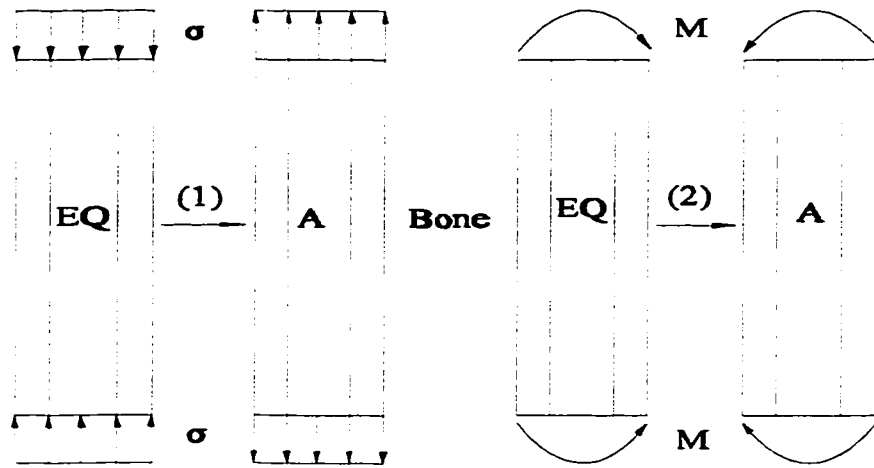
Figure 2.6 Two loading cases used to test modeling theories where EQ represents modeling equilibrium state, A refers to the actual loading environment.

Just as with Carter and Fyhre's theory, Huiskes' theory also takes the cortical bone as the "densified" cancellous bone although it separates the adaptive behaviour of bone into modeling and remodeling. For cancellous bone, the terms modeling and remodeling haven't been well defined.

Huiskes's theory may explain the densification or resorption of cancellous bone around an implant, but it can't explain the densification of secondary osteons, so it is not an ideal model to fully explain the experimental

results. Moreover, the unstable solution of the computational algorithm of Huiskes' model makes it difficult to accept.

2.2.3 Cowin's theory

2.2.3.1 Hypothesis and objective

Of all the remodeling theories, Cowin's theory is the most rigorous one. Unlike Carter and Fyhre's theory or Huiskes' theory, Cowin et al. (1989b) consider the cortical bone as a different material from the cancellous bone. Thus his theories for cortical bone and cancellous bone are separated. The following will mainly discuss his theory for cortical bone.

Cowin's theory uses the strain as the mechanical signal sensor. Like Huiskes' theory, it also attempts to describe the adaptive behaviour of bone from one loading condition to another. It is assumed that bone tissue has a site specific natural or homeostatic equilibrium strain state. With a change of load, an abnormal strain state will stimulate the bone tissue to regain the equilibrium.

Cowin's theory also separates internal remodeling (remodeling) and external remodeling (modeling). While Cowin's theory allows large elastic deformations, we will only address the small strain theory which is specialized from the general theory.

2.2.3.2 Formulation

(1) Modeling (external remodeling)

The theory of surface remodeling acknowledges the observed fact that external changes in bone shape are induced by changes in the loading environment. The bone is considered to be an open system with regard to mass transport and the mass of bone will vary as the external shape varies. The rate of surface deposition or resorption is proportional to the change in the strain in

the surface from a reference value of strain. The hypothesis for the surface remodeling is that the speed of the remodeling surface is linearly proportional to the strain tensor.

$$\frac{dX}{dt} = C_{ij}(\xi_{ij} - \xi_{ij}^0)$$

(2-8)

where $\dfrac{dX}{dt}$ is the speed of modeling surface normal to the surface, C_{ij} are the modeling coefficients, ξ_{ij} are the coponents of the actual strain tensor, and ξ_{ij}^0 are the equilibrium strains.

The time scale for the derivatives in the above constitutive equation are for a very long time scale, on the order of the modeling time and not on the order of the loading time for bone. These time scales differ by many orders of magnitude (Cowin et al. 1993). Let $T(r)$ denote the time that biological processes take to complete significant growth (or modeling) associated with a mechanical loading, and let $T(l)$ denote the characteristic period of mechanical loading. Rough estimates of these numbers are two weeks and one second, respectively; thus $T(l)/T(r)$ is a small number. The time scale for all modeling rate equations is necessarily $T(r)$. On the other hand, all modeling models assume that the new increment of bone tissue that is added to the whole bone (or subtracted from the whole bone) has exactly the same strain as the bone tissue at the site where it is to be added or subtracted. This assumption may seem unreasonable on the loading time scale, but on the modeling time scale which covers million of loading cycles in the bone formation period, it is not an unreasonable assumption (Cowin, private letter).

(2) Remodeling (internal remodeling)

In the theory of internal remodeling, the bone matrix, that is to say the solid extra-cellular material and the bone cells, are modeled as a solid structure

with interconnected pores. This solid is assumed to be a porous anisotropic linear elastic solid. The extracelluar fluid and blood are modeled as a single fluid. As a result of the chemical reactions, mass, momentum, energy and entropy are transferred to or from the solid porous bone matrix. Because the characteristic time of adaptation is so large compared to a characteristic time for inertia effects, only mechanically quasi-static processes are considered. Using the balance equations for mass, momentum, energy, and the entropy inequality, Cowin and his co-workers have developed a rigorous thermomechanical continuum theory as a model for the adaptation of cortical bone (Cowin et al. 1976).

In the processes of remodeling, the mass of the porous elastic solid is changed by increasing or decreasing its porosity but not by changing the overall dimensions of bone. The bulk density ρ of the porous solid is written as the product of γ and v:

$$\rho = \gamma v \qquad (2\text{-}9)$$

where γ is the density of material that composes the matrix structure and v is the volume fraction of that material present.

The change in volume fraction ζ from a reference volume fraction ζ_0 is denoted by:

$$e = \zeta - \zeta_0 \qquad (2\text{-}10)$$

where ζ denotes the value of the volume fraction v of the matrix material in an unstrained reference state, the conservation of mass yields the relationship between v and ζ.

The governing system equations for the theory are:

$$2\xi_{ij} = u_{i,j} + u_{j,i} \qquad (2\text{-}11)$$

$$\sigma_{ij,j} + \gamma(\zeta_0 + e)b_i = 0 \tag{2-12}$$

$$\sigma_{ij} = (\zeta_0 + e)C_{ijkm}(e)\xi_{km} \tag{2-13}$$

$$\frac{de}{dt} = a(e) + A_{ij}(e)\xi_{ij} \tag{2-14}$$

where a(e), A_{ij}(e), and C_{ijkm}(e) are material coefficients. For the small strain, (2-13) and (2-14) can be approximated by:

$$\sigma_{ij} = (\zeta_0 C^0_{ijkm} + eC^1_{ijkm})\xi_{km} \tag{2-15}$$

$$\frac{de}{dt} = a_0 + a_1 e + a_2 e^2 + A^0_{ij}\xi_{ij} + eA^1_{ij}\xi_{ij} \tag{2-16}$$

where a_0, a_1, a_2, A^0_{ij}, A^1_{ij} are remodeling coefficients, ξ_{ij} are components of strain tensor, σ_{ij} are components of stress tensor, C^0_{ijkm}, C^1_{ijkm} are elastic coefficients which are all constants, u_i is the displacement in i direction.

2.2.3.3 Convergence of computational algorithm

(1) external remodeling

Hart et al. (Hart et al. 1984; Hart, 1983) have applied Cowin's theory to predict the surface movement in the central or diaphyseal region of the femur due to changes in axial loading. A hollow circular cylinder, shown as Figure 2.7, is employed to represent the diaphyseal region of the femur. The problem is

to determine the surface remodeling that would occur in the diaphyseal region of a long bone if the compressive load carried by the bone were suddenly raised to a new level and held there indefinitely. It has been shown that there are a total eight stable modeling solution types for this kind of problem (Cowin et al. 1981, Figure 2.8). If the inner radius is initially equal to a_0, and if the outer radius is initially equal to b_0, then after remodeling, the inner radius is a $_\infty$, and the outer radius is b $_\infty$.
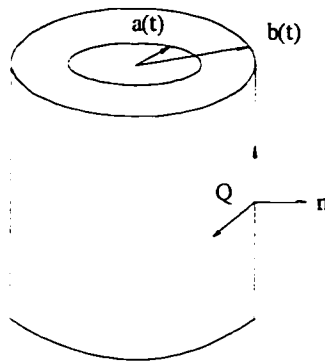
Figure 2.7 A cylinder representing the diaphysis of the femur

Hart et al. (1984b) developed a computational method based on Cowin's theory to model the first three solution types (Figure 2.8) by changing the modeling coefficients and equilibrium states. Numerical results showed good agreement with the analytical ones.

(2) Internal remodeling

Cowin et al. (1981) applied their internal remodeling theory to get a
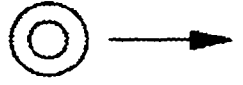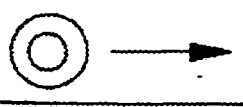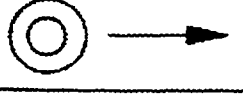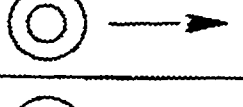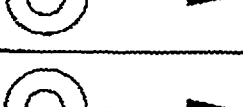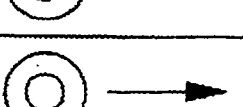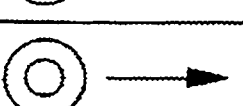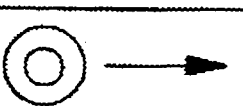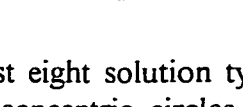
SOLUTION TYPE	SURFACE MOVEMENT	AREA CHANGE	
1	$a_\infty > a_0$ $b_\infty < b_0$	−	
2	$a_\infty > a_0$ $b_\infty > b_0$	+ or −	
3	$a_\infty < a_0$ $b_\infty > b_0$	+	
3°	$a_\infty = 0$ $b_\infty > b_0$	+	
4	$a_\infty < a_0$ $b_\infty < b_0$	+ or −	
4°	$a_\infty = 0$ $b_\infty < b_0$	+ or −	
5	$a_\infty = a_0$ $b_\infty > b_0$	+	
6	$a_\infty = a_0$ $b_\infty < b_0$	−	
7	$a_\infty < a_0$ $b_\infty = b_0$	+	
8	$a_\infty > a_0$ $b_\infty = b_0$	−	

Figure 2.8 An illustration of the first eight solution types of the diaphyseal modeling problem. The concentric circles in the left column represent the cross section before the additional load is applied and the circles in the right column represent the shape of the cross section when modeling is complete (Cowin 1981).

theoretical solution for a cylindrical section with material properties that varied along its length. The initial inhomogeneity chosen was one cycle of a sinewave (Figure 2.9). The cylinder was loaded axially and as time processed, the amplitude of the sine wave decreased rapidly at first and then more slowly. At large time the sine wave became a straight line signifying that the cylinder had become homogeneous.
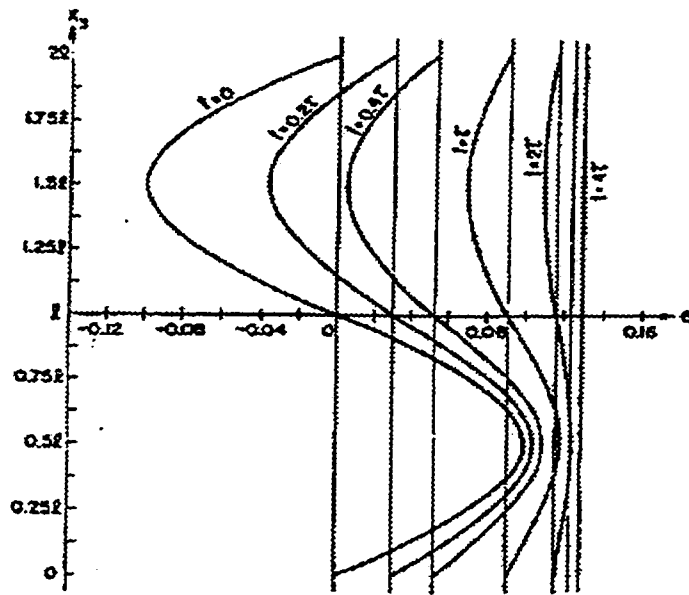
Figure 2.9 Development of initial inhomogeneity e (Cowin, 1981)

Hart et al. (1984b) used a numerical solution to mimic Cowin's solution for the same problem. The numerical solution for this internal remodeling example gave the same results as the analytical solution.

2.2.3.4 Discussion

Biological studies and remodeling experiments have suggested that if strain is the mechanical variable responsible for the adaptive response, there are

several other strain-related factors, in addition to strain magnitude, that may affect the generation of such signals. These are strain mode (tension, compression, or shear), strain direction and strain distribution. Cowin's theory adopts the strain tensor as the remodeling signal sensor to reflect these effects. On the one hand, the strain tensor, unlike the strain energy density, itself has features of both the magnitude and the direction and on the other hand, the term $C_{ij}(\xi_{ij} - \xi_{ij}^0)$, with arbitrary coefficients C_{ij} can include the effect of the strain mode and strain distribution (the effects of strain distribution can be reflected by the fact that the adaptation is localized, and different C_{ij} at each location accounts for this localization). At present, this complete strain tensor is a better candidate as a remodeling signal sensor than the strain energy density.

While values of these coefficients are necessary if the theory is to be any of use for predicting adaptive in vivo behaviour of bone these coefficients must be determined from experiments. For surface remodeling as an example, they were assumed to be different for the endosteal and periosteal surfaces, different for deposition and resorption of tissue, and different depending on whether the tissue is in tension or compression. By changing the magnitude of the remodeling coefficients, the predicted cross sectional shape of the bone may be made to approximate the experimental cross-section. The calculation which predicts a cross-sectional shape which is closest to the experimental cross-sectional shape could yield the calculated remodeling rate constant for that experiment.

It is noted that different coefficients are required for different experiments. This means the theory is incapable of describing adaptation to mechanical usage in any sort of generalized way. However, due to the high degree of complexity and uncertainty in adaptive behaviour of biomaterials, (which depends on species, age, anatomical site etc.), there is perhaps no generalized way to describe it from a practical application standpoint. For the same bone in the same animal of same age with similar activity, one could expect these coefficients to be similar. If we can determine these remodeling coefficients for one of them, the adaptation of others could be predicted with the same coefficients.

2.2.4 Miscellaneous

In addition to the theories introduced above, there are several other ways to study the adaptation of bone.

(1) Prediction of bone adaptation using damage accumulation

Predergast and Taylor (1994) recently proposed an interesting method to predict the adaptation of bone. They assumed that bone adapts to attain an optimal strength by regulating the damage generated in its microstructural elements.

In this method, two hypotheses are invoked. The first one is that there exists damage in the form of inter-constituent microcracks present within the bone even at remodeling equilibrium (RE). The stimulus for remodeling is the change in damage from this equilibrium amount $\Delta W = W - W_{re}$, where W denotes the actual damage in the microstructure, W_{re} is the damage in remodeling equilibrium. The second hypothesis is that the rate of repair of damage is determined by the homeostatic stress.

If $\dot{W}$ denotes the rate of production of damage at a particular stress, temperature, and bone density and $\dot{W}_{re}$ denotes the damage repair rate which, as a first approximation, remains equal to the rate of production of damage at remodeling equilibrium, then at remodeling equilibrium, there exists two equalities.

$$W = W_{re}(\Delta W = 0) \qquad \dot{W} = \dot{W}_{re} \qquad (2\text{-}17)$$

The remodeling equilibrium they proposed is quite similar to Cowin's external remodeling rate equation which is:

$$\frac{dX}{dt} = C \cdot \Delta W = C \cdot \int_{t_0}^{t} (\dot{W} - \dot{W}_{re})dt \qquad (2\text{-}18)$$

where X denotes the extent of bone deposition or resorption and C is a rate constant.

In this approach damage is defined by the remaining life approach. In the particular case of fatigue, failure occurring at a cyclic stress equal to $\Delta\sigma_i$ (some measurement of stress components), the damage increase is a function of n_i/N_{fi}, where N_{fi} is the number of cycles to failure at $\Delta\sigma_i$, and n_i is the number of cycles accumulated at $\Delta\sigma_i$. For a load history including various values of $\Delta\sigma_i$:

$$W = \sum_{i=1}^{m} \frac{n_i}{N_{fi}} \qquad (2\text{-}19)$$

where m is the number of loading blocks.

Because damage values range from 0 to 1, so the rate of damage can be calculated as the reciprocal of the fatigue life, for a given $\Delta\sigma_i$, as

$$\dot{W} = \frac{1}{N_{fi}} \qquad (2\text{-}20)$$

N_{fi} is associated with $\Delta\sigma_i$ by

$$\log(N_{fi}) = H\log(\Delta\sigma_i) + JT + K\rho + M \qquad (2\text{-}21)$$

where $\Delta\sigma_i$ (in MPa), T (in ^{0} C), and ρ (in gcm^{-3}) representing cyclic stress, temperature, and density respectively. H, J, K and M are constants.

This model has been applied to an external remodeling problem of a bone diaphysis under reduced torsional load. The bone is modeled as a right

circular cylinder. The calculation gave a physically reasonable prediction which corresponds to one of the solutions in Figure 2.8. The authors claim "it is not known for certain whether accumulative damage is involved in stimulating the bone adaptation process. However, it is known that damage (in the form of microcracks in the nonhomogeneous bone tissue) will be generated and that damage can accumulate, even *in vivo*. Therefore, under certain conditions, the response of bone making and resorbing cells is not sufficient to repair the damage and it accumulates. It is also known that cyclic loading generates a greater remodeling stimulus than constant loading. From these two observations alone, it is reasonable to infer that accumulative damage is a stimulus that will bring us closer to the mechanism of bone remodeling than either strain or strain energy density." This conclusion needs to be tested. On the other hand, equation (2-21) does not indicate how to calculate the N_{fi} for a complex stress field and intrinsically assumed tensile stress and compressive stress have the same effect on the damage life, and in turn on the remodeling. In addition, when there is more than one load block, $\dot{W}$ is not defined.

(2) Bone ingrowth

Sadegh, Luo and Cowin (Sadegh et al., 1993) have combined the Cowin's surface bone remodeling theory and the boundary element method to investigate the microstructural remodeling of bone at the bone-implant interface. In clinical applications of orthopaedics, many bone implants function as load bearing structures. The screws used in the application of bone plate and dental prothesis, transfer the load of the prothesis to the bone tissue. Other bone prostheses have slots or ridges into which bone may grow. It is desirable that the remodeling of the bone architecture, after the surgical placement and adjacent to the implanted prothesis, create a strong mechanical interlocking between bone and implant.

A model for the architectural changes that occurs in bone tissue around or near an implant is developed based on the assumption that bone surface strain controls the adaptive response. In their paper, three situations are considered: remodeling induced penetration between the screw threads of an implant screw, penetration of bone tissue into a slot or cavity in an implant, and the interaction of individual trabeculae in the remodeling processes near an implant. For comparison (1) in Figure 2.10 shows the result of adaptive bone
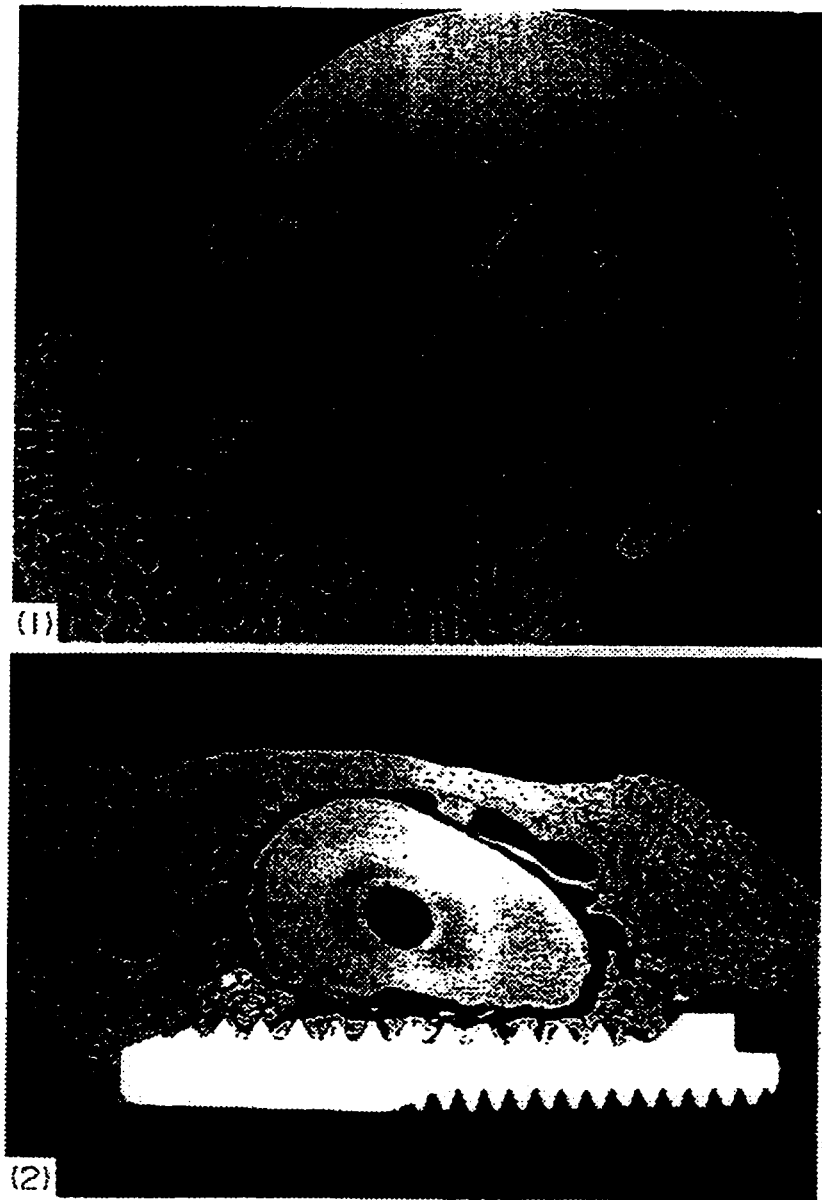
Figure 2.10 (1) Remodeled cancellous architecture under the femoral component of a hip joint. (2) Microradiograph of a cross section through an implant and an incisor in the dog mandible. Note the bony ingrowth into the implant (Sadegh el al. 1981).

remodeling in a canine hip experiment while (2) is a microradiograph of a cross section through an implant and incisor in the dog mandible.

Because the concern is the position of the surface of bone ingrowth into the screw or slot, surface remodeling theory is used, and the boundary element method (BEM) was employed to reduce the dimension of the problem. As the basic idea underlying BEM is that the governing differential equation of the domain of interest is transformed into an integral equation on the boundary of the domain, the amount of calculation could be largely reduced.

This is the first time that the surface remodeling theory of Cowin has been used for cancellous bone. Although these results are preliminary and restricted by an inadequate knowledge of the numerical values of certain physical and biological parameters as well as being for two dimensional isotropic case with a specific and a single RE strain as opposed to a range of RE strains, the result is encouraging.

(3) Remodeling theory for cancellous bone

Unlike other remodeling theories developed by Carter and Fyhre or Huiskes, which take the cortical bone as the same material as that of cancellous bone at different density, Cowin's theories for cortical bone (especially for the internal remodeling theory) are not suitable for cancellous bone. Cowin and associates (Cowin el al. 1992) developed a continuum model to describe the temporal evolution of both the density changes and the reorientation of the trabecular architecture given the applied stress state in the bone and certain material parameters of the bone.

The model they proposed is necessarily nonlinear, and associated with many experimentally determined remodeling coefficients and quantitative anisotropic elastic constant measurements of cancellous bone. A significant limitation of the proposed continuum model is the length scale below which it can not be applied (about 5 mm) because of the inhomogeneity of the porous structure. This precludes application of the model at a bone implant interface.

2.3 Numerical Results of Evaluation

Several simple problems have been employed to evaluate those mathematically based theories. This allows an evaluation and comparison of the ability of each to predict bone response as well as comparing them to specific known results.

2.3.1 Evaluation of Huiskes' theory

(1) External Remodeling (Modeling)

The problem considered was a classical cantilever beam with a concentric force at the tip as shown in Figure 2.11. The finite element method and Huiskes' modeling equation (2-7) are combined to investigate the external remodeling of the beam. The 2-D beam was divided into four quadratic isoparametic serendipity elements and the magnitude load is 4 KN. The $\Delta t \cdot C_x$ (where Δt is the time difference of each time step and C_x is the modeling coefficient at surface point x) is 0.1×10^{-7} and is the same at all surface points. The bone is assumed as an isotropic material and Young's modulus is 0.2×10^{12} Pa. Poisson's ratio is 0.3. The objective was to develop uniform maximum stress on the surfaces under the same loading environment which means that equilibrium strain is the uniform axial strain equal to the axial strain at the fixed end of the beam.

The final external shape is shown in Figure 2.11. The upper curve is the theoretical solution while the bottom curve was predicted by the numerical solution. The iteriation converged in 30 steps. It shows that two solutions are very close. The positions of each surface point is also given in Table 2.2

Table 2.2 Final position of each surface point

Point	1	4	6	9	11	14	16	19	21
Analy. (x10^{-3})	7.071	6.614	6.124	5.592	5.000	4.330	3.536	2.500	0.000
Iterat. (x10^{-3})	7.087	6.606	6.147	5.575	5.039	4.307	3.827	2.271	1.009
Error (%)	0.226	0.121	0.376	0.304	0.78	0.531	8.23	9.16	∞

Four Quadratic Isoparametric Serendipity Elements

Analytic
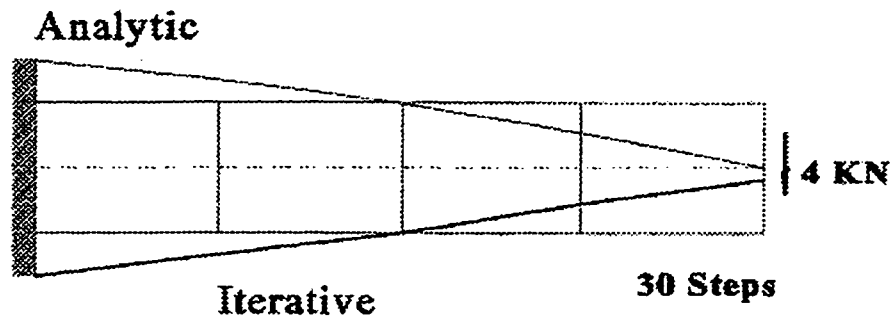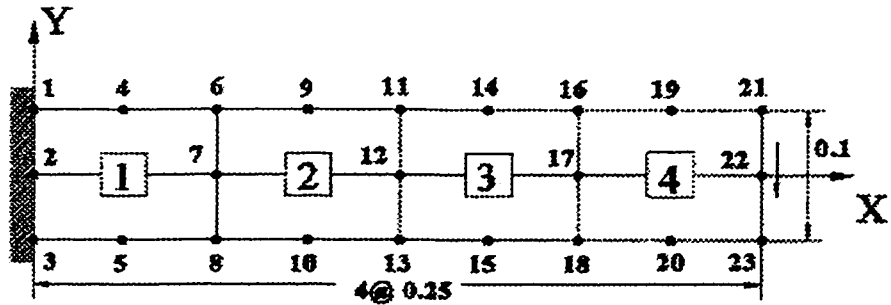
Figure 2.11 Adaptive shape optimization of a cantilever beam, loaded at the end by a transverse force, using Huiskes' external method.

Table 2.3 Final values of modulus at each Gauss point

Element	Element 1		Element 2		Element 3		Element 4	
Point	1,1	2,2	1.1	2.2	1,1	2,2	1,1	2.2
Theoretical $(x10^{12}$	0.538	0.386	0.292	0.183	0.12	0.55	0.233	0.167
Numerical $(x10^{12})$	0.502	0.374	0.289	0.184	0.12	0.536	0.246	0.162
Error (%)	6.691	3.108	1.027	0.546	0	2.545	1.3	2.99

(2) internal remodeling

The size of the beam and loading were the same as that of the external remodeling problem described in the last section. For internal remodeling, the objective is to find the changes of modulus at Gauss points. An initial arbitrarily chosen uniform strain energy density of 0.16×10^5 and initial uniform Young's modulus value of 0.2×10^{12} were assigned to all Gauss points. $\Delta t \cdot C_e$ (C_e is the remodeling coefficient at a Gauss point) is chosen as 0.16×10^6. The final values of modulus at each Gauss point are shown in Table 2.3. The time stepping took 350 steps to get this solution.

(3) remarks

For Huiskes' model, the adaptation coefficients control modeling or remodeling rate. For the numerical calculations presented, $\Delta t \cdot C_e$ and $\Delta t \cdot C_x$ were selected after a trial run, ensuring that the modulus change ΔE or position change ΔX in the first iterative step was small relative to its actual value at the location where $(U - U_n)$ had the highest value. The calculation results showed that the convergence rate is high for the external remodeling but very low for internal remodeling even for this simple problem.

2.3.2 Evaluation of Cowin's Theory

(1) internal remodeling

Considering a cylinder with inner and outer radii a and b respectively, the applied loads S_1 and S_2 were uniform on the inside and outside surfaces respectively (Figure 2.12). The evolution of initial inhomogeneous volume fraction e to the homogeneous one under different stress fields was investigated.
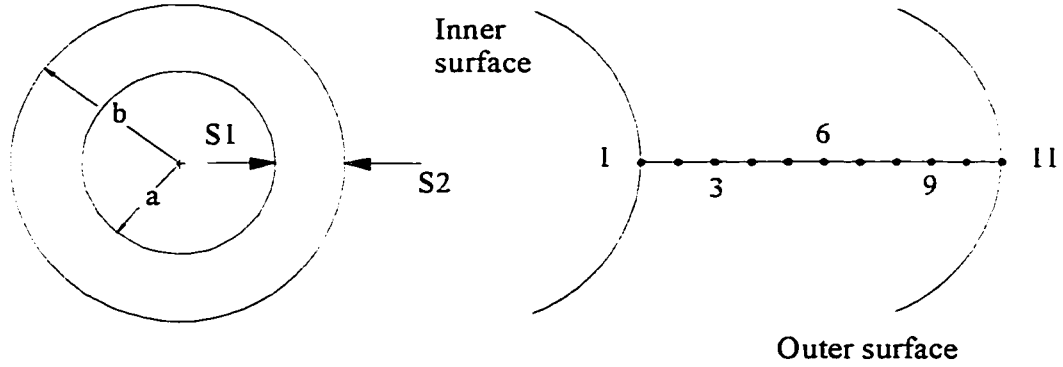
Figure 2.12 Bone model as a cylinder with uniform loading on inside and outside surface. The right side is an illustration of knots used by finite difference method.

◆ Governing equations

$$\frac{de(r,t)}{dt} = C_0 + C_1 e(r,t) + C_2 tr(\underline{\xi}) \tag{2-22}$$

$$r^2[\kappa_0\zeta_0 + \kappa_0 e(r,t) + \frac{3}{4}G]\frac{\partial^2 u_r}{\partial r^2} + [\kappa_0\zeta_0 + \kappa_0 e(r,t) + \frac{3}{4}G +$$

$$\kappa_0 r\frac{\partial e(r,t)}{\partial r}]\frac{\partial u_r}{\partial r} - [\kappa_0\zeta_0 + \kappa_0 e(r,t) + \frac{3}{4}G - \kappa_0 r\frac{\partial e(r,t)}{\partial r}]u_r = 0 \tag{2-23}$$

where κ_0 is the modulus of compression, G is the shear modulus, ζ_0 is the reference volume fraction, $e(r,t)$ is the change in volume fraction of the point r at time t, u_r is the displacement at the point r, $\underline{\xi}$ is the strain tensor.

◆ Method

Because the governing equations were first order differential equation and second order partial differential equation, the finite difference method and forward Euler method were used to solve them.

$$(\frac{\partial u}{\partial r})_i = \frac{u_{i+1} - u_{i-1}}{2h}$$

(2-24)

$$(\frac{\partial^2 u}{\partial r^2})_i = \frac{u_{i+1} + u_{i-1} - 2u_i}{h^2}$$

$$e(r_i, t_{j+1}) = e(r_i, t_j) + \Delta t(C_0 + C_1 e(r_i, t_j) + C_2(\frac{\partial u_i}{\partial r} + \frac{u_r}{r}) \qquad (2\text{-}25)$$

Where i means the *ith* node on the radius, and j means jth time step. By assuming initial $e(r,0)$, the combination of equations (2-22), (2-23), (2-24), (2-25) can be used to solve this initial value problem. The constants used in the examples are as follows: $\kappa_0 = 0.744 \times 10^4$ GPa, $G = 0.36 \times 10^4$ GPa, $\zeta_0 = 0.8$. The bone inner radius a is 1.0mm and outer radius is 2.0mm. The stress boundary condition is that $\sigma_r|_{r=a} = S_1/2\pi a$, and $\sigma_r|_{r=b} = S_2/2\pi b$.

◆ Results

Three different initial inhomogeneous volume fraction distributions along the radius are assumed $e(r, 0)$: a linear increase with radius, a parabolic shape and a linear decrease with radius. As time step progressed, the initial inhomogeneous $e(r,0)$ finally became homogeneous ($e(r, t)$ are all the same along the radius) even under a inhomogeneous stress field (S_1 was not equal S_2) as shown in Figure 2.13-2.15. The convergence rate in all cases was rapid as only 15-20 iterative steps were enough to make the solution converge. This result has never been reported before. The relationship between the final volume fraction and remodeling coefficients C_0, C_1, C_2 are also investigated. When two of coefficients are fixed, the final $e(r, t)$ vs. another coefficient are shown in Figure 2.16-2.18 The results showed that the convergence rate was not sensitive to the remodeling coefficients.

Initial Forwardslash Shape e
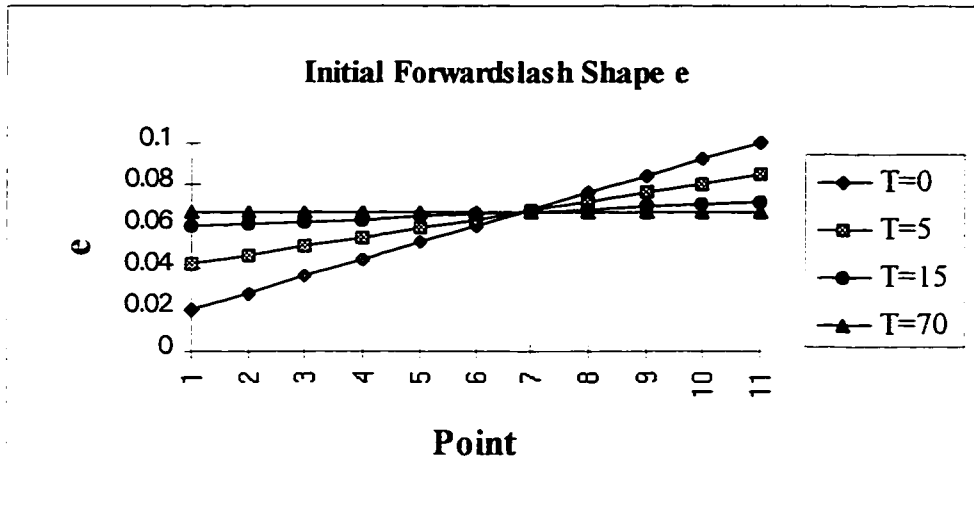
Figure 2.13 Evaluation of an initial inhomogeneous volume fraction of e
(linear increasing along the radius) to a homogeneous one

Initial Parabolic Shape e
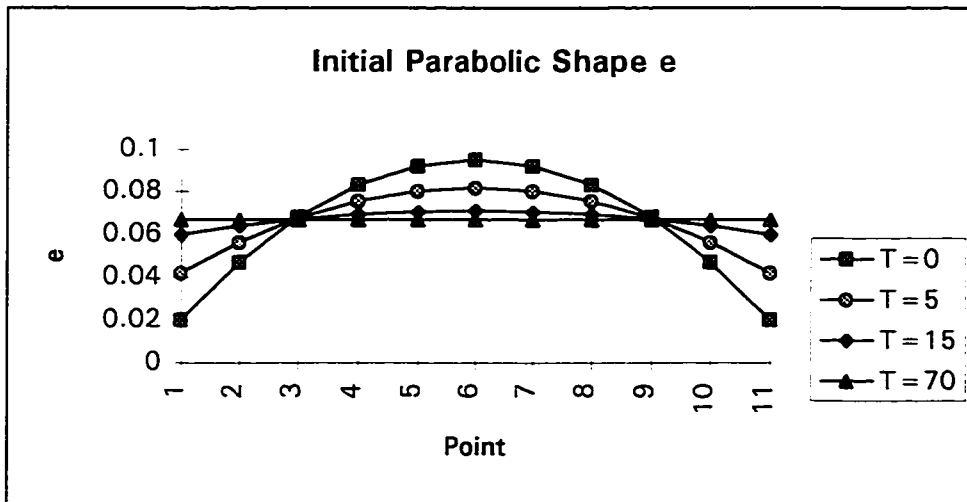
Figure 2.14 Evaluation of an initial inhomogeneous volume fraction of e
(parabolic along the radius) to a homogeneous one

Initial Backslash Shape e
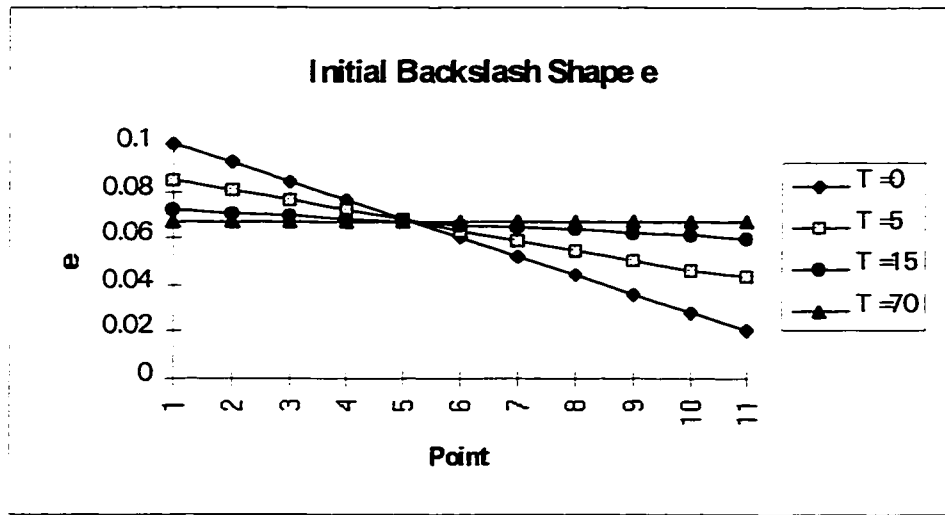
Figure 2.15 Evaluation of an initial inhomogeneous volume fraction of e (linear decreasing along the radius) to a homogeneous one

e Via C2
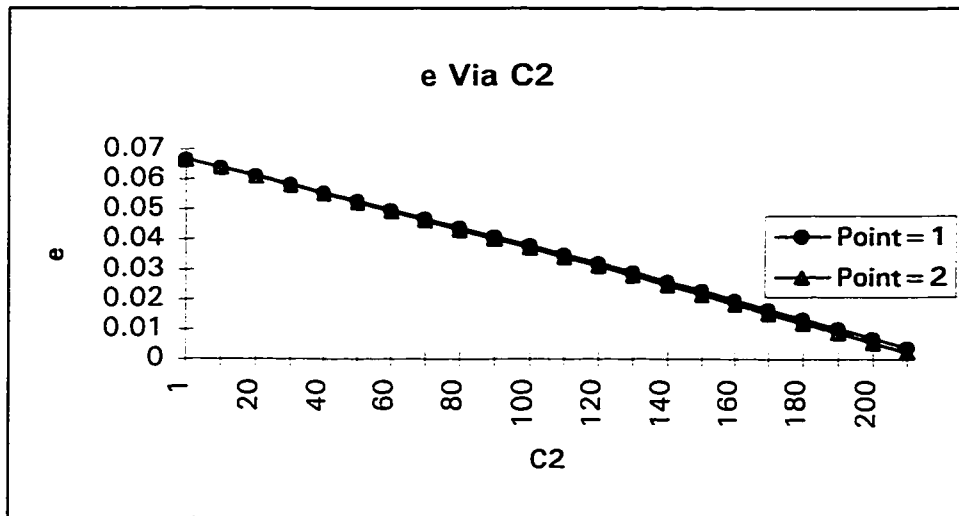
Figure 2.16 The relationship between the final volume fraction andremodeling coefficient C_2
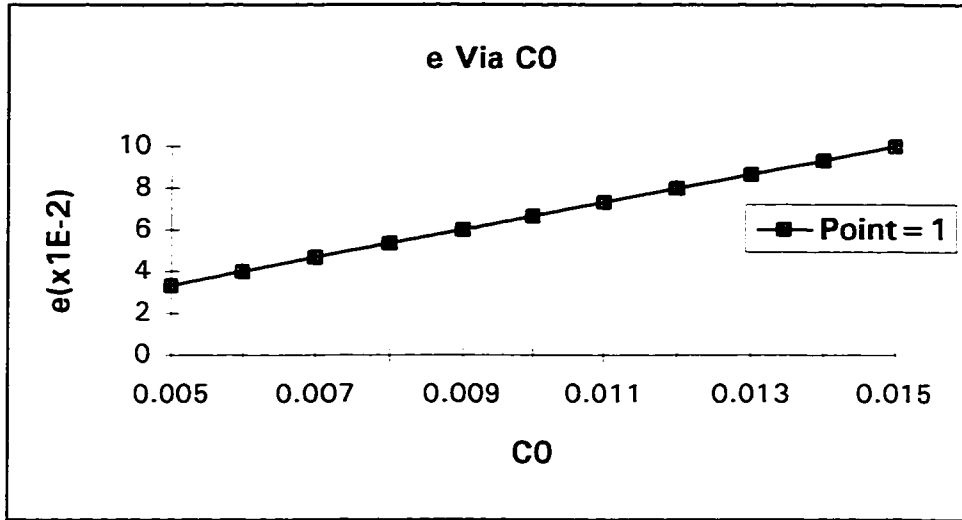
Figure 2.17 The relationship between the final volume fraction and remodeling coefficient C_0
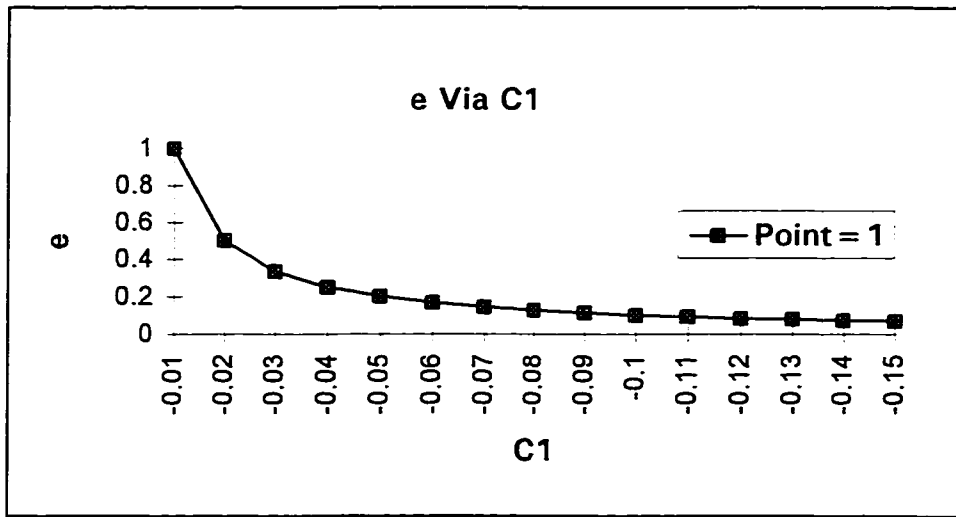
Figure 2.18 The relationship between the final volume fraction remodeling coefficient C_1

(2) external remodeling (modeling)

Cowin's external remodeling theory is used to investigate the bending problem as in shown in Figure 2.19.
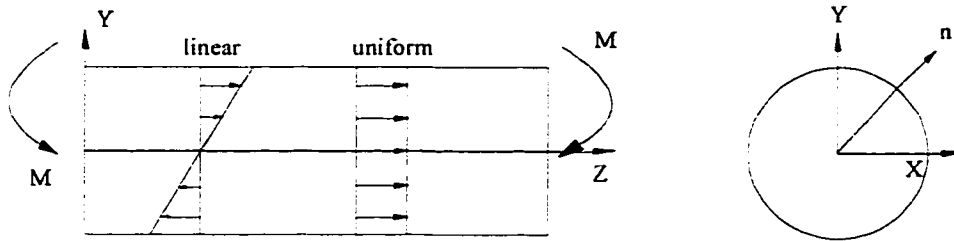
Figure 2. 19   Bone modeled as a cylinder with a circle cross section. The initial equilibrium stress is uniform, the actual loading is a bending moment.

The bone is assumed as an isotropic material and its surface was divided into 72 sections. Each point at the connection of two sections serves as a node to calculate geometric properties of the bone cross-section (Hrudey private notes) and were also used to generate Lagrange interpolating polynomials (Charpra 1988) which was employed to calculate the normal direction of each surface point by fitting the curve through five adjacent points. The uniform equilibrium strain is in tension or compression, and the actual loading is a bending movement. No matter what value for the coefficient was chosen, no equilibrium state could be reached on the compressive /tensile side.

2.3.3 Evaluation of Carter and Fyhre's Theory

The internal remodeling theory modified from Carter and Fyhre's theory by Huiskes et al. (Weinans 1992) (Equation 2-6, 2-7) was used to investigate the problem similar to Figure 2.12.

◆ governing equations

$$\rho\frac{\partial^2 u_r}{\partial r^2} + (2\frac{\partial\rho}{\partial r} + \frac{\rho}{r})\frac{\partial u_r}{\partial r} + (\frac{2}{r} \times \frac{\mu}{1-\mu} \times \frac{\partial\rho}{\partial r} - \frac{\rho}{r^2})u_r = 0 \qquad (2\text{-}26)$$

$$\frac{\partial\rho}{\partial t} = \frac{3790B \times \rho}{2(1+\mu)(1-\mu)}[(\frac{\partial u_r}{\partial r})^2 + (\frac{u_r}{r})^2 + \frac{2\mu}{1-\mu} \times \frac{u_r}{r} \times \frac{\partial u_r}{\partial r}] \qquad (2\text{-}27)$$

where ρ is the apparent density of bone, u_r is the displacement at the point on the radius. B is the remodeling coefficient.

◆ Method

The finite difference method and second order Runge-Kutta method (Charpra 1988) were used to solve the coupled differential equations (2-24) and (2-25) in the same manner as the method employed to solve Cowin's internal remodeling problem (Section 2.4.2). The radius was divided into ten sections.

◆ Results

No matter what value of remodeling coefficient B was chosen and how small the time step was, all solutions diverged. When a bound was put on the apparent density ρ, i.e., $\rho_{cb} \leq \rho \leq 0.01 \text{gcm}^{-3}$ where ρ_{cb} is the cortical bone density, value at each point along the radius converged to the boundary value-- either to that of cortical bone or to the minimum density 0.01gcm^{-3} (complete resorption). There was no smooth transition between the two values, which seems impossible. According to the theoretical study (Weinans el al. 1992), stability criterion for this kind of problem is $v < 1.0$ where v is the value of the exponent from the relationship $E=C\rho^v$. In the current model, $v = 2$, and as a result, no stable solution exists.

2.4 Summary

Several modeling and remodeling theories from both a biological and mechanical point of view have been discussed. The limitations and shortcomings of these theories are briefly summarized as follows.

The biological approaches to adaptive behaviour of bone are essentially the FNT and Mechanostat theories proposed by Frost. The FNT theory suggests that increased surface concavity causes bone resorption whereas decreased surface convexity initiates bone deposition. It does not however, explain the behaviour of bone in other loading situations. The Mechanostat theory tries to set up a more general rule for all bones and uses an absolute value of strain rather than a value relative to some equilibrium state. Overall these two theories attempt to link bone-cell activity and the biomechanical loading conditions to explain experimental results. However, because of the specific nature of these approaches, they can explain only some experimental findings but not others.

As for mathematical theories, Carter and Fhyre's theory tries to predict the bone apparent density at remodeling equilibrium rather than to predict the modeling and remodeling process due to the disturbance of loading environment. It uses strain energy density as the mechanical signal sensor. As discussed previously, this is not a good candidate. The computational algorithm based on Carter and Fyhre's theory has a well known chaos mechanism and the numerical solution obtained by this algorithm is unstable.

The goal of Huiskes' theory is to investigate the "stress shielding" phenomenon in total hip replacement. This theory is in fact modified from Cowin's theory but adopts a different mechanical signal sensor, i.e. strain energy density rather than strain tensor.

Cowin's theory may be the most rigorous one among all remodeling theories. It uses the strain tensor as the mechanical signal sensor which can reflect to some degree the effects of strain mode, strain direction, and strain distribution on the adaptive behaviour of bone. From the published literature and the current study presented here, all solutions obtained by the computational algorithm based on Cowin's theory were convergent.

Chapter 3

Development of New Modeling Model

As stated above the strain and the strain energy density have been considered by most researchers as the mechanical signal sensor which triggers the modeling/remodeling process. There are however several other strain-related factors that may also affect the generation of such signals. These include the strain mode (tension, compression, or shear), the strain direction, and the strain distribution etc.

Obviously the strain energy density contains less information than the strain tensor because it has no characteristic of direction. The fact that it is always positive basically assumes that the tensile and compressive strains play like roles on the bone remodeling/modeling. This, as discussed in the last chapter, is contradictory to the conclusion that the direction of strain is an important factor affecting bone remodeling. In fact, little experimental evidence has been found to relate the adaptive changes of bone to the strain energy density.

Among all existing remodeling/modeling theories, only Cowin's theory adopts the strain tensor as the remodeling/modeling signal sensor. The strain tensor can reflect more or less the effects of several strain-related factors. On the one hand, the strain tensor, unlike the strain energy density, itself has features of both the magnitude and the direction. On the other hand, equation (2-8) with arbitrary coefficients C_{ij}, intrinsically includes the effect of the strain distribution (the effects of strain distribution can be reflected by the fact that the adaptation is localized, and different C_{ij} at each location accounts for the localization).

A review by Cowin and his colleagues (Cowin et al. 1991) of the existing experimental data on bone and bone cell response to mechanical

64

loading suggests that either strain or an electrical charge system is the source of bone cell excitation and, therefore, bone modeling and remodeling. Cowin pointed out that since the principal electrical charge mechanism considered is also strain-driven, strain emerges as the principle mechanical candidate for a biological sensor system.

A rationale behind the argument that the strain tensor is a better than strain energy is also provided by Cowin (Cowin et al. 1993). They argued that bone cells have recently been shown to have stretch and voltage receptors (Cowin et al. 1991) while there is no indication that bone cell have strain energy receptors. A consideration of underlying physics or biophysics suggests that the existence of strain energy receptor is unlikely.

Given all the facts mentioned above, it is believed at present that the complete strain tensor is a better candidate as a remodeling/modeling signal sensor than the strain energy density.

All mathematically based remodeling/modeling theories assume that bone material obeys the Hooke's law in the normal small strain range of loading. It means that the bone material is modeled as a continuum although the bone material itself is not a real continuous material. As a result, a length scale over which material properties of bone are averaged should be established.

In a recently published paper, Cowin (1993) gave more credibility to the surface remodeling (modeling) theory. He claims that since all bone remodeling occurs by deposition or resorption from surfaces, surface remodeling rate equations have the potential advantage of mimicking the actual behaviour of bone. Another important advantage of surface remodeling rate equations is that homogeneous elasticity theory can be employed and thus one is more assured of existence of the solutions. This conclusion is based on the fact that surface rate equations require a length scale which is 100 times less than the length scale required by the internal remodeling rate equation. The length scale is determined by the homogenization volume (the volume in which inhomogeneous stress and strain field are averaged). Taking cancellous bones for example, the remodeling theory is supposed to be applied to a single trabecular and the length scale has to be at least several trabeculae widths (5mm) while the modeling theory is applied to trabeculum (the trabecular bone

as the whole) and the length scale is determined by the hole within it ($50\mu m$) which is much smaller.

For internal remodeling, if the loading is inhomogeneous, the internal remodeling will make the associated adaptive elasticity nonlinear in time and space. It has been the practice in computational bone stress adaptation studies to employ the standard finite element techniques based on linear elasticity. When these methods are applied to nonlinear adaptive elasticity problems for materially inhomogeneous objects, there is no assurance that there is a solution.

Even though the current study only focuses on the modeling model and chooses the strain tensor as a mechanical signal sensor, the use of Cowin's theory alone brings with it other problems.

Cowin's external modeling theory is flawed in a different way to Huiskes'. It fails to correctly predict the adaptation under two loading cases shown in Figure 2.6. In contrast to Huiskes' theory which predicts that no remodeling would happen, Cowin's theory predicts that either the bone completely resorbs, or deposits indefinitely, thus modeling equilibrium would never be regained. In fact, Cowin's theory assumes that tension and compression (the strain mode) have opposite effects on the bone adaptation. If the compression is osteogenic, then the tension is bone destructive, and vice versa.

As was discussed in the previous chapter, tension and compression play different roles in bone adaptation. They could be both osteogenic but the degree of their effects on bone adaptation may be different. Also, it appears that each bone and each part of each bone has its own loading environment, appropriate functional strain level and strain distribution. For example, the ovine radius (Lanyon et al. 1979b, 1982) and the porcine radius (Goodship, et al., 1979) are loaded in combined bending and compression, with the convex surface in tension; the ovine tibia (Lanyon et al., 1979a) is subjected to combined bending and torsion with the concave surface as the tension side, while the ovine calcaneus (Lanyon, et al., 1973) is in bending with some direct shear. In view of the diversity of strain fields observed on the various bones, it is reasonable to ask whether all the strain components of bone in normal *in vivo* loading (compression, bending with its implied tension and compression, and torsional

and direct shear) promote functional adaptation, or whether a bone could be sensitive to one strain component and less sensitive to another.

In order to help resolve the difficulty when Cowin's external remodeling theory is applied to the two loading cases in Figure 2.6, and to reflect the different strain components on the modeling/remodeling, a new modeling model is developed.

3.1 New Modeling Model

Basically the new model adopts all the assumptions that Cowin's external remodeling theory made, i.e. at the external surface of the solid bone material there are chemical reactions which convert the body fluids to solid bone material and vice versa. As a result of the chemical reactions mass is transferred from the body fluid to the bone. In particular, bone is considered as an open system with regard to mass transport.

From the biological point of view, the chemical reaction involves activation of osteoblast which is associated with the formation of primary lamellar bone (A-F process), or activation of osteoclast which is associated with the resorption of lamellar bone from the surface (A-R process). The formation and resorption of lamellar bone on the bone surface is independent to each other. The whole modeling process is as follows: a local change in the strain field is sensed by the bone (the motion of bone fluid is driven by strain), and transferred by osteocytes and osetocyte network (cell processes surrounded by a bone fluid space) to activate the osteoblast or osteoclast.

Another two basic assumptions are: (1) only modeling time scales which are much larger than loading time scale) is considered; (2) the new increment of bone tissue that is added to the whole bone (or subtracted from the whole bone) has the exactly the same strain energy as the bone tissue at the site where it is to be added or subtracted. The first assumption means that the inertia effects are neglected while the second one assumes that the new bone material and old bone material share the same referential unstrained state.

Let Q denotes a surface point on the linear elastic body representing the one tissue (Figure 2.7) and $\underline{n}$ denotes an outward unit normal vector of the tangent plane to the surface of the body at Q.

The modeling model is presented as the modeling rate equation:

$$U = C_{ij}(Q)[K_{ijkm}(\underline{\xi},\underline{\xi}^0,Q)\xi_{km}(Q) - \xi_{ij}^0(Q)] \qquad (3\text{-}1)$$

where U is the speed of movement of the modeling surface normal to the surface, i.e. $\underline{n}$ direction; $\xi_{km}(Q)$ is the Cartesian components of the strain tensor at Q; $\xi_{ij}^0(Q)$ is the equilibrium value of the strain where no modeling happens.

$C_{ij}(Q)$ are surface modeling rate coefficients which control the speed of the modeling process. Generally speaking , they are dependent on the point Q.

$K_{ijkm}(\underline{\xi},\ \underline{\xi}^0,\ Q)$ are the weighting factors which reflect the effects of different strain components, and are dependent on the actual and equilibrium strain states. The physical meaning of each component of $K_{ijkm}(\underline{\xi},\ \underline{\xi}^0,\ Q)$ is that if one unit of equilibrium strain component $\xi_{ij}^0(Q)$ maintain the modeling equilibrium, $1/\ K_{ijkm}(\underline{\xi},\ \underline{\xi}^0,\ Q)$ units of actual strain component $\xi_{km}(Q)$ are needed to regain the modeling equilibrium.

The surface modeling rate coefficients, weighting factors and equilibrium strain components are phenomenological coefficients of the bone surface point and must be determined by experiment. One would hope that surface modeling rate coefficients and weighting factors are essentially independent of the specific point, and in reality this could be the case.

By introducing alternative notations, equation (3-1) can be written in another form:

$$U = C_i(Q)[K_{ij}(\underline{\xi},\underline{\xi}^0,Q)\xi_j - \xi_i^0] \qquad (3\text{-}2)$$

where [1]

$$
\left\{
\begin{array}{l}
\xi_1 = \xi_{11} \\
\xi_2 = \xi_{22} \\
\xi_3 = \xi_{33} \\
\xi_4 = 2\xi_{23} = 2\xi_{32} \\
\xi_5 = 2\xi_{13} = 2\xi_{31} \\
\xi_6 = 2\xi_{12} = 2\xi_{21}
\end{array}
\right.
\qquad (3\text{-}3)
$$

and assume $C_{23} = C_{32}$, $C_{13} = C_{31}$, and $C_{12} = C_{21}$, which can be justified by the fact that corresponding pair shear strains contribute the same to the modeling;

$$
\left\{
\begin{array}{l}
C_1 = C_{11} \\
C_2 = C_{22} \\
C_3 = C_{33} \\
C_4 = C_{23} = C_{32} \\
C_5 = C_{13} = C_{31} \\
C_6 = C_{12} = C_{21}
\end{array}
\right.
\qquad (3\text{-}4)
$$

and

$$K_{ij} = K_{iijj} \qquad \text{(no sum, and } i, j = 1, 2, 3);$$

$$K_{i4} = (K_{ii23} + K_{ii32})/ 2 \qquad \text{(no sum, and } i = 1, 2, 3);$$

$$K_{i5} = (K_{ii13} + K_{ii31})/ 2 \qquad \text{(no sum, and } i = 1, 2, 3);$$

$$K_{i6} = (K_{ii12} + K_{ii21})/ 2 \qquad \text{(no sum, and } i = 1, 2, 3);$$

---

[1] The notations $C_i (Q)$ and $K_{ij} (\xi . \xi^0 . Q)$ can be exchangeable with the notations C_i and K_{ij} in the text.

$$K_{4i} = (K_{23ii} + K_{32ii}) \qquad (\text{no sum, and } i = 1, 2, 3);$$

$$K_{5i} = (K_{13ii} + K_{31ii}) \qquad (\text{no sum, and } i = 1, 2, 3);$$

$$K_{6i} = (K_{12ii} + K_{21ii}) \qquad (\text{no sum, and } i = 1, 2, 3);$$

$$K_{44} = (K_{2323} + K_{2332} + K_{3223} + K_{3232})/2;$$

$$K_{45} = (K_{2313} + K_{2331} + K_{3213} + K_{3231})/2;$$

$$K_{46} = (K_{2312} + K_{2321} + K_{3212} + K_{3221})/2;$$

$$K_{54} = (K_{1323} + K_{1332} + K_{3123} + K_{3132})/2;$$

$$K_{55} = (K_{1313} + K_{1331} + K_{3113} + K_{3131})/2;$$

$$K_{56} = (K_{1312} + K_{1321} + K_{3112} + K_{3121})/2;$$

$$K_{64} = (K_{1223} + K_{1232} + K_{2123} + K_{2132})/2;$$

$$K_{65} = (K_{1213} + K_{1231} + K_{2113} + K_{2131})/2;$$

$$K_{66} = (K_{1212} + K_{1221} + K_{2112} + K_{2121})/2;$$

3.2 Simplified form of new model

Introducing another new notation:

$$\xi_i' = K_{ij}\xi_j \qquad (3\text{-}5)$$

where ξ_i' is a bulk strain component which reflects the comprehensive effect of different strain components on the modeling equilibrium in the direction i.

Generally speaking, K_{ij} is a 6x6 matrix:

$$[K_{ij}] = \begin{bmatrix} K_{11} & K_{12} & K_{13} & K_{14} & K_{15} & K_{16} \\ K_{21} & K_{22} & K_{23} & K_{24} & K_{25} & K_{26} \\ K_{31} & K_{32} & K_{33} & K_{34} & K_{35} & K_{36} \\ K_{41} & K_{42} & K_{43} & K_{44} & K_{45} & K_{46} \\ K_{51} & K_{52} & K_{53} & K_{54} & K_{55} & K_{56} \\ K_{61} & K_{62} & K_{63} & K_{64} & K_{65} & K_{66} \end{bmatrix}$$

(3-6)

At present, there is no experimental data available for K_{ij}. For tsimplicity and practicality, it could be assumed that only actual strain components ξ_i make the contribution to the ξ_i, which means that $[K_{ij}]$ is a diagonal matrix.

$$[K_{ij}] = \begin{bmatrix} K_{11} & & & & & \\ & K_{22} & & & & \\ & & K_{33} & & & \\ & & & K_{44} & & \\ & & & & K_{55} & \\ & & & & & K_{66} \end{bmatrix}$$

(3-7)

This assumption will be justified in section 3.3.4. As a result, equation (3-2) becomes:

$$U = C_i[\xi_i' - \xi_i^0]$$

(3-8)

where

$$\xi_i^{'} = K_{ii}\xi_i \qquad \text{(no sum)} \qquad (3\text{-}9)$$

For the axial loading or bending cases in which only ξ_3 is taken as the variable, (3-2) can be simplified as:

$$U = C_i^{'}(K_{33}^{'}\xi_3 - \xi_3^0) \qquad (3\text{-}10)$$

where $K_{33}^{'}$ reflects the fact that the effects of strains in other two directions are included.

(A) Remember that K_{33} is a function of ξ_3 and ξ_3^0:

(B) If ξ_3 and ξ_3^0 are both compressive or both tensile, $K_{33}^{'} = 1$;

(C) If ξ_3 is tensile, and ξ_3^0 is compressive, then $K_{33}^{'} < 0$, and the interpretation of $K_{33}^{'}$ is as following:

(1) $K_{33}^{'} < -1$, the adaptation of bone is more sensitive to the tension than the compression;

(2) $K_{33}^{'} = -1$; the tension has the same effect on the modeling as the compression does;

(3) $-1 < K_{33}^{'} < 0$, the degree of the effect of tension on the modeling is less than that of compression;

(D) The interpretation is similar for the situation that ξ_3 is compressive and ξ_3^0 is tensile.

For a loading case where only torsional load is applied on a bone diaphysis, only $\tau_{z\theta}$ is taken as the variable, and (3-2) can be simplified as:

$$U = C_4(K_{44}\xi_4 - \xi_4^0)$$

(3-11)

If ξ_4 and ξ_4^0 have the same sign, then $K_{44} = 1$;

If the sign of ξ_4 is different from that of ξ_4^0, $K_{44} = -1$.

There is no reason to assume that shear strains in an opposite direction have the different effects on bone modeling. But if ξ_4 is direct shear and ξ_4^0 is generated by a torsional load or vice versa, it can be assumed that $|K_{44}|$ is not necessary to be equal to 1. Up to now, no report on the effects of direct shear on bone modeling has been found, and it is not known if direct shear and torsional shear have the same effect on the adaptive behaviour of bone.

3.3 Restriction on the modeling coefficients and weighting factors

Generally speaking, $|K_{ij}|$ is a 6x6 full matrix. But by making certain assumptions, the modeling surface rate equation (3-1) can be simplified just like cases shown in last section. U in equation (3-1) is a scalar and the equation must be independent of coordinate systems. As a result, the tensors such as modeling coefficients C_{ij} and weighting factors K_{ijkl} are subjected to some restrictions. The restrictions on those tensors come from the symmetry of the tensor as the bone is often modeled as a material which has certain material symmetry. The choice of material symmetry for an elastic model of bone depends to a large extent on the intended application although cortical bone is generally considered as an orthotropic material as discussed in section 1.2.1.

3.3.1 Bone modeled as an isotropic material

Let the coordinates x, y, z be transformed to x', y', z' according to the orthogonal scheme:

	x	y	z
x'	l_1	m_1	n_1
y'	l_2	m_2	n_2
z'	l_3	m_3	n_3

where l_i, m_i, n_i are the direction cosines associated with the transformation.

As bone is modeled as an isotropic material, any transformation of strain components should not change the value of U on the left side of equation (3-2). The transformation of strain components can be done by arbitrarily choosing l_i, m_i, and n_i : (1) reflexion in a plane, (2) rotation about an axis, (3) rotation about an axis combined with reflection in a plane at right angles to the axis. In the case of isotropic material, every plane is a plane of symmetry and every axis is an axis of symmetry.

Assume that the plane (x, y) is the plane of symmetry, and the axis of symmetry is z.

The reflexion in the plane (x, y) is represented by the equations:

$$x' = x, \quad y' = y, \quad z' = -z$$

The rotation about z through an angle θ is represented by equations:

$$x' = x \cos \theta + y \sin \theta, \quad y' = - x \sin \theta + y \sin \theta, \quad z' = z$$

When only term $C_i \xi_1^0$ is considered, it can be concluded by the above transformations without changing U:

$$C_1 = C_2 = C_3 = C$$

$$C_4 = C_5 = C_6 = 0$$

(3-12)

When the term $C_i K_{ij} \xi_j$ is considered, the following relationships must hold:

$$
\begin{cases}
K_{14} + K_{24} + K_{34} = 0 \\[2ex]
K_{15} + K_{25} + K_{35} = 0 \\[2ex]
K_{16} + K_{26} + K_{36} = 0 \\[2ex]
K_{11} + K_{21} + K_{31} = K_{12} + K_{22} + K_{32} \\[2ex]
K_{11} + K_{21} + K_{31} = K_{13} + K_{23} + K_{33}
\end{cases}
$$

(3-13)

3.3.2 Bone modeled as a transversely isotropic material

For the transversely isotropic material if the plane of isotropy is assumed to be the x , y plane, the operation of rotation about z and reflexion in the plane (x,y), (x,z), and (y,z) must keep U unaltered.

When only term $C_i \xi_i^0$ is considered, the following relationship must hold:

$$C_1 = C_2 = C$$

$$C_4 = C_5 = C_6 = 0$$

(3-14)

When the term $C_i K_{ij} \xi_j$ is examined, the following relationships must hold:

$$
\begin{cases}
CK_{14} + CK_{24} + C_3 K_{34} = 0 \\
\\
CK_{15} + CK_{25} + C_3 K_{35} = 0 \\
\\
CK_{11} + CK_{21} + C_3 K_{31} = CK_{12} + CK_{22} + C_3 K_{32}
\end{cases}
$$

(3-15)

3.3.2 Bone modeled as an orthotropic material

For an orthotropic material, the coordinate system is chosen to be coincident with the symmetry coordinate system of material. The operation reflexion in the plane (x,y), (x,z), and (y,z) must keep U unaltered.

When only term $C_i \xi_i^0$ is considered, the following relationship must hold:

$$C_4 = C_5 = C_6 = 0 \qquad\qquad \text{(3-16)}$$

When term $C_i K_{ij} \xi_j$ is examined, the following relationships must hold:

$$\begin{cases} C_1 K_{14} + C_2 K_{24} + C_3 K_{34} = 0 \\[2mm] C_1 K_{15} + C_2 K_{25} + C_3 K_{35} = 0 \\[2mm] C_1 K_{16} + C_2 K_{26} + C_3 K_{36} = 0 \end{cases} \qquad \text{(3-17)}$$

3.3.4 Remarks

The equations (3-13), (3-15) and (3-17) reveal that the independent variables of K_{ij} are 31, 33 and 33 respectively corresponding to the isotropic, transversely isotropic or orthotropic bone material assumptions. That means that subject to the constraints (3-13), (3-15), or (3-17) the components of K_{ij} can be selected to produce specific effects. In particular K_{ij} matrix can be assumed to be a diagonal matrix (3-7) in which only K_{ii} (no sum and i = 1,2,3,4,5,6) exist. It is obvious that (3-13), (3-15) or (3-17) won't be violated by this assumption and it is justified in this sense. It implies that for an isotropic material $K_{11} = K_{22} = K_{33}$, for a transversely isotropic material $K_{11} = K_{22}$.

Equation (3-2) is a general modeling rate equation. However, equations (3-10) and (3-11) are more often used in practice. In addition, certain research results about the effects of shear stresses on modeling can be used to reduce the number of modeling coefficients for some problems.

For example, Moreland (1980) conducted an experimental study on the effect of torsion on the immature rabbit. Radiographic and histological analyses failed to show any evidence of cortical modeling. Cowin (1987) conducted a theoretical study on this problem. He found that the predictions of the theory of surface remodeling are different for small and large torsion. It was shown that

the surface velocity can only depend upon the square of shear strains. For small torsional loads, no modeling will be induced. For large torsional loads, modeling will be induced but it is likely to occur at a slower rate than that for axial loads.

Although there is no quantitative data on the degree to which long bones are subjected to torsion, it is suggested that these bones do not carry much torsional load (Moreland 1980, Cowin, 1987). As a result, if the shear stress is induced by a torsional load the effect of shear strain will be neglected, and the new modeling rate equation will become:

$$U = C_i (K_{ii} \xi_i - \xi_i^0) \qquad \text{(no sum for } K_{ii}, \ i = 1,2,3) \qquad \textbf{(3-18)}$$

However Carter et al. (1980) found that significant longitudinal and shear stress were present in the midshaft of the radius and ulna, and Lanyon et al. (1979a) also found ovine tibia was subjected to combined bending and torsion. As a result it is not clear if bones carry much torsion or not. In addition, no report of the effects of direct shear on bone modeling has been found.

If bone is assumed to have some degree of material symmetry, (3-18) can be definitely simplified no matter what kind of load caused the shear strain. Of course the simplified form is based on the assumption that the K_{ij} matrix is a diagonal one.

If bone is assumed as an isotropic material, (3-18) can be further simplified as:

$$U = C \ [K(\xi_1 + \xi_2 + \xi_3) - (\xi_1^0 + \xi_2^0 + \xi_3^0)] \qquad \textbf{(3-19)}$$

If bone is taken as an transversely isotropic material, (3-18) will becomes:

$$U = C_1[K_{11}(\xi_1 + \xi_2) - (\xi_1^0 + \xi_2^0)] + C_3(K_{33}\xi_3^0 - \xi_3^0) \tag{3-20}$$

Similarly, the modeling rate equation for orthotropic bone material is:

$$U = C_i(K_{ii}\xi_i - \xi_i^0) \qquad \text{(no sum for } K_{ii} \text{ and } i = 1, 2, 3) \tag{3-21}$$

3.4 The advantage of the new model

The new model has several advantages as follows:

The new model can explain the adaptive behaviour of bone in the two loading cases in Figure 2.6 while Cowin's theory can not explain them. For example, for the loading case (1) in Figure 2.6, Cowin's theory predicts either the bone resorbs completely ($C_{11} < 0$) or deposits infinitely ($C_{11} > 0$), which is obviously unrealistic. Using the new model and if tension and compression make no difference in their effects on the bone adaptation, it will predict that no modeling will occur ($K_{11}=-1$).

A more plausible situation is that tensile and compressive strains affect bone adaptation to different degrees. Under this condition, by choosing K_{11} as a negative number whose absolute value is not 1 ($|K_{11}| < 1.0$ or > 1.0 depending on the different roles of tensile and compressive strain on the bone adaptation), the new theory will predict a finite modeling shape corresponding to modeling coefficient C_1 and weighting factor K_{11}.

The comprehensive comparison between the new model and Cowin's new theory is shown in Table 3.1. For the cases 5, 7, 9, and 11 which is highlighted in the table, the new model is successful in predicting the bone modeling while Cowin's theory fails to do so.

Table 3.1 Comparison between the new model and Cowin's modeling theory for one dimensional cases

Case	C_I	K_{I1}		$C_I(K_{I1}E_I - E_I^0)$	Cowin's Theory	New Model
1	> 0	= 1	$E_I > 0. E_I^0 > 0.$ $E_I > E_I^0$	> 0	Bone size increases	same
2	> 0	= 1	$E_I > 0. E_I^0 > 0.$ $E_I < E_I^0$	< 0	Bone size decreases	same
3	< 0	= 1	$E_I < 0. E_I^0 < 0.$ $|E_I| > |E_I^0|$	> 0	Bone size increases	same
4	< 0	= 1	$E_I < 0. E_I^0 < 0.$ $|E_I| < |E_I^0|$	< 0	Bone size decreases	same
5	< 0	= -1	$E_I > 0, E_I^0 < 0,$ $|E_I| > |E_I^0|$	> 0	**Bone resorbs to nothing**	**Bone size increases**
6	> 0	= -1	$E_I > 0. E_I^0 < 0.$ $|E_I| > |E_I^0|$	> 0	Bone size increase forever	same
7	< 0	= -1	$E_I > 0, E_I^0 < 0,$ $|E_I| < |E_I^0|$	< 0	**Bone resorbs to nothing**	**Bone size decreases**
8	> 0	= -1	$E_I > 0. E_I^0 < 0.$ $|E_I| < |E_I^0|$	< 0	Bone size increase forever	same
9	> 0	= -1	$E_I < 0, E_I^0 > 0,$ $|E_I| > |E_I^0|$	> 0	**Bone resorbs to nothing**	**Bone size increases**
10	< 0	= -1	$E_I < 0. E_I^0 > 0.$ $|E_I| > |E_I^0|$	> 0	Bone size increase forever	same
11	> 0	= -1	$E_I < 0, E_I^0 > 0,$ $|E_I| < |E_I^0|$	< 0	**Bone resorbs to nothing**	**Bone size decreases**
12	< 0	= -1	$E_I < 0. E_I^0 > 0.$ $|E_I| < |E_I^0|$	< 0	Bone size increase forever	same

While some evidence supports the contention that tensile and compressive strain affect the bone adaptation to different degrees (see Martin et al., 1989) two experiments have been found that indirectly indicate tensile and compressive strains are both osteogenic and their influences on bone adaptation are the same.

In the first experiment (Hert et al. 1972), tibiae of rabbits were loaded in bending. In the first series, the lateral side of the tibia was exposed to compressive stress and the medial side to tensile stress. In the second series, the load direction was reversed. Similar modeling results were obtained in both series (Figure 3.1).
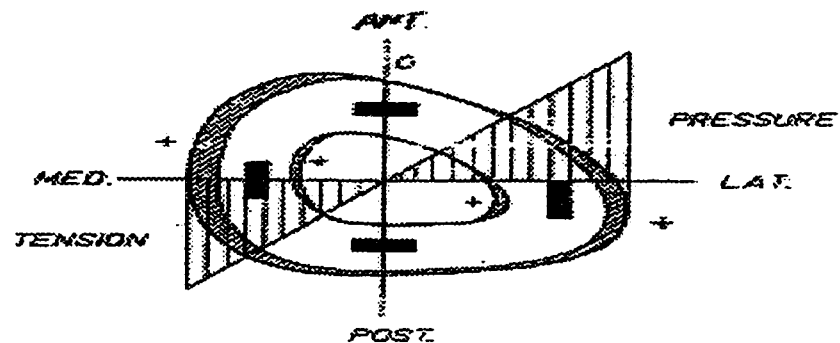
Figure 3.1 Diagram of section of diaphysis of tibia illustrating distribution of stress in compact bone. In both loaded sides (medial and lateral), apposition of new bone occurred on the periosteal and endosteal surfaces (+) (Hert et al. 1972).

Figure 3.2 Transverse undecalcified section from the midshaft of the artificial loaded radius and ulna showing a substantial thickness of new bone periosteally and a small amount endosteally(O'Conner et al., 1982).
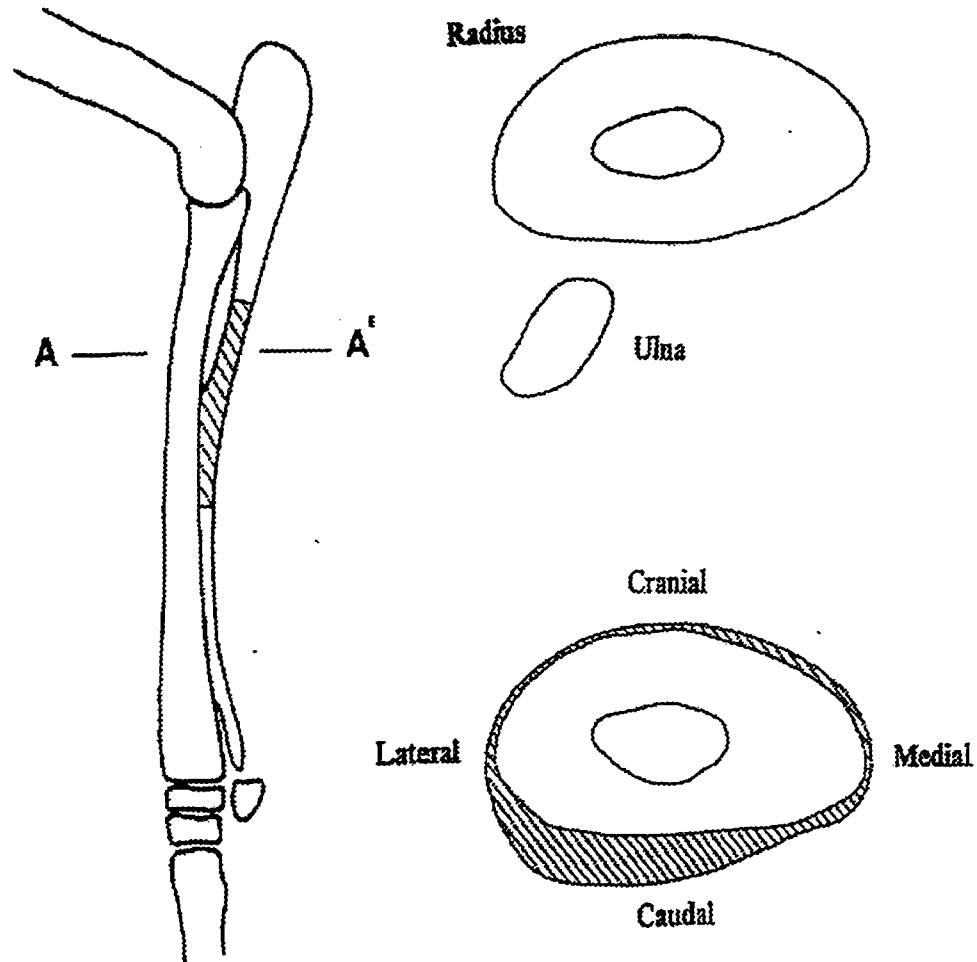
Figure 3.3 Diagram of the radius and ulna of the adult sheep showing the region of ulna removed in the osteomy experiments and distribution of new bone deposited at the level A-A' over 1 year period following. The new bone formation was predominantly on the bone caudal surface (Lanyon et al., 1982).

In the second experiment (O'Conner et al., 1982), bending and compressive were applied intermittently on the radius and ulna of experimental sheep. The plane of bending was the same as that imposed during locomotion.

It was found that direction of bending (tension and compression) appeared to have no effect on the course of the modeling observed (Figure 3.2).

The new model developed intrinsically embraces Cowin's external remodeling theory and can be transformed to Huiskes's and Carter's external remodeling theories. It also has much flexibility.

With $K_{ij} = 0$ ($i \neq j$) and $K_{ii} = 1$ (no sum), the new model automatically becomes Cowin's external remodeling theory. Moreover, by changing the values of K_{ij}, the new model can explain the modeling phenomenon for which Cowin's theory failed to explain.

For example, in the famous experiment about ulnar osteotomy studies (Lanyon et al., 1982, see Figure 3.3), mature sheep were subjected to an ulnar osteotomy (removal of a section of the ulna diaphysis) which caused a slight increase in peak principal walking strain in the radius. The increase of strain on the cranial surface was 20% while it was 10% on the caudal. After the modeling was complete, the principal peak strain showed a reduction in cranial region of 20% and in caudal of 10% compared to the strain in the control side.

This phenomenon can not be explained by Cowin's theory because Cowin's theory predicts that there would be a recovery of radius strain from larger value immediately after osteotomy to normal value once modeling was complete. But by introducing $K_{11} > 1$, this overcompensation can be predicted by the new model although the physical meaning is not clear (may be due to biological effect or different effects of other strain components besides the peak axial strain component)

By choosing $C_1 = C_2 = C_3 = C$, $K_{11}=K_{22}=K_{33}=K$, $K_{44}=K_{55}=K_{66} = 0$, and $K_{ij} = 0$ ($i \neq j$), equation (3-2) becomes:

$$U = C[K(\xi_1 + \xi_2 + \xi_3) - (\xi_1^0 + \xi_2^0 + \xi_3^0)] \qquad (3\text{-}22)$$

If $K = \dfrac{W / (\xi_1 + \xi_2 + \xi_3)}{W^0 / (\xi_1^0 + \xi_2^0 + \xi_3^0)}$, where $W = \dfrac{1}{2}\sigma_{ij}\xi_{ij}$, $W^0 = \dfrac{1}{2}\sigma_{ij}^0\xi_{ij}^0$,

Then the new model becomes Huiskes' external remodeling theory. As the modified Carter and Fyhre's external remodeling theory is actually the same as Huiskes' theory, the new model also can represent Carter and Fhyre's theory.

In addition, by choosing $K = \dfrac{W_e / (\xi_{11})}{W_e^0 / (\xi_{11}^0)}$, where $W_e = \dfrac{1}{2}\sigma_{kk}\xi_{11}$ and $W_e^0 = \dfrac{1}{2}\sigma_{kk}^0\xi_{11}^0$, then (3-2) becomes:

$$U = C(W_e - W_e^0) \tag{3-23}$$

The modeling objective is W_e, and the trigger of modeling is the bone volume change.

By choosing a different modeling objective, the modeling equation (3-2) can also have different forms. This model allows the introduction of more flexibility in bone response than existing modeling theories.

The new model can reflect that different roles of the same strain components in the modeling objective before modeling occurs and after modeling completes.

The objective in Cowin's modeling theory is:

$$C_i \xi_i = C_{ij} \xi_i^0 = S \tag{3-24}$$

where S is a constant, ξ_{ij} and ξ_{ij}^0 share the same weight in the total objective.

While for the new model, the objective is:

$$C_i K_{ij} \xi_j = C_j \xi_j^0 = S \tag{3-25}$$

for the same strain component, say j, if $K_{ij} \neq 0$ (i ≠ j) or $K_{ij} \neq 1$ (i = j), ξ_j and ξ_j^0 will be different in their weight to the modeling objective.

On the other side, if the bone is assumed to be an isotropic or a transversely isotropic or an orthotropic material, Cowin's theory automatically rules out any effects of shear strains on the modeling. But for the new model, the effects of shear strain on the bone modeling can be reflected as long as one of K_{ij} is not equal to zero (i ≠ j).

The new model can reflect the effects of other factors such as diseases, drugs, toxic agents etc. on modeling.

Each mechanism of bone adaptation should have a mathematical and a biological aspect. Mechanical load (L) on a bone (B) generates a primary mechanical signal (S_1) that in effect monitors the mechanical usage. Some kinds of cells should then detect (D) that signal and react by delivering another signal (S_2) to the responding modeling (R_m) and remodeling (R_r) system. The mechanical aspect includes process L to S_1 whereas D-->S_2-->(R_m, R_r) can be considered as the biological aspect.

Frost (1987) proposed that some circulating and local agents such as hormones, drugs, diseases and genetics might act on cells in the biological aspect of MES mechanism to make Mechanostat either insensitive or somewhat overactive to a mechanical usage. The mode of action would deceive the Mechanostat into perceiving a spurious excess or deficit by raising or lowering respectively effective MES setpoints. Many clinical-pathological facts and situations strongly suggest that biological action on MES setpoints do occur (Frost, 1987).

The new model can explain to some degrees the biological effects on bone adaptation but Cowin's theory fails to do so. According to Cowin's theory,

if the loading condition does not change, there will be no bone adaptation. If bone disease or other biological agents take action while the loading condition does not change, the new model can predict the bone adaptation by changing the K_{ij} to account for the new equilibrium strain (MES setpoint) caused by diseases or other factors.

3.5 Summary

In this chapter, the new modeling model is developed. Compared with other modeling theories, the new model has much flexibility and can be transformed to other modeling theories easily.

The proposed new model can not only solve the problem showed in Figure 2.6 that Cowin's theory fails to explain but also can explain to some degrees the biological effects on bone adaptation which Cowin and other modeling theories also fail to explain.

The new model has the basic form (3-2) which can be simplified under certain conditions. If bone material is assumed to be isotropic, transversely isotropic or orthotropic, and bone is loaded in bending or axial tension and compression, the number of modeling coefficients and weighting factors are dramatically reduced.

Actually, it is generally accepted that cortical bone can be considered as an orthotropic material. Our study focuses on the cortical bone and emphasize on the loading cases such as combined bending and axial tension and compression which are the most common loading environment for long bones.

As a result, the modeling rate equation (3-10) is the most commonly used form.

In this chapter, the restrictions on the modeling coefficients and weighting factor have been considered. In addition, the implications of the model and comparison with existing theories have been discussed.

Chapter 4

Modeling Model Examples

This chapter is concerned with the methods for applying the new modeling theory to describe and predict the shape changes of bone when its loading environment is changed. The primary goal is to test the new modeling theory and evaluate its flexibility.

It was mentioned in previous chapters that one characteristic of mathematical modeling theories is the computational feature of their applications. The computational modeling of the bone adaptation process involves two aspects: one is the theoretical "model" of the bone adaptation mechanism which includes modeling rate equations; the other is the computer simulation which is basically thought of as a computer program and its associated numerical methods.

The first feature of the computational modeling was described in the last chapter, and the second aspect will be addressed in this chapter. The new modeling theory is validated by incorporating it with the numerical methods to predict the shape changes of bone. The reason that numerical techniques are employed is that bones is considered to have irregular geometry and variable material properties. Numerical methods have to be used to perform the stress analysis for the complicated stress/strain environment caused by the shape of the bone and its material properties. For different problems, different numerical techniques are employed. These numerical methods are discussed later with specific problems.

The solution procedures based on adaptive elasticity are time stepping: the bone surface points are relocated in each time step according to the prediction of the new modeling model. The direction of change is assumed to be normal to the old surface. With the time step increasing, the bone modeling continues until the iteration converges and modeling equilibrium is reached.

87

The modeling coefficients are found by a trial-and-error approach. After several trial calculations, only those coefficients that guarantee the iteration to converge are used. The weighting factor values are essentially fixed to reflect the effects of different strain components on the modeling along certain direction. At present, there is no specific data to determine the values of those factors.

In this chapter, the bone is considered as an isotropic or an orthotropic material. The parameter studies are undertaken in several aspects:

◆ Model studies which include
    (1) different bone shapes: circle or elliptical cylinder;
    (2) different bone cross-sections: single or double connected;

◆ Loading studies which include:
    (1) different stress analysis types: 2D or 3D;
    (2) different loading environment: axial, radial, bending or combined loading;

◆ Modeling parameters
    (1) different modeling coefficients;
    (2) different weighting factors;

There are three kinds of problems and they will be discussed separately.

4.1 Bone modeled as a right cylinder with a circular cross-section

The bone is modeled as a right cylinder with a circular double connected cross-section as shown in Figure 4.1. The inner and outer radii are represented as a(t) and b(t) and equal to 1mm and 2mm respectively at modeling equilibrium. The bone is loaded in the radial direction and on both inner and outer surfaces. The load on both surfaces are uniformly distributed. The magnitude of total load on the inner and outer surfaces are $1\pi(N)$ and $2\pi(N)$ respectively at the modeling equilibrium state. As in this case the purpose is to

test the new model, the bone is assumed as an isotropic material and weighting factors are all equal to 1. The Young's modulus E is 0.0000115GPa and Poisson's ratio is equal to 0.3.

The problem here is similar to the problem described in section 2.2.3.3. The difference is that the loading environment is different. The load applied in this problem is in the radial direction while the load in the problem presented by Hart et al. (1993) is in the axial direction.
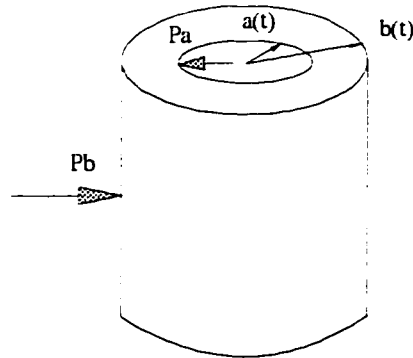
Figure 4.1 A cylinder representing the diaphysis of bone. The surface a(t) is the endosteal surface and b(t) is the periosteal surface. P_a is the magnitude of the total distributed applied load on the endosteal surface and P_b is the magnitude of the total distributed load on the periosteal surface.

(1) Governing equations :

Assuming $K_{rr} = K_{\theta\theta} = K_{zz} = 1$, the modeling rate equation in the coordinate becomes:

$$U = C_r \xi_r + C_\theta \xi_\theta - C_r \xi_r^0 - C_\theta \xi_\theta^0 \qquad \text{(4-1)}$$

Hooke's law:

$$\xi_r = \frac{1-\mu^2}{E}(\sigma_r - \frac{\mu}{1-\mu}\sigma_\theta) \qquad (4\text{-}2)$$

$$\xi_\theta = \frac{1-\mu^2}{E}(\sigma_\theta - \frac{\mu}{1-\mu}\sigma_r) \qquad (4\text{-}3)$$

and substituting (4-2) and (4-3) into (4-1), (4-1) becomes:

$$U = B_r\sigma_r + B_\theta\sigma_\theta - C^0 \qquad (4\text{-}4)$$

where

$$C^0 = C_r\xi_r^0 + C_\theta\xi_\theta^0 \qquad (4\text{-}5)$$

$$B_r = \frac{1-\mu^2}{E}(C_r - \frac{\mu}{1-\mu}C_\theta), \qquad B_\theta = \frac{1-\mu^2}{E}(C_\theta - \frac{\mu}{1-\mu}C_r) \qquad (4\text{-}6)$$

The solution (Timoshenko and Goodier, 1951)for the problem at time t shown in Figure 4.1 is:

$$\sigma_r = \frac{\frac{b^2}{r^2}-1}{\frac{b^2}{a^2}-1} \times \frac{P_a}{2\pi a} + \frac{1-\frac{a^2}{r^2}}{1-\frac{b^2}{a^2}} \times \frac{P_b}{2\pi a}$$

$$\sigma_\theta = -\frac{\frac{b^2}{r^2}+1}{\frac{b^2}{a^2}-1} \times \frac{P_a}{2\pi a} + \frac{1+\frac{a^2}{r^2}}{1-\frac{b^2}{a^2}} \times \frac{P_b}{2\pi a}$$

$$(4\text{-}7)$$

By combining (4-7), (4-4) with stress boundary conditions:

$$\frac{da}{dt} = B_r \frac{P_a}{2\pi a} + B_\theta (-\frac{b^2 + a^2}{b^2 - a^2} \times \frac{P_a}{2\pi a} + \frac{2b^2}{b^2 - a^2} \times \frac{P_b}{2\pi b}) - C_a^0 \qquad (4\text{-}8)$$

$$\frac{db}{dt} = B_r \frac{P_b}{2\pi b} + B_\theta (-\frac{2a^2}{b^2 - a^2} \times \frac{P_a}{2\pi a} + \frac{b^2 + a^2}{b^2 - a^2} \times \frac{P_b}{2\pi b}) - C_b^0 \qquad (4\text{-}9)$$

where

$$C_a^0 = C_r \xi_r^0|_a + C_\theta \xi_\theta^0|_a, \qquad C_b^0 = C_r \xi_r^0|_b + C_\theta \xi_\theta^0|_b$$

(2) Numerical method

The coupled differential equations are solved by using the fourth order Runge-Kutta method.

$$a_{n-1} = a_n + \frac{1}{6}(k_1 + 2k_2 + 2k_3 + k_4) \qquad (4\text{-}10)$$

$$b_{n-1} = b_n + \frac{1}{6}(l_1 + 2l_2 + 2l_3 + l_4) \qquad (4\text{-}11)$$

where

$$k_1 = hf(a_n, b_n) \quad l_1 = hg(a_n, b_n)$$

$$k_2 = hf(a_n + \frac{hk_1}{2}, b_n + \frac{hl_1}{2}) \quad l_2 = hg(a_n + \frac{hk_1}{2}, b_n + \frac{hl_1}{2})$$

$$k_3 = hf(a_n + \frac{hk_2}{2}, b_n + \frac{hl_2}{2}) \quad l_3 = hg(a_n + \frac{hk_2}{2}, b_n + \frac{hl_2}{2})$$

$$k_4 = hf(a_n + hk_3, b_n + hl_3) \quad l_3 = hg(a_n + hk_3, b_n + hl_3)$$

here h is the time step and

$$f(a, b) = B_r \frac{P_a}{2\pi a} + B_\theta (-\frac{b^2 + a^2}{b^2 - a^2} \times \frac{P_a}{2\pi a} + \frac{2b^2}{b^2 - a^2} \times \frac{P_b}{2\pi b}) - C_a^0$$

$$g(a, b) = B_r \frac{P_b}{2\pi b} + B_\theta (-\frac{2a^2}{b^2 - a^2} \times \frac{P_a}{2\pi a} + \frac{b^2 + a^2}{b^2 - a^2} \times \frac{P_b}{2\pi b}) - C_b^0$$

(3) Results

It is assumed that P_a and P_b are always uniformly distributed on the surfaces they apply at during the modeling process. By changing the magnitude of actual P_a and P_b, the loads raised from the equilibrium loads, and modeling coefficients, totally five group of solutions are obtained as shown in Figure 4.2. In the first solution, the cross-sectional area decreases due to inward movement of the periosteal surface (b < b_0) and outward movement of the endosteal surface (a > a_0), one example is that if $P_a = 2\pi(N)$, $P_b = 3\pi(N)$, and $C_r = C_\theta =$ 1000 mm/day, the final a = 1.28572 mm ($a_0 = 1.0$ mm) and b = 1.71428 mm ($b_0 = 2.0$ mm). In the second solution, the endosteal and periosteal surfaces move out, and the area can either increases or decreases depending on the relative rate of movement of the two surfaces. For example, $P_a = 3\pi(N)$, $P_b = 5\pi(N)$, and $C_r = C_\theta = 100$ mm/day, the final a = 1.49998 mm and b = 2.49994 mm. The third solution, the endosteal surface moves in and the periosteal surface moves out, and the area increases. The example is: $P_a = 2\pi(N)$, $P_b = 5\pi(N)$, and $C_r = C_\theta = 1000$ mm/day, the final a = 0.59998 mm and b = 2.40002 mm. Solution four is just a special sub class of the solution three. Both surfaces move in. The fifth solution and the cross-sectional area either increases or decreases depending on the load and modeling coefficients.

It is interesting to know that the solution types in this case are quite similar to the solution types in Figure 2.8 in which loading is in the axial direction. As B_r and B_θ are chosen to be the same for both inner surface and

b0=2.0

9.42

12.57

a0=1.0

1 a > a0
   b < b0

2 a > a0
   b > b0

3 a < a0
   b > b0

4 a = 0
   b > b0

5 a < a0
   b < b0
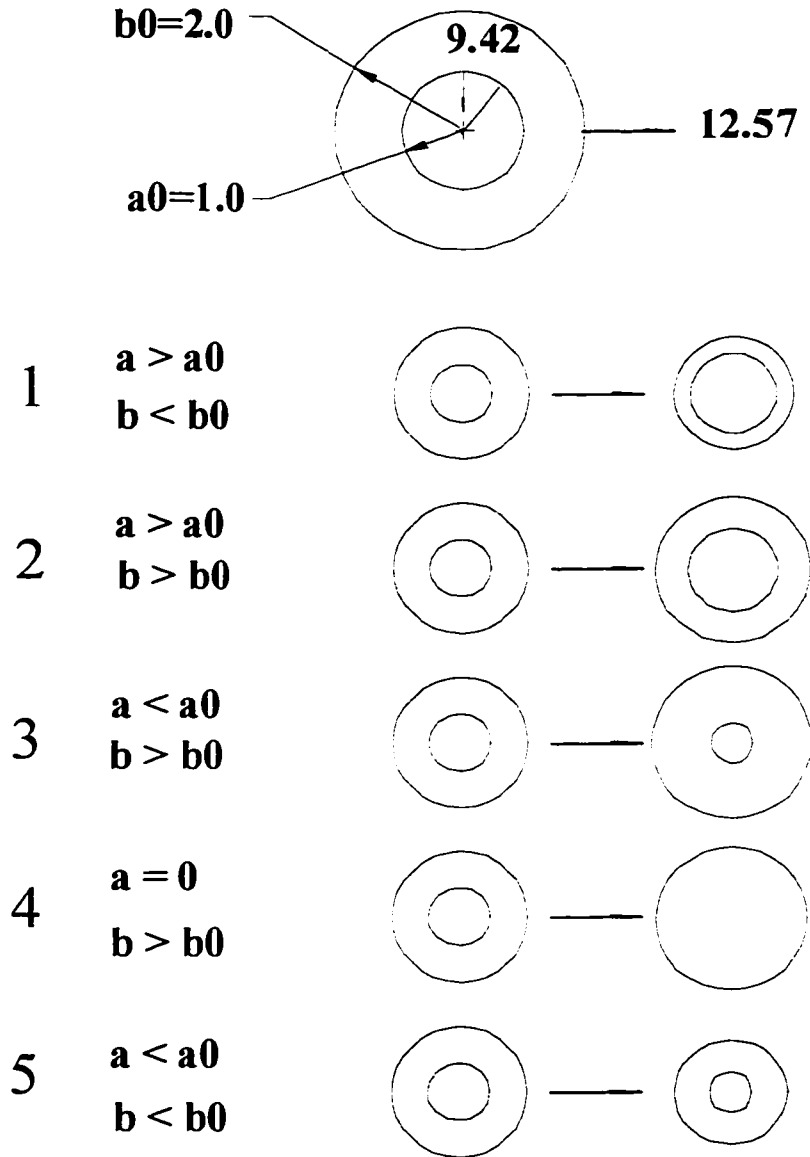
Figure 4.2 Five solution types of diaphyseal modeling problem

outer surfaces, the number of solution types are limited. The different B_r and B_θ may provide other solution types.

All solutions in the calculation converge very quickly.
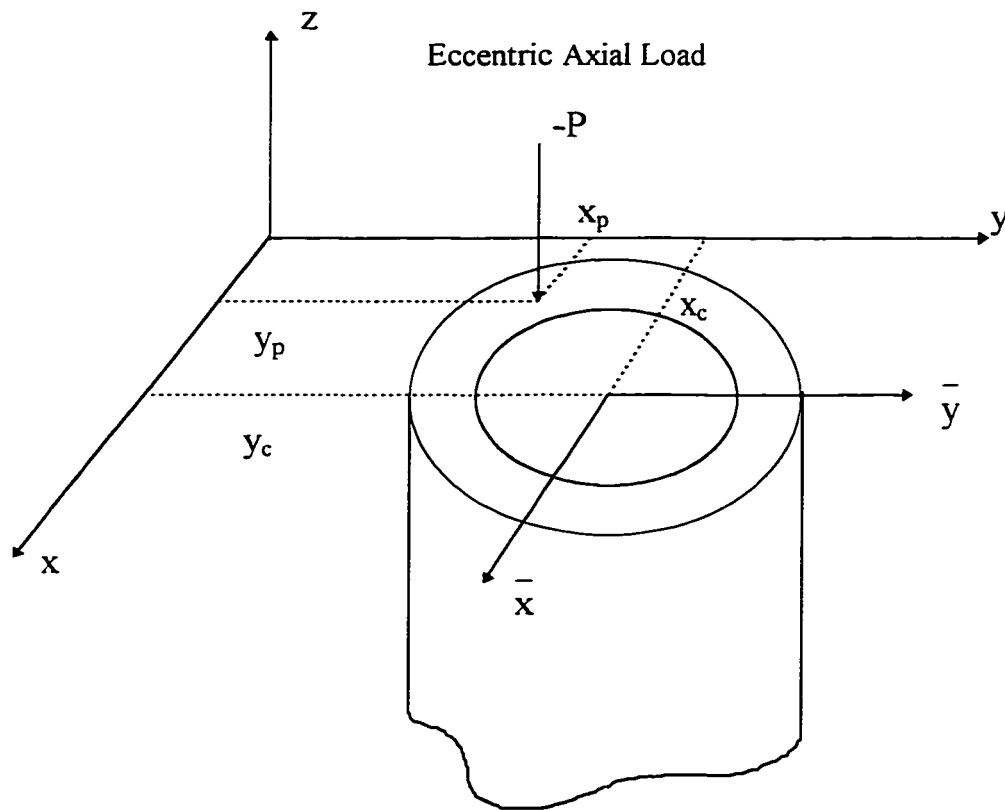
Figure 4.3 Cross-sectional bone model. Global coordinate system (x,y). The coordinates of centroid are given by (x_c, y_c). The point of load is given in the global coordinates by (x_p, y_p).

4.2 Combined axial and bending loading for an elliptical cross-section

The bone is modeled as a right cylinder with an elliptical cross-section oriented in a global coordinate system (x,y) as shown in Figure 4.3. The coordinates of centroid are given by (x_c, y_c), and the centroid is the origin of the centroidal coordinates system ($\bar{x}$, $\bar{y}$) with axes parallel to the global coordinate axes. The long and short axes of the ellipse are 4.0mm and 2.0mm respectively. For the cases in which bone has a doubly connected cross-section, the long and short axes of the inner ellipse are 2.0mm and 1.0mm respectively and the long and short axes of the outer ellipse are 4.0mm and 2.0mm respectively. The bone is loaded by a distributed load which is equivalent to an axial compressive or tensile force at (x_p, y_p). If (x_p, y_p) are (0, 0), the bone is subjected to the uniform compression or tension along the z direction, and when the yp, xp are nonzero , the bone is subjected to the compression/tension and bending.

4.2.1 Computer formulation and the numerical technique to solve problems

Substitution of Hooke's law into equation (3-10), yields

$$U = B_3(K'_{33}\sigma_3 - \sigma_3^0)$$
(4-12)

σ_3 is calculated by using beam theory (Cowin et. al. 1985):

$$\sigma_{bend} = \frac{P(x_p - x_c)[I_{xy}(y - y_c) - I_{xx}(x - x_c)] + P(y_p - y_c)[I_{xy}(x - x_c) - I_{yy}(y - y_c)]}{I_{xx}I_{yy} - I_{xy}I_{xy}}$$

$$\sigma_3 = -\frac{P}{A} - \sigma_{bend} \qquad\qquad (4\text{-}13)$$

Where σ_3 is the magnitude of the axial stress at the point (x, y), P is the magnitude of the equivalent axial load which acts in the z direction, A is the total cross-sectional area of bone in the x-y plane, x_p, y_p are the coordinates of the point of load application, x_c, y_c are the coordinates of the centroid of bone lying in the x-y plane. $I_{\overline{xx}}$ is the area moment of inertia of the cross-sectional area with respect to the centroidal $\overline{x}$ axis, $I_{\overline{yy}}$ is the area moment of inertia of the cross-sectional area with respect to the centroidal $\overline{y}$ axis, and $I_{\overline{xy}}$ is the area product of inertia of the cross-sectional area with respect to the centroidal and $\overline{x}$ and $\overline{y}$ axes.

For this calculation, the bone tissue is assumed to be orthotropic and therefore only axial stresses exist (see Cowin et al., 1985). The bone surfaces (periosteal and endosteal surfaces) are divided into fifty sections. Each point at the conjunction of any two sections is used as the knot for the cubic spline calculation which is employed to fit the bone surfaces. Since the bone surfaces are closed curves, the end conditions for the spline are periodic. The geometric properties of the cross-section and the normal direction at each knot are calculated by the combination of the cubic spline and the Gaussian integration method.

Let S(x) represent the bone surface, then:

$$S(x) = \sum_{i=1}^{N-1} \Phi_i(x) f_i + \sum_{i=1}^{N-1} \Psi_i(x) m_i \qquad\qquad (4\text{-}14)$$

where f_i, m_i are prescribed values and slopes at knots x_1, x_2 ......x_{N-1} and

$$\Phi_i(x_j) = \delta_{ij} \qquad \Phi_i'(x_j) = 0 \qquad \Psi_i(x_j) = 0 \qquad \Psi_i'(x_j) = \delta_{ij}$$

For $k = 2, \cdots N,$ define:

$$h_k = x_k - x_{k-1}$$

$$\lambda_k = \frac{1}{h_k}$$

$$b_k = 2.0 \times (\frac{1}{h_k} - \frac{1}{h_{k+1}})$$

$$\mu_k = \frac{1}{h_{k+1}}$$

$$C_k = 3 \times \frac{f_k - f_{k-1}}{h_k^2} + 3 \times \frac{f_{k+1} - f_k}{h_{k+1}^2}$$

From the condition that $S''(x)$ is continuous at the interior knots x_2, ...x_N.

$$\frac{1}{h_k} m_{k-1} + b_k m_k + \mu_k m_{k+1} = C_k \qquad (k = 2, \cdots N) \tag{4-15}$$

Another two conditions (periodic condition) $S'(x_1) = S'(x_{N+1})$ and $S''(x_1) = S''(x_{N+1})$ produce:

$$m_1 = m_{N+1}$$

$$\mu_{N+1} m_2 + \lambda_{N+1} m_N + b_{N+1} m_{N+1} = C_{N+1}$$

where

$$\mu_{N+1} = \frac{1}{h_2}$$

$$\lambda_{N+1} = \frac{1}{h_{N+1}}$$

$$b_{N+1} = 2 \times (\frac{1}{h_2} + \frac{1}{h_{N+1}})$$

$$C_{N+1} = 3 \times (\frac{f_{N+1} - f_N}{h_{N+1}^2}) + 3 \times (\frac{f_2 - f_{N+1}}{h_2^2})$$

The final equations are:

$$
\begin{bmatrix}
b_2 & \mu_2 & 0 & \cdots & 0 & 0 & \lambda_2 \\
\lambda_3 & b_3 & \mu_3 & \cdots & 0 & 0 & 0 \\
0 & \lambda_4 & b_4 & \cdots & 0 & 0 & 0 \\
\cdot & \cdot & \cdot & & \cdot & \cdot & \cdot \\
\cdot & \cdot & \cdot & & \cdot & \cdot & \cdot \\
0 & 0 & 0 & \cdots & b_{N-1} & \mu_{N-1} & 0 \\
0 & 0 & 0 & \cdots & \lambda_N & b_N & \mu_N \\
\mu_{N+1} & 0 & 0 & \cdots & 0 & \lambda_{N+1} & b_{N+1}
\end{bmatrix}
\begin{Bmatrix}
m_2 \\
m_3 \\
m_4 \\
\cdot \\
\cdot \\
m_{N-1} \\
m_N \\
m_{N+1}
\end{Bmatrix}
=
\begin{Bmatrix}
C_2 \\
C_3 \\
C_4 \\
\cdot \\
\cdot \\
C_{N-1} \\
C_N \\
C_{N+1}
\end{Bmatrix}
\qquad \textbf{(4-16)}
$$

The algorithm for solving the equation (4-9) (see Ahlberg 1967) is:

for $k = 2, \cdots N + 1$, define

$$\begin{cases} p_k = \lambda_k q_k + b_k & (q_0 = 0) \\[2mm] q_k = -\mu_k \Big/ p_k \\[2mm] \mu_k = (C_k - \lambda_k \mu_{k-1}) \Big/ p_k & (\mu_0 = 0) \\[2mm] s_k = -\lambda_k s_{k-1} \Big/ p_k \end{cases}$$

Then

$$m_{N+1} = \frac{C_{N+1} - \mu_{N+1} v_1 - \lambda_{N+1} v_N}{\mu_{N+1} t_2 + \lambda_{N+1} t_N + b_{N+1}}$$

$$m_k = t_k m_{N+1} + v_k \qquad (k = 2, \cdots N)$$

$$m_1 = m_{N+1}$$

where

$$t_k = q_k t_{k+1} + s_k \qquad (t_{N+1} = 1)$$
$$v_k = q_k v_{k-1} + \mu_k \qquad (v_{N+1} = 1)$$

The geometric properties are calculated by combining spline equation and Gausian integration:

Area:

$$A = \int_A \frac{\partial}{\partial y}(y)dA = \int_S y \times n_y dS = \int \rho \sin\theta \times (-\rho' \cos\theta + \rho \sin\theta)d\theta$$
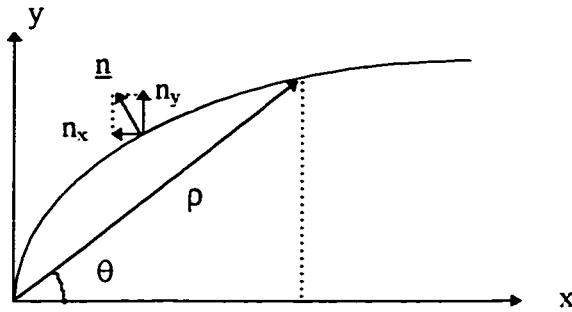
Figure 4.4 Polar coordinate

The static moment:

$$A_x = \frac{1}{2}\int \rho^2 \sin^2\theta \times (-\rho'\cos\theta + \rho\sin\theta)d\theta$$

$$A_y = \frac{1}{2}\int \rho^2 \cos^2\theta \times (\rho'\sin\theta + \rho\cos\theta)d\theta$$

and the moment of inertia are:

$$I_x = \frac{1}{3}\int \rho^3 \sin^2\theta \times (-\rho'\cos\theta + \rho\sin\theta)d\theta$$

$$I_y = \frac{1}{3}\int \rho^3 \cos^2\theta \times (\rho'\sin\theta + \rho\cos\theta)d\theta$$

$$I_{xy} = \frac{1}{2}\int \rho^3 \sin^2\theta\cos\theta \times (\rho'\cos\theta + \rho\sin\theta)d\theta$$

In all above integrals, ρ is the distance from the original point of polar coordinate (Figure 4.4) and can be represented by using the spline equation in terms of θ, and the integrals can be calculated by three-point Gauss-Legendre formula.

The time stepping method is used to simulate the modeling process. The procedure can be divided into several steps:

A. Calculate the geometric properties of the bone cross-section;
B. Calculate the axial stress at each knot by using (4-13);
C. Calculate the surface speed at each point by (4-12) which is multiplied by the prescribed time step to get the magnitude of the surface modeling;
D. Find the normal direction at each knot (actually get from m_i);
E. Relocate each point by the magnitude of surface modeling in the normal direction;
F. Increase the time by the time step;
G. Repeat the step 1 to step 6 until the time stepping converges.

In the calculation, the different modeling coefficients are chosen to guarantee the convergence. The units used in the examples are: P (N), x_p, y_p (mm), B_{33} (mm day^{-1} GP$_a^{-1}$), K_{33} (1).

4.2.2 Modeling model examples

In order to examine the capabilities of the new model to deal with the problems in Figure 2.6 for which the Cowin's theory fails, it is assumed that the equilibrium strain is negative, and the actual strain is positive (see section 2.2.2.4).

The bone is modeled as a right cylinder with a single connected elliptical cross-section. The equilibrium load is $P^0 = 1.0$ (compression) with $x_p = 0$ and y_p = 0, and the actual load is P = -1.5 with $x_p = 0$ and $y_p = 0$. $B_3 = -2.0$, three different weighting factors $K_{33} = 0.5$, 1.0, and 1.5 are used, and three cases converged. The results are shown in Figure 4.5. It can be seen from the results
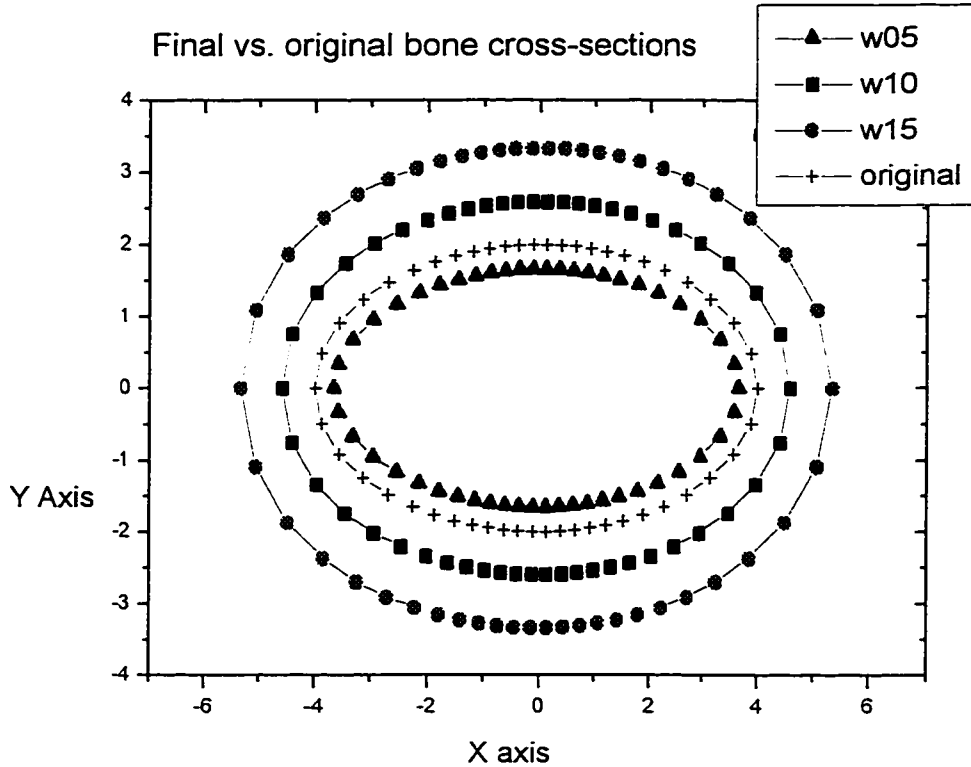
Figure 4.5 The final shapes of bone cross-section after the modeling complete. P =1.5 (tension), y_p = 0.0, weighting factors K_{33} = 0.5, 1.0, 1.5.

that with a small weighting factor (K_{33} = 0.5), the bone resorbed which means that, even with $|P| > |P^0|$, it is not enough to maintain the bone mass, and with a large weighting factor (for example, K_{33} =1.5 or 1.0), the deposition of bone occurred.

In Figure 4.5, w05 represents K_{33} = 0.5, w10, w15 represent K_{33} = 1.0, and K_{33} = 1.5 respectively.

To further examine the loading cases which are inconsistent in Cowin's theory, the following problem is considered. At the equilibrium state, the load is centric, and the equilibrium strain is thus uniformly compressive while the actual

load is eccentric, and the strain has two parts: one is uniform axial compression and the other is the strain caused by eccentricity. In this case, the bone is also modeled as a right cylinder with a single connected elliptical cross-section.
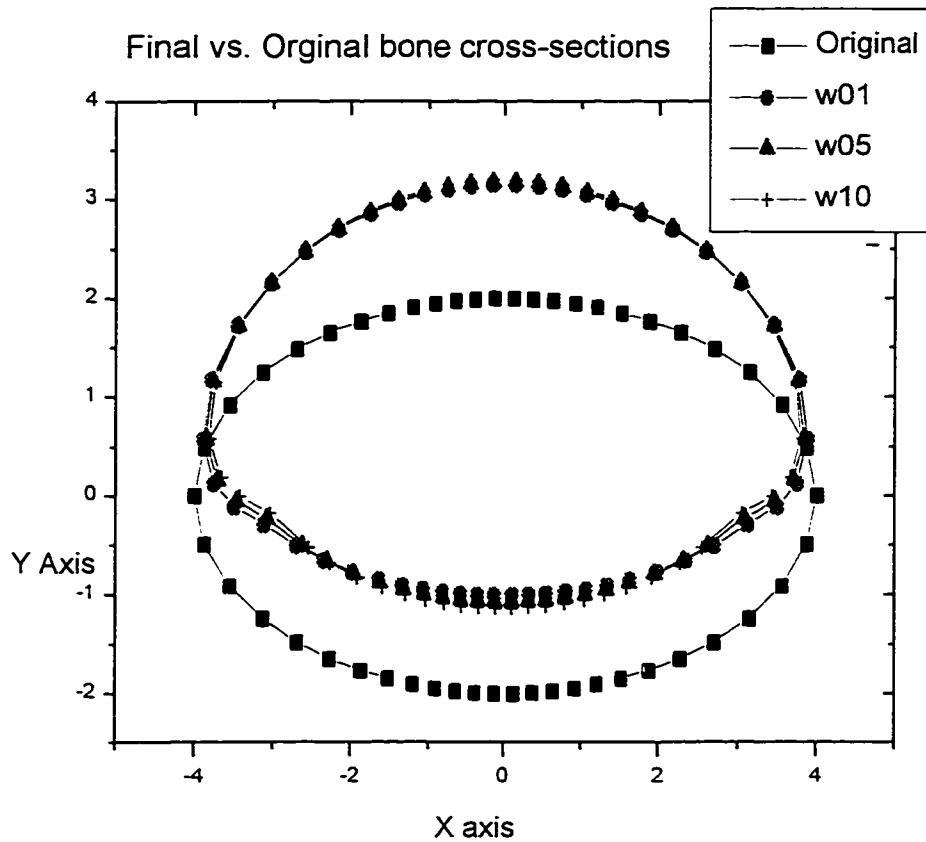
Figure 4.6 The final shapes of bone cross-section after modeling. The equilibrium loading is uniform axial compression and the actual loading is an eccentric compression. $P = 1.0$, $y_p = 1.0$, $K_{33} = 0.1$, 1.0, and 0.5, $B_3 = -10.0$.

The equilibrium load is $P^0 = 1.0$ (compression), the actual load is the same but with $x_p = 0$ and $y_p = 1.0$, $B_3 = -10.0$. In this case, on the one side of bone, the actual strain is tensile, and on the other side, compressive. Also, three different weighting factors $K_{33} = 0.1$, 0.5, and 1.0 are adopted, all cases

converged. Even though the change in point of application $y_p = 1.0$ is quite big compared to the short axis of the ellipse, the new model can still handle it.

It can be seen from the Figure 4.6, for the three different weighting factors, the differences between the final shapes are not prominent in comparison with the cases in Figure 4.5. This is because most points at bone surface have the same sign for the actual strains and the corresponding equilibrium strains, the effect of K_{33} is not obvious.
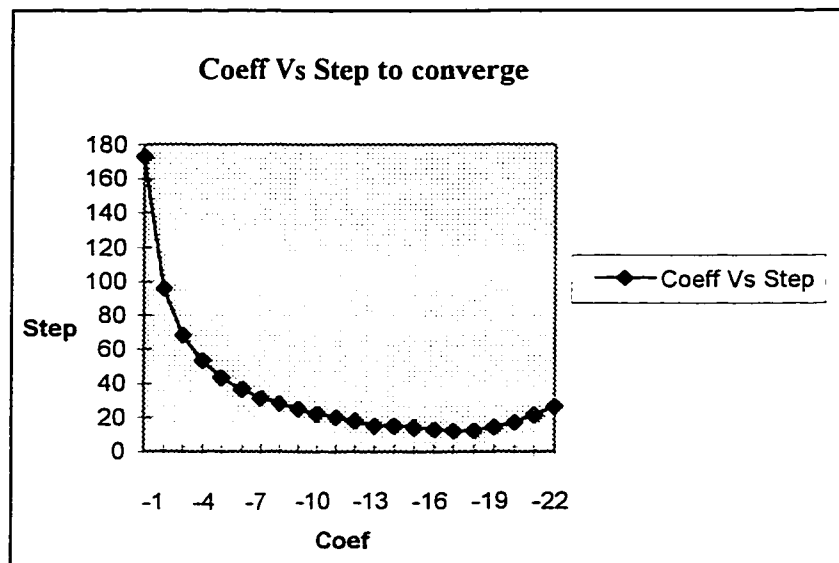
Figure 4.7 The effect of modeling coefficient B_3 on the speed of convergence. $P = 1.0$, $y_p = 0.1$, $K_{33} = 1$

To investigate the effect of modeling coefficient B_3 on the speed of the convergence, a similar problem but with a small $y_p = 0.1$ is considered. The relationship between B_3 and the time steps to converge are shown in Figure 4.7. This suggests that the larger the modeling coefficient, the faster the speed of the convergence. There is quite a large range of B_3 which can guarantee the convergence of the modeling process. However if the coefficient is too large, the convergence might not be possible.
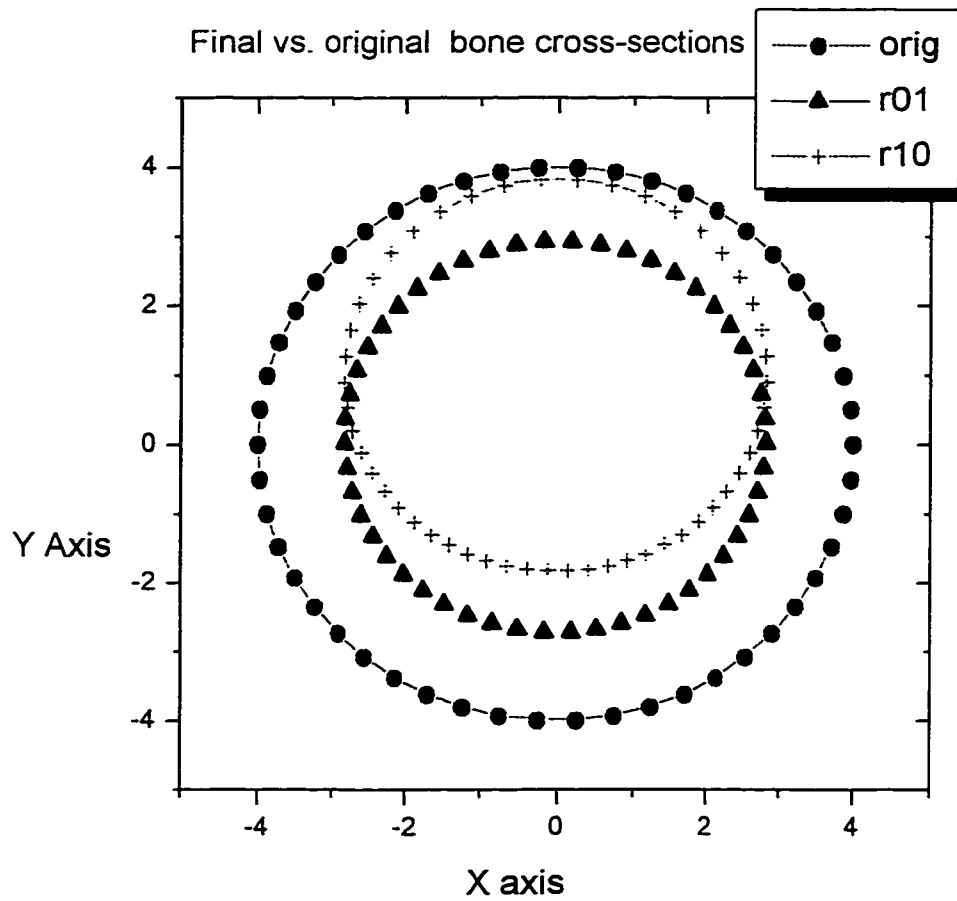
Figure 4.8 The final shape and position of cross-section of bone. The magnitude of actual load is smaller than that of equilibrium load. $P^0 =$ 2.0, $P = 1.0$ and $y_p = 0.1$ (r01), 1.0(r10), the original cross-section is a circle and the radius $= 4$, $K_{33} = 0.5$, $B_3 = -3.0$
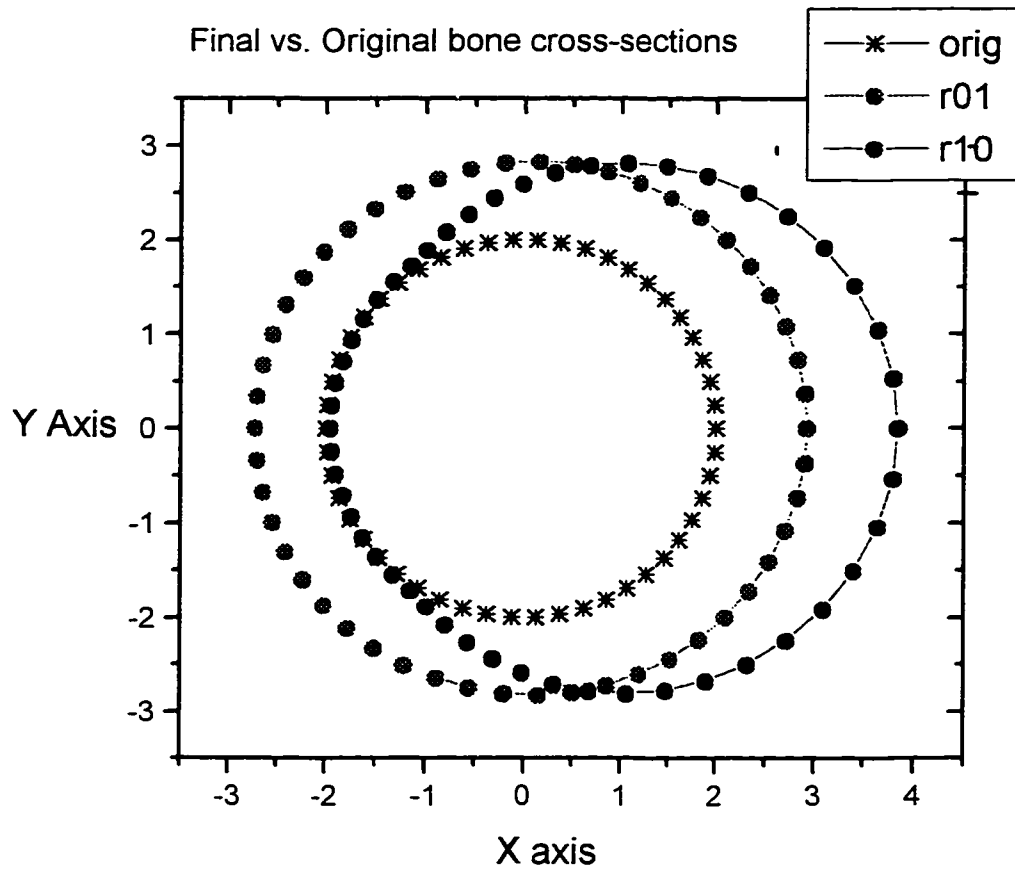
Figure 4.9 The final shape and position of cross-section of bone after modeling complete. The magnitude of actual load is larger than that of equilibrium load. $P^0 = 0.5$, $P = 1.0$ and $x_p = 0.1(r01)$, $1.0(r10)$, the original cross-section is a circle and the radius = 2, $K_{33} = 0.5$, $B_3 = -3.0$

In the previous two examples above, the actual load had the same magnitude as the equilibrium load. The problem in which not only the loading position of the actual load changes (from the equilibrium load), but also the magnitude of the actual load changes, is considered. The bone considered here is a right cylinder with a single connected circular cross-section.

The first case is one when the magnitude of the actual load is smaller than that of the equilibrium value and the point of application of the actual load is different from that of equilibrium load in the y direction. The equilibrium load is $P^0 = 1.0$ (compression) with $y_p = 0$ and $x_p = 0$, and the actual load is $P = 0.5$ with $y_p = 0.1$, and 1.0 and $x_p = 0$. The modeling coefficient $B_3 = -3.0$, and the radius of the original circle is 2.0.

The second case assumes the magnitude of the actual load is larger than that of the equilibrium value and the point of application is different from that of the equilibrium load in the x direction. The equilibrium load is $P^0 = 0.5$ (compression) with $y_p = 0$ and $x_p = 0$, and the actual load $P = 1.0$, with $y_p = 0$, and $x_p = 0.1$, and 1.0. The modeling coefficient $B_3 = -3.0$, and the radius of the original circle is 2.0.

Figure 4.8 shows that with smaller actual load (compared with equilibrium load) and small eccentricity $y_p = 0.1$, the final area of the bone cross-section decreases but the centroid of the bone cross-section remains near the original position. With larger eccentricity $y_p = 1.0$, the whole bone cross-section moves, and the area of the cross-section also decreases.

From Figure 4.9, it can be seen that with a small eccentricity $x_p = 0.1$, the final area of the bone cross-section increases while the centroid moves little. With a large eccentricity $x_p = 1.1$, the bone cross-section not only swells a lot but also drifts considerably.

In all cases, the weighting factor $K_{33} = 0.5$. The final shapes of the bone cross-section are circular. This is different with the cases that have the original shape of bone cross-section elliptical. Generally speaking, if the original shape of bone cross-section is elliptical, the final shape won't be elliptical again.
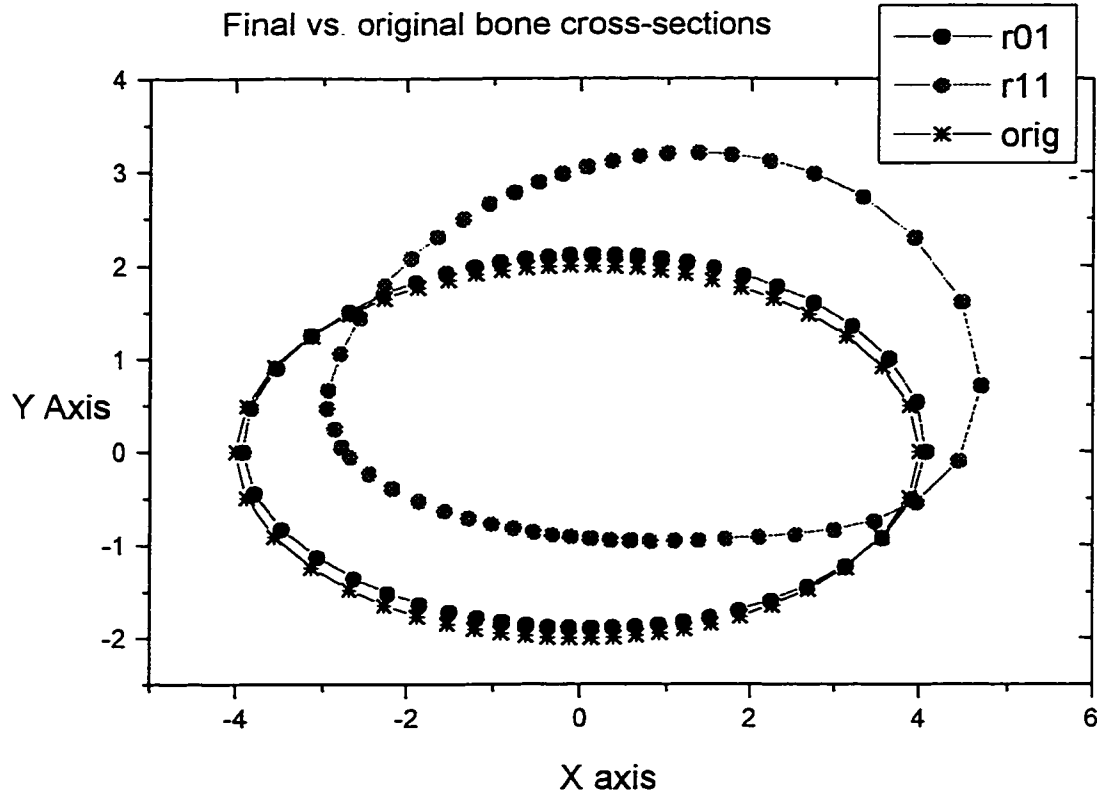
Figure 4.10 The final shapes of the bone cross-section after the modeling. The original bone cross section is elliptical. $P = P^0 = 1.0$, $x_p = 0.1$, $y_p = 0.1$ (r01) and $x_p = 1.1$(r11), $y_p = 1.0$, $K_{33} = 0.5$, $B_3 = -3.0$.

As up to the present, only cases in which the load eccentricity is in one direction is considered. To consider the load applied at an arbitrary point, another problem is examined. The equilibrium load is $P^0 = 1.0$ (compression) with $x_p = 0$ and $y_p = 0$, the actual load $P = 1.0$, with $x_p = 0.1$, $y_p = 0.1$ (represented by r01), and $x_p = 1.0$, $y_p = 1.0$ (represented by r11). $B_{33} = -3.0$, the weighting factor is 0.5. The final shapes of bone cross-section after modeling is shown in Figure 4.10.

For most of cases, the area of the bone cross-section remains constant during the iteration if the actual load has the same magnitude with the equilibrium load. But for the problem considered here, the situation is a little bit different. The modeling predicts 'overshoot' of the bone cross-sectional area at the beginning, then gradually converge to the target area.(see Figure 4.11). The overshooting of bone cross-section area is also reported by Prendergas and Taylor (1993).
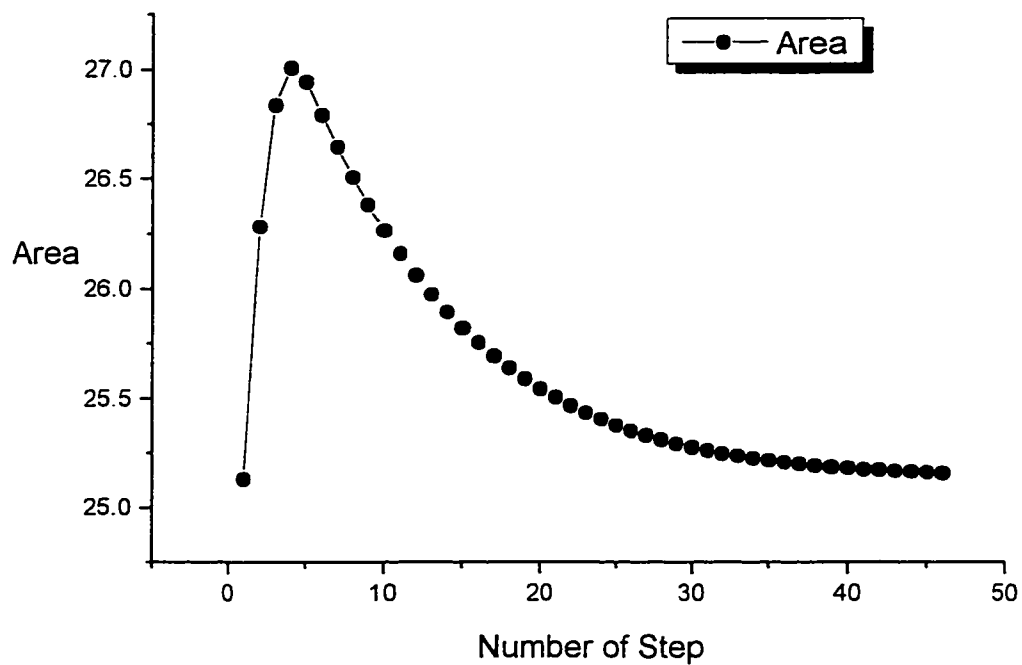
Figure 4.11 The bone cross-section area changes during the modeling. At the time step 5 to step 20, the area 'overshoot' the equilibrium area and gradually converge to the target area.

A more realistic representation of long bone is a right cylinder with a doubly connected elliptical cross-section. The long and short axes of the outer ellipse are taken as 4.0 and 2.0 while for the inner ellipse, they are 2.0 and 1.0 respectively. The equilibrium load is 1.0 with $x_p = 0$, and $y_p = 0$. The actual load is 2.0 with $x_p = 1.0$ and $y_p = 1.0$. The modeling coefficient $B_3 = -3.0$ for both surfaces. The weight factor $K_{33} = -0.5$.
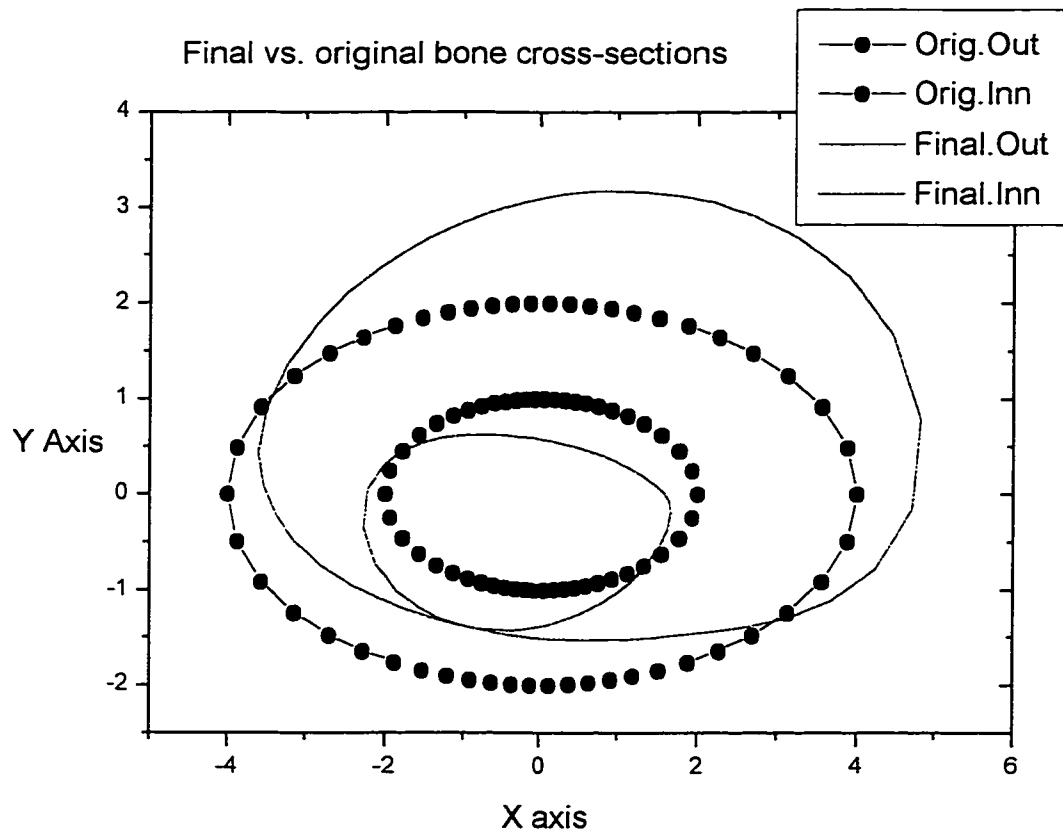
Figure 4.12 The final shapes of the bone cross-section after the modeling. The original bone was doubly collected. At outer surface, long axis A = 4, and short axis B =2, at the inner surface, A= 2.0, B =1.0. Load P = P^0 = 1.0, x_p = 1.0 and y_p = 1.0. B_3 = -3.0, K_{33} = -0.5.

The final shape of bone cross-section is shown in Figure 4.12. It is interesting to note that there is a section along the bone surface in which the outer surface coincides with the inner surface. This is to be expected as on the region that is close to the point of application, the strain is composed by two compressive parts, one is from the uniform compressive strain, and the other comes from bending due to an eccentric load. The magnitude of compressive strain is increased and causes the bone deposit on this side while for the side that is far from the load, the strain composes of a compressive part which comes from the uniform compressive strain, and a tensile part which is introduced by the bending. As a result, the resultant strain on the far end is tensile. As the weight factor is 0.5, the effect of actual tensile strain is less than that of equilibrium compressive strain on the modeling, the bone gradually resorbs.

4.3 3D Modeling Model Examples
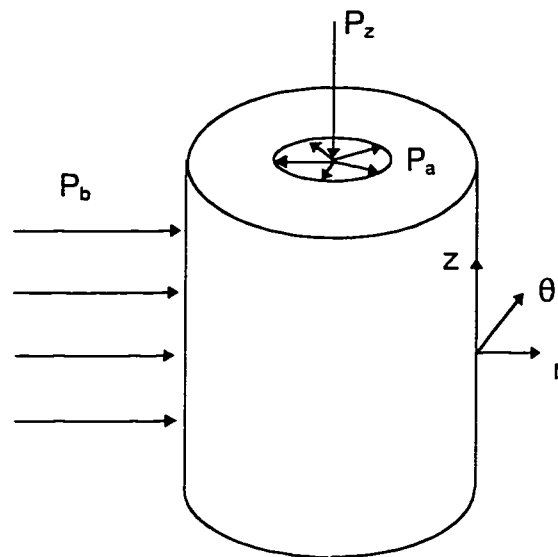
Figure 4.13 The diaphysical region of bone represented by a hollow circular cylinder.

All the examples above are loaded in one direction and therefore the simplified formulation (3-10) is used. To more fully examine the new modeling theory, a 3D problem is considered.

The bone is modeled as a right cylinder with a circular doubly connected cross-section. As before, the bone is considered as an isotropic material, and a cylindrical coordinate system (r, θ, z) is employed to describe the orthotropic elastic stress-strain relationship. P_z is axial load on the top and bottom surfaces, and P_a, P_b are radial loads on the inner and outer surfaces. They are all uniformly distributed.

The problem is to determine the surface modeling that would occur if the loads carried by the bone on three different surfaces were suddenly raised or lowered to a new level.

The modeling equation becomes:

$$U = B_r(K_{rr}\sigma_r - \sigma_r^0) + B_\theta(K_{\theta\theta}\sigma_\theta - \sigma_\theta^0) + B_z(K_{zz}\sigma_z - \sigma_z^0) \qquad (4\text{-}17)$$

And the stress-strain relationships:

on the inner surface are:

$$\sigma_z = \frac{P_z}{\pi(b^2 - a^2)} - E_z(\frac{\gamma_{rz}}{E_r} \times \frac{P_a}{2\pi a} + \frac{\gamma_{\theta z}}{E_\theta} \times \sigma_\theta|_a)$$

$$\sigma_r = \frac{P_a}{2\pi a} - E_r(\frac{\gamma_{zr}}{E_z} \times \frac{P_z}{\pi(b^2 - a^2)} + \frac{\gamma_{\theta r}}{E_\theta} \times \sigma_\theta|_a)$$

$$\sigma_\theta = \sigma_\theta|_a - E_\theta(\frac{\gamma_{z\theta}}{E_z} \times \frac{P_z}{\pi(b^2 - a^2)} + \frac{\gamma_{r\theta}}{E_r} \times \frac{P_a}{2\pi a})$$

on the outer surface are:

$$\sigma_z = \frac{P_z}{\pi(b^2 - a^2)} - E_z \left(\frac{\gamma_{rz}}{E_r} \times \frac{P_b}{2\pi b} + \frac{\gamma_{\theta z}}{E_\theta} \times \sigma_\theta|_b \right)$$

$$\sigma_r = \frac{P_b}{2\pi b} - E_r \left(\frac{\gamma_{zr}}{E_z} \times \frac{P_z}{\pi(b^2 - a^2)} + \frac{\gamma_{\theta r}}{E_\theta} \times \sigma_\theta|_b \right)$$

$$\sigma_\theta = \sigma_\theta|_b - E_\theta \left(\frac{\gamma_{z\theta}}{E_z} \times \frac{P_z}{\pi(b^2 - a^2)} + \frac{\gamma_{r\theta}}{E_r} \times \frac{P_b}{2\pi b} \right)$$

where

$$\sigma_\theta|_a = -\frac{b^2 + a^2}{b^2 - a^2} \times \frac{P_a}{2\pi a} + \frac{2b^2}{b^2 - a^2} \times \frac{P_b}{2\pi b}$$

$$\sigma_\theta|_b = -\frac{2a^2}{b^2 - a^2} \times \frac{P_a}{2\pi a} + \frac{b^2 + a^2}{b^2 - a^2} \times \frac{P_b}{2\pi b}$$

The problem is solved by the same method used in last section. The only difference is that the modeling equation is different. In the calculation, E = 21.5GP, γ = 0.24 (as the solutions for σ's are for an isotropic material).

The initial inner and outer radii a_0 and b_0 are 2.0mm and 4.0mm respectively. The magnitude of equilibrium axial load and radial load on inner and outer surfaces are all 1.0 N.

Table 4.1 3D Modeling Results

Case	$B_r\|_a$, $B_\theta\|_a$, $B_z\|_a$ $B_r\|_b$, $B_\theta\|_b$, $B_z\|_b$ (mm day GP_a^{-1})	P_z, P_a, P_b (N)	K	a (mm)	b (mm)
1	50, 50, 50 50, 50, -50	1.5, 1.5, 1.5	1.0	4.466 ↑	6.037↑
2	50, 50, -50 -50, -50, 50	-1.5, 1.5, 1.5	1.0	9.057 ↑	10.99↑
3	50, 50, 50 -50, -50, -50	-1.5, 1.5, 1.5	1.0	2.409 ↑	4.874↑
4	50, 50, 50 -50, -50, -50	-1.5, 1.5, 1.5	0.5	2.418 ↑	4.833↑
5	50, 50, -10 -50, -50, -10	-1.5, 1.5, 1.5	1.0	5.270 ↑	6.541↑
6	50, 50, 10 -50, -50, -10	-1.5, 1.5, 1.5	1.0	3.622 ↑	6.111↑
7	50, 50, -10 -50, -50, 10	-1.5, 1.5, 1.5	1.0	5.467 ↑	7.012↑
8	50, 50, 10 -50, -50, 10	-1.5, 1.5, 1.5	1.0	0.533 ↓	9.479↑
9	20, 20, 10 -20, -20, -10	0.5, 0.5, 0.5	1.0	1.051 ↓	1.959↓
10	20, 20, 100 -20, -20, -100	0.5, 0.5, 0.5	1.0	2.591 ↑	3.661↓
11	20, 0, 100 -20, 0, -100	1.5, 0.5, 0.5	1.0	1.728 ↑	4.849↓

Table 4.2 Area changes

Case	1	2	3	4	5	6	7	8	9	10	11
Area diff	4.5 π	26.8 π	5.9 π	5.5 π	3.0 π	12.2 π	7.2 π	77.5 π	-9.3 π	-5.7 π	8.5 π

With different actual loading environment, the final shapes of bone cross-section will be different. In the calculation, choosing the right B_r, B_θ. and B_z are crucial. They are chosen by a trial and error method to guarantee the convergence of problems.

The result is shown in table 4.1. The a and b are the final inner and outer radii after the modeling finishes. The symbol↑ and↓ mean increase and decrease from the equilibrium values. B_r, B_θ and B_z are the modeling coefficients of modeling rate equations for the inner and outer surfaces. The symbol (-) means that the actual load has the different sign from its corresponding value in equilibrium state. K represents the weighting factor where $K_{rr} = K_{\theta\theta} = K_{zz} = K$.

Table 4.2 lists the area changes for eleven cases of 3D modeling examples. In the one dimensional problem, the modeling coefficient B_i do not affect the final shape of bone cross-section. But for the 3D problems, the B_i do have the effects on them.

For the first modeling example, the actual loads are raised to 1.5N from the equilibrium load 1.0N. The modeling coefficients are all 50 (mm day^{-1}GPa^{-1}) except for B_z on the outer surface. The final radii a and b increase from their original values.

In the second example, the actual axial load has the different sign as the equilibrium axial load and it is assumed that the tension has the same the effect as the compression (K = 1). By choosing different B_r, B_θ and B_z on the inner and outer surfaces, the final a and b also increase.

The third example indicates that different modeling coefficients may have quite different effects on the final a and b by comparing it with the second case.

The fourth example examined the difference that the different weighting factor will make on the modeling. It shows that cases three and four have no big difference on the modeling in terms of a and b under this special circumstance.

The fifth, sixth and seventh examples basically examine the effects of different modeling coefficients on the final shape of bone cross-section.

The eighth example shows a different behavior of bone modeling. For the seven examples shown before it, all a and b increase from their equilibrium values. But the eighth case indicates that a decreases from its original value while b still increases.

The ninth and tenth examples examined the modeling of bone assuming that the actual loads decrease to 0.5N and are held there. The ninth case indicates that a and b both decrease from their equilibrium values while the tenth example shows that a increases but b decreases from their original values.

In the eleventh example, the actual axial load increases while another two are reduced. The final a decreases while b increases.

Basically, when the magnitude of loads is raised from their equilibrium values, the final areas of bone cross-section increase and vice versa. This can be concluded from the table 4.2.

4.4 Summary

In this chapter, the new modeling theory is fully examined by quite a few examples under different loading environment. Several parameters that affect the modeling , such as different bone shape, different loading, different modeling coefficients as well as different model structure (2D, 3D) are studied.

All results of examples shown in this chapter are very satisfactory. Most of examples can only be solved by the new modeling model while Cowin's modeling theory failed to explain them due to changing direction of load or bending load as a result of eccentric loadings.

Some examples in this chapter are very close to the real bone modeling situation. The capability of new modeling model to predict the final shape of those examples proves the flexibility of new modeling model.

It can be concluded from the examples that for the one dimensional problem, the final shape of bone cross-section is insensitive to the modeling

coefficients but quite sensitive to the weighting factors. For 3D problems, it is reversed.

Chapter 5

FEM Modeling Examples

The last chapter discussed the methods to predict strain-history-dependent modeling in long bones by utilizing the new modeling theory. However, all examples examined in that chapter were concerned with the initial regular boundary geometry of long bones..

In reality, the irregular shape, the inhomogeneity of bone material and the anisotropy of structural material properties render the problem of determining bone strain history in terms of closed form solution impossible. This is why the numerical methods are employed to tackle the modeling problems.

The numerical methods adopted in last chapter have their limits. With the complicated bone shape or material properties, the problem of calculating snode position on the surface as well as bone strains at those points are often intractable. Historically the finite element method (FEM) has been used for the stress/strain analysis of solids with the complicated shape or material properties and this is also the case for biomechanics. The FEM has become the method of this choice for computational bone modeling especially for bones with irregular shape or material properties.

In this chapter, several examples are examined by applying the new modeling theory combined with FEM. The assumption underlying this computational model is that the stress-strain behavior at any point at any time is linear in stress and strain, with coefficients dependent only on the current state of modeling, and not on modeling rate. The solution of the problem can be solved iteratively estimating the current modeling state, and then calculating the corresponding strain distribution using the FEM. The modeling rate equations (new modeling theory) can then be used to obtain the values for the new

118

surface, and the bone shape as well as the FEM model will be updated accordingly. This process will go on until the modeling equilibrium is reached.

Like the examples in the last chapter, the parameter study for this FEM model are also undertaken in several aspects:

(1) different sizes of bone cross-section;
(2) different loading (tension, compression, bending , combined tension and bending;
(3) different meshing;

In this chapter, all bones are assumed as isotropic materials and elements are 8-nodes quadratic isoparametric serendipity elements although the program developed in this study can deal with anisotropic linear elastic two-dimensional stress analysis as well as modeling processing for both plane stress or plane strain problems using linear, quadratic or cubic isoparametric serendipity elements. The development of our own FEM program is because most commercial FEM packages can not handle modeling processes as for each time stepping the bone shape will change and requires the update of surface values and may need re-meshing the bone model if the surface elements are out of shape.

5.1 Computer formulation

The FEM model is constructed by combining the FEM with new modeling theory. The assumption underlying the model is that bone obeys Hooke's law in the normal small strain physiological range of loading:

$$\sigma_{ij} = E_{ijkl}\xi_{kl} \qquad\qquad (5\text{-}1)$$

where σ_{ij} = stress tensor components; i,j = 1, 2, 3
ξ_{ij} = strain tensor components; i,j = 1, 2, 3
E_{ijkl} = elastic coefficients tensor

The strain is defined in terms of the displacement as

$$\varepsilon_{ij} = \frac{1}{2}(\frac{\partial u_i}{\partial X_j} + \frac{\partial u_j}{\partial X_i}) \qquad (5\text{-}2)$$

where $\underline{X} = (X_1, X_2, X_3)$ represents a material point while $u_i = u_i(\underline{X}, t) =$ displacement; $i = 1,2,3$.

The stress at any point, $\underline{X}$, time t, must satisfy the equilibrium equations

$$\frac{\partial \sigma_{ji}}{\partial X_j} + F_i = 0 \qquad (5\text{-}3)$$

where $F_i = F_i(\underline{X}, t) =$ body force, $i=1,2,3$. The boundary conditions for the problem can be expressed as

$$T_i^{(n)}(Q, t) = \overline{T}_i(Q, t) \quad \text{on } S_1 \qquad (5\text{-}4a)$$
$$u_i(Q, t) = \overline{u}_i(Q, t) \quad \text{on } S_2 \qquad (5\text{-}4b)$$

where $T_i^{(n)} = \sigma_{ij} n_j =$ stress vector component i corresponding to direction n = (n_1, n_2, n_3), $\overline{T}_i =$ applied boundary traction component i, $\overline{u}_i =$ applied boundary displacement component i, $Q =$ point on boundary

and the surface S is a function of time

$$S(t) = S_1(t) + S_2(t) \qquad (5\text{-}5)$$

The relation between $S(t)$ and $\xi_{ij}(t)$ is defined by the new modeling theory

$$U = C_{ij}(K_{ijkl}\xi_{kl} - \xi_{ij}^{0})\qquad\qquad(5\text{-}6)$$

where U = surface velocity of bone normal to bone surface at point Q and is a function of S(t).

Since the FEM is a widely recognized procedure that is presented in a number of references, the description here is abbreviated to include only those details of particular relevance to the modeling procedure presented.

Global Coordinate System

Generic Coordinate System
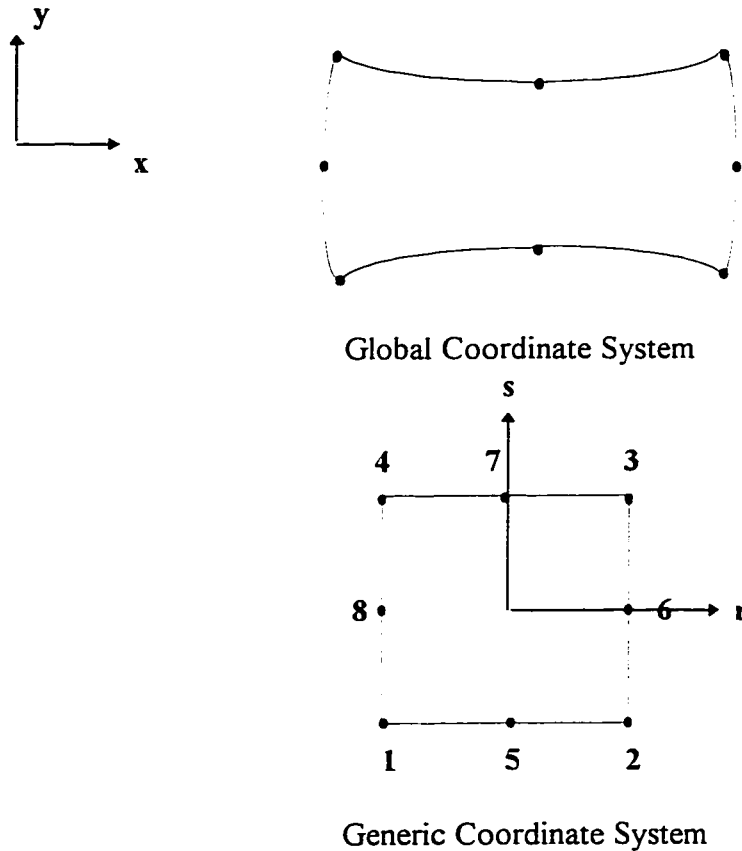
Figure 5.1 8-node modeling finite element shown in global and generic coordinates

The integration of the stiffness matrix is accomplished by using 2x2 Gausian integration rules. In order to calculate the strain and stress at the surface points, Jacobian matrices are not only evaluated at Gauss points but also at surface points, the strain displacement matrix and stress-strain matrix are also evaluated at surface points. If there are two elements which share the same point, the strain or stress at this point will be averaged.

$$
|J| = \begin{vmatrix} \dfrac{\partial x}{\partial r} & \dfrac{\partial y}{\partial r} \\ \dfrac{\partial x}{\partial s} & \dfrac{\partial y}{\partial s} \end{vmatrix}
\tag{5-7}
$$

The direction of surface modeling is taken to be the normal direction to the element's surface at a node.

Figure 5-2   one element in global coordinate system

For the point on the r surface, the components of unit normal direction can be determined by

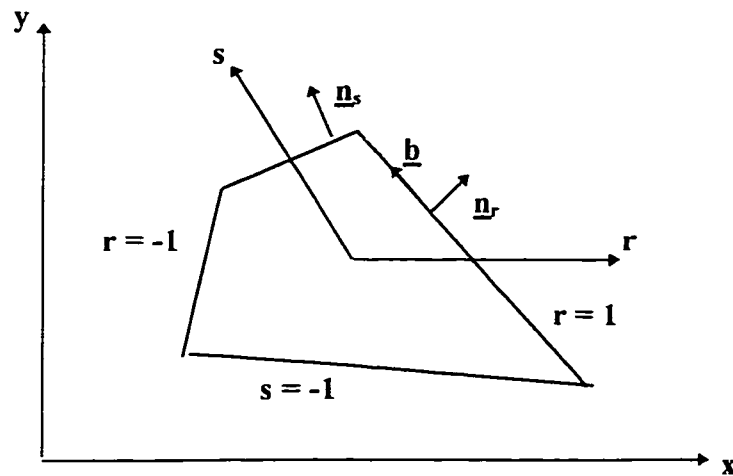$$l_r = \cos(\underline{n}_r, \underline{x}) = \left.\frac{\partial y}{\partial s}\middle/\sqrt{(\frac{\partial x}{\partial s})^2 + (\frac{\partial y}{\partial s})^2}\right. \qquad (r = 1)$$

(5-8)

$$m_r = \cos(\underline{n}_r, \underline{y}) = -\left.\frac{\partial x}{\partial s}\middle/\sqrt{(\frac{\partial x}{\partial s})^2 + (\frac{\partial y}{\partial s})^2}\right. \qquad (r = 1)$$

For the point on the s surface, the components of unit normal direction can be determined by:

$$l_s = \cos(\underline{n}_s, \underline{x}) = -\left.\frac{\partial y}{\partial r}\middle/\sqrt{(\frac{\partial x}{\partial r})^2 + (\frac{\partial y}{\partial r})^2}\right. \qquad (s = 1)$$

(5-9)

$$m_s = \cos(\underline{n}_s, \underline{y}) = \left.\frac{\partial x}{\partial r}\middle/\sqrt{(\frac{\partial x}{\partial s})^2 + (\frac{\partial y}{\partial s})^2}\right. \qquad (s = 1)$$

Those values can be obtained from the Jacobian matrix evaluated at the node. In the case where two elements meet at the same node, the unit normal vectors are averaged by summing them and renormalizing.

A 2D program has been developed to study the FEM modeling model discussed above. The program can be used to do the static stress analysis as well as surface modeling process.

The flow chart of the computational algorithm is shown in Figure 5.3.

```
                    ┌─────────────────┐
                    │   Input Data    │
                    └─────────────────┘
                             │
                             ▼
                    ┌─────────────────┐
         ┌─────────►│      FEM        │
         │          └─────────────────┘
         │                   │
         │                   ▼
         │        ┌────────────────────────┐
         │        │  Compute Nodal modeling │
         │        └────────────────────────┘
         │                   │
         │                   ▼
         │              ╱────────────╲        Y    ┌──────┐
         │         ◄───  Modeling Equilibrium ─────►│ Stop │
         │              ╲────────────╱              └──────┘
         │                   │
         │                  N│
         │                   ▼
         │        ┌────────────────────────┐
         └────────┤     Increment Time     │
                  └────────────────────────┘
```
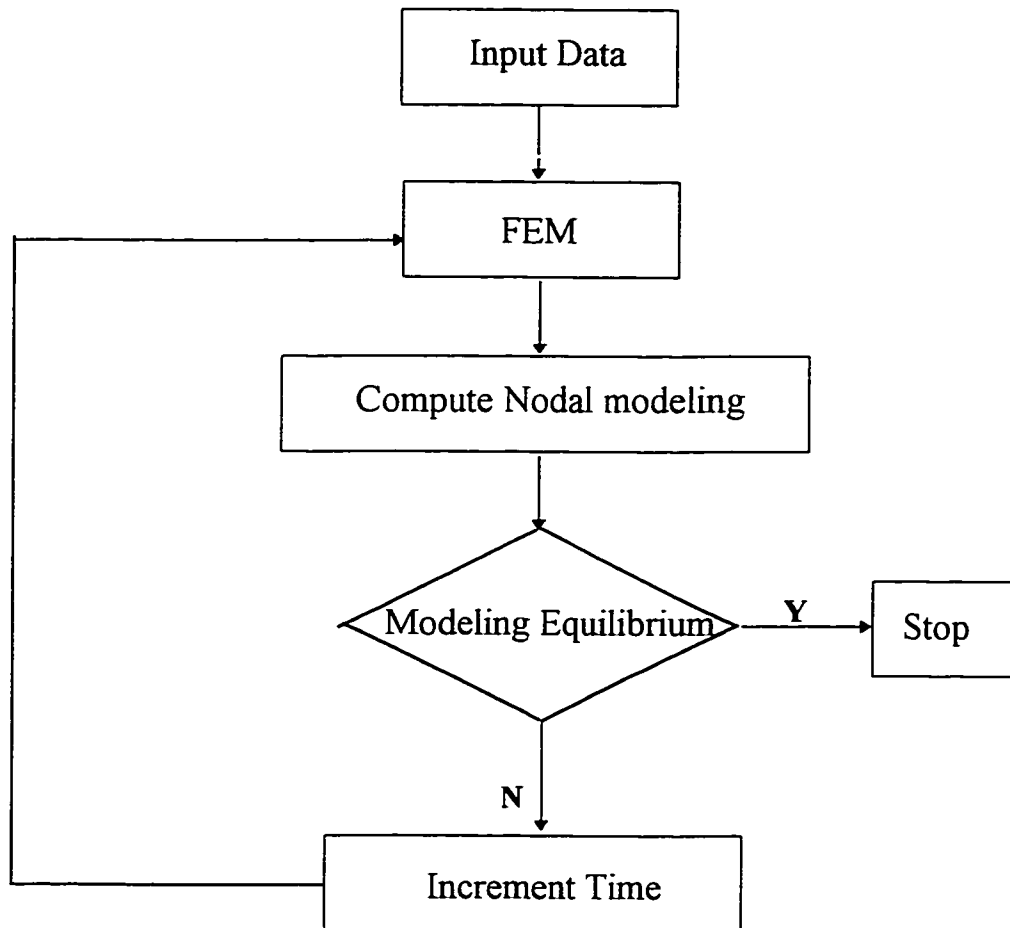
Figure 5-3 Flow chart for computational algorithm

5.2 Applications

The program has been used to solve several examples of adaptive elasticity problems. The FEM model (Figure 5.4) is two dimensional. This is accomplished by choosing its element characteristics in such a way that the dimensions in the mid-longitudinal section and the moments of inertia of the bone in the axis symmetric model are precisely reproduced in the two dimensional model.
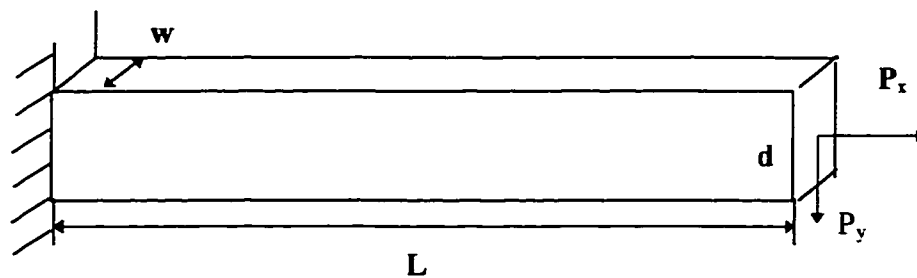

Figure 5.4 The FEM model of simplified bone

In the examples, w is chosen as 1 so that the radius of bone simulated by the model is equal to $\sqrt[4]{\frac{d^3}{3\pi}}$. The bone is assumed as an elastic isotropic material. The examples are classified by their loading environment: (1) $P_y = 0$, $P_x \neq 0$; (2) $P_y \neq 0, P_x = 0$; (3) $P_y \neq 0, P_x \neq 0$; For all examples, the FEM results (Figure 5.3) for the first time step are compared with the results obtained with ANSYS in order to guarantee that stress/strain analysis of the model is correct.

For the loading along the y direction, the load distribution is assumed to be parabolic while for the loading in the x direction, a uniform load distribution is enforced. The units used in the examples are: P_x, P_y (N); w, L, d (mm), E (GPa).

(1) Loading only in the x direction ($P_y = 0$)

Two examples are examined under this kind of loading environment. For the first example, $P_x^0 = 2000$, $P_x = 4000$, $L = 1.0$, $d = 0.01$. E(Young's modulus) $= 0.2 \times 10^{10}$, v (Poisson's ratio) $= 0.3$, $C_1 = 2.0$, $C_2 = C_3 = 0$, $K_{11} = 1.0$, other K_{ij}'s $= 0$. In order to simulate the real bone material, all data for the second example are chosen in a way that the strains produced are within the normal strain range. $P_x^0 = 55000$, $P_x = 110000$, $L = 1.0$, $d = 0.01$. $E = 0.12 \times 10^{11}$, v $= 0.376$ (Cowin et al. 1989), $C_1 = 2.0$, $C_2 = C_3 = 0$, $K_{11} = 1.0$, other K_{ij}'s $= 0$.

The FEM model is shown in Figure 5.5. The beam is divided into four elements and the uniform loading is evenly distributed at three nodes.
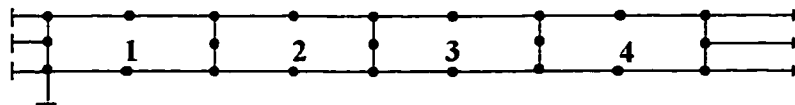

Figure 5.5 The FEM model of cantilever beam with axial loading

In examples, the magnitude of actual strains are twice as big as that of equilibrium strain, bone is supposed to be added simultaneously from both surfaces and the final d is two times of original depth d^0. This is just the case obtained with two examples. The final shape is illustrated in Figure 5.6. During the modeling process, the magnitude of the geometry change is the largest after the first time step and smaller with each succeeding step. This is because the difference between the axial strain in the structure and the axial equilibrium strain is smaller after each time step until the difference is equal to zero, and modeling stops. In the figure, the added bone material is shown by the shaded areas.
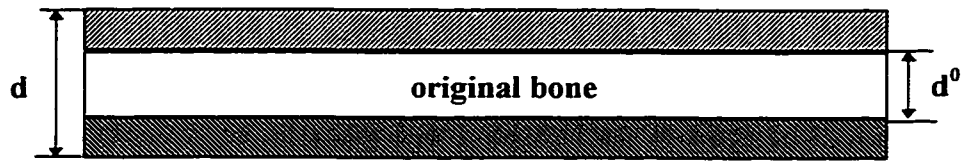
Figure 5.6 Final vs. original bone geometry after modeling

Generally speaking, by changing the constants (C_1, C_2, C_3), the predicted bone shape is made to approximate the experimental or analytic results. The calculations that predicts a final shape closest to the experimental/analytic results yield the modeling rate constants. The choice of C_1, C_2, C_3 also determines the speed at which the modeling process will approach modeling equilibrium. In the calculations of our examples involved in FEM model, only C_1 is used and its value is determined by values which cause the modeling processes to converge.

(2) Loading only in the y direction ($P_x = 0$)

To illustrate another potential modeling problem, the bone subjected to a bending load is studied. Three types of problem are modeled. The first one studies the bone response to an actual load whose magnitude is twice of that of the equilibrium load and in the same direction. The load is uniformly distributed at three end points P_1, P_2, and P_3. The second problem is included here to validate the new modeling model. It is similar to the first one but the actual load is in the opposing direction of the equlibrium load and its magnitude is also twice of that of the equlibrium load. The third example is to examine the effect of different weighting factors on the final shape of bone after modeling equilibrium is reached for the second example.

The FEM is shown in Figure 5.7. The bone is also divided into four elements. The load is lumped to three nodes at the end of the beam.

For the first example, P_1 = P_3 = -100, P_2 = -200, $P_1^0 = P_3^0 = -50$, $P_2^0 = -100$, L = 1.0, d = 0.01. E = 0.2×10^{10}, v = 0.3, $C_1 = -0.5$,
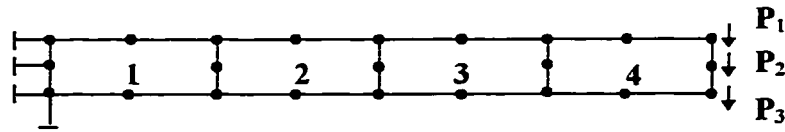
Figure 5.7 The FEM model of a cantilever beam with bending load

$C_2 = C_3 = 0$, $K_{11} = 1.0$, other K_{ij}'s $= 0$. The second example is almost the same except that the actual load is reversed ($P_1 = P_3 = 100$, $P_2 = 200$, $P_1^0 = P_3^0 = -50$, $P_2^0 = -100$,), and $K_{11} = 1$, other K_{ij}'s $= 0$, The third model assumes that $K_{33} = -0.8$ and all other data are the same as those of the second example.

The assumption behind the third example is that as long as the strain mode changes (the actual strain is tensile and the equilibrium strain is compressive or the actual strain is compressive and the equilibrium strain is tensile), the magnitude of the actual strain has to be larger than that of the equilibrium strain to regain the equilibrium state because the weighting factor is 0.8.

Since for the first and second examples, the magnitude of actual load is twice as much as that of the equilibrium load, the final depth d_1 of the bone should be $\sqrt{2}$ times original d^0 in order to maintain the equilibrium strain. For the third examples, d_2 should be $\sqrt{2K_{11}}$ times original d^0 (Figure 5.8).

All examples gave results very close to the analytical solutions. The errors are less than 1/10000.
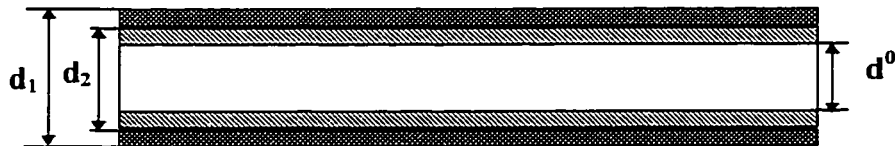

Figure 5.8 Final & original geometry of bone where d^0 is the original depth, while d_1 is the final depth for the first and second examples and d_2 is the final depth for the third example

(3) Loading in both the x and the y directions

In order to fully validate the new modeling theory under a more complicated loading environment, the third group of problems are examined. The beam was loaded at the free end in both the x direction and the y direction while the equilibrium strain at all points are tensile. Cowin's theory can not solve this problem because the actual strains at the bottom of the beam are compressive which are opposite in the direction to the equilibrium strains at the same place. The beams of different size under different loading environment are modeled. The first example is shown in Figure 5.9.
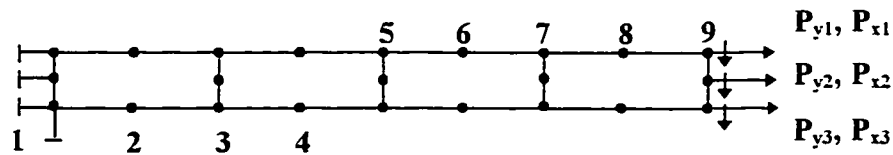

Figure 5.9 The FEM model of a cantilever beam with tip loads at both the x and y directions

The actual loads: $P_{x1} = P_{x2} = P_{x3} = 20000$, $P_{y1} = P_{y3} = 0$, $P_{y2} = -100$. The equilibrium loads: $P_{x1}^0 = P_{x2}^0 = P_{x3}^0 = 20000$, $P_{y1}^0 = P_{yx2}^0 = P_{y3}^0 = 0$. The size of beam: $L = 1.0$, $d^0 = 0.01$. The coefficient and weights: $C_1 = 0.2$, $C_2 = C_3 = 0$, $K_{11} = -1$, other K_{ij}'s = 0. The material properties: $E = 2 \times 10^9$, $v = 0.3$.

The result of strains at different surface nodes after first time step is compared with the result obtained from ANSYS. Two results are listed in Table 5.1 and shows good agreement between the two formulations.

Table 5.1 Strains at different surface points obtained from FEM model and ANSYS in Figure 5.9

$\times 10^{-6}$	1	2	3	4	5	6	7	8	9
FEM	-4.3533	374	750	1124	4500	4124	3751	3376	3003
ANSYS	-4.3288	N/A	750	N/A	4500	N/A	3750	N/A	3001
ERR	0.6%	N/A	0.0%	N/A	0.0%	N/A	0.2%	N/A	0.6%

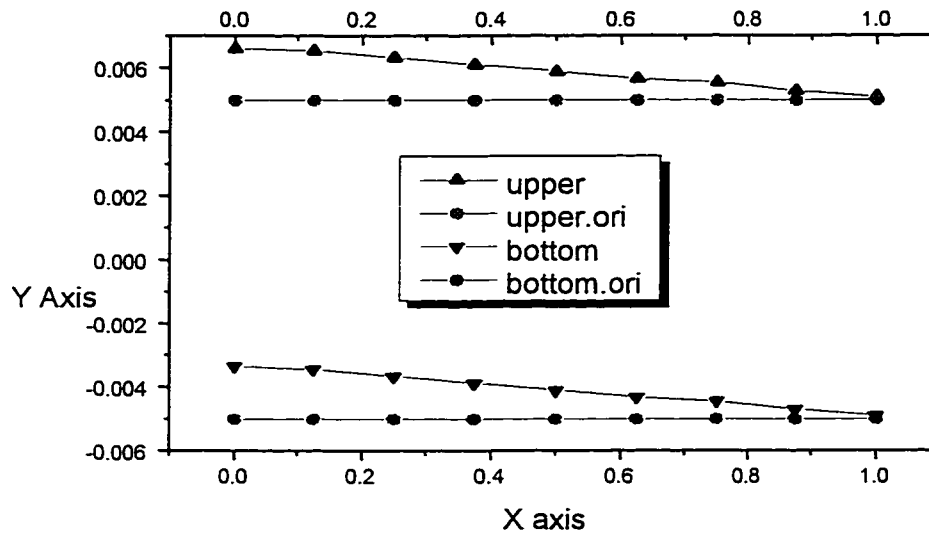The final shape Vs original geometry are shown in Figure 5.10.

Figure 5.10 The original geometry of bone (between two parallel straight lines: upper.ori and bottom.ori) vs. final geometry (between two arch lines: upper and bottom) for problem in Figure 5.9

The final shape of bone indicates that while the points at which the load was applied did not move much, the surface at the top of the bone moved up in

order to reduce the strains to return to the equilibrium strains while the nodes at the bottom of bone also moved up so that the actual strain at those bottom points gradually change the strain pattern from the negative to the positive.

The second example in third group is the similar to the first but the depth of beam is different. The d^0 of the first example is 0.01 while the d^0 of the second example is 0.1. As a result, finer meshing is needed for the second FEM model. By trial and error, the 10x4 meshing as shown in Fgure 5.11 is adopted.
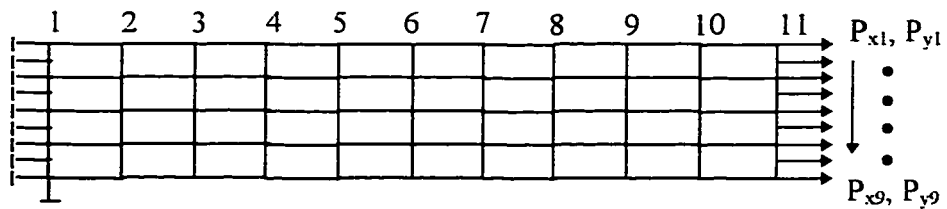

Figure 5.11 The FEM model of cantilever beam with parabolically load distribution in the y direction and uniformly load distribution in the x direction

For the second example, the size of bone: $L = 1.0$, $d^0 = 0.1$; The actual loading: $P_{x1} = P_{x9} = 37500$, and $P_{x2} = P_{x3} = P_{x4} = P_{x5} = P_{x6} = P_{x7} = P_{x8} = 75000$, $P_{y1} = P_{y9} = -7.8125$, $P_{y2} = P_{y8} = -531.25$, $P_{y3} = P_{y7} = -484.375$, $P_{y4} = P_{y6} = -1156.25$, $P_{y5} = -640.625$. The equilibrium loading: $P_{x1}^0 = P_{x9}^0 = -37500$, $P_{y1}^0 = P_{y2}^0 = P_{y3}^0 = P_{y4}^0 = P_{y5}^0 = P_{y6}^0 = P_{y7}^0 = P_{y8}^0 = P_{y9}^0 = 0$; The coefficients and weight factors: $C_1 = 2$, $C_2 = C_3 = 0$, $K_{11} = -1$, other K_{ij}'s $= 0$. The material properties: $E = 2 \times 10^9$, $v = 0.3$.

The total amount of actual load in x direction is 600000, and the total amount of actual load in y direction is -5000. The total amount of equilibrium load in x direction is -600000, and the total amount of equilibrium load in y direction is 0. The actual load distribution in the y direction is parabolic while both actual and equilibrium load distribution in the x direction are uniform.

The result of strains at different surface nodes after the first time step is also compared with the result obtained from ANSYS. Two results are listed in Table 5.2. It is obvious that the results for the middle surface points from FEM and ANSYS are very close while the difference between two results are relatively large at the end surface points of the beam (2%).

The final and original geometry of bone are shown in 5.12. The pattern is quite similar to the one in Figure 5.10.
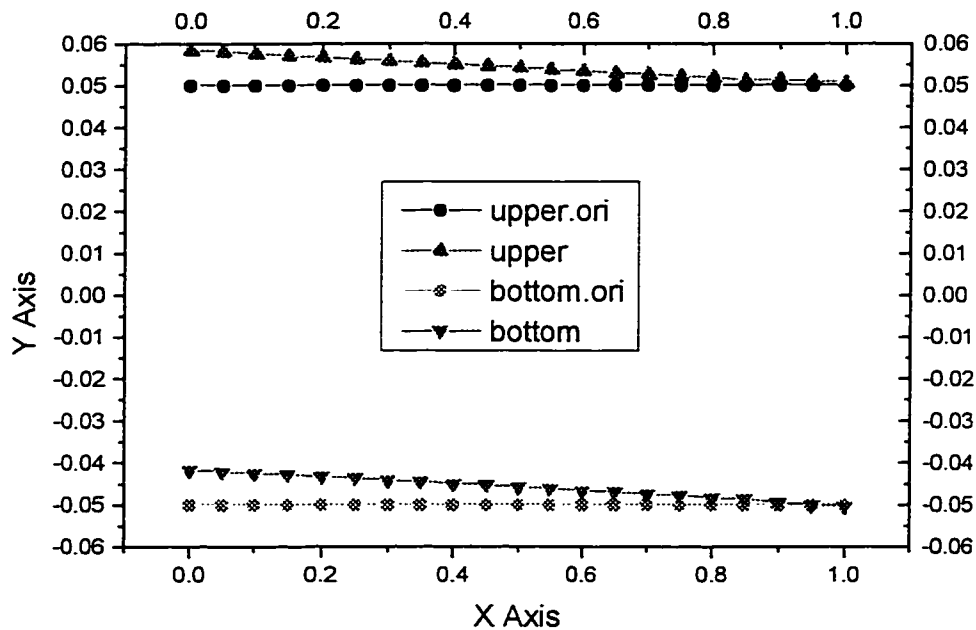

Figure 5.12 The original geometry of bone (between two parallel straight lines: upper.ori and bottom.ori) vs. final geometry (between two arch lines: upper and bottom) for problem in Figure 5.11

Table 5.2 Strains at different surface points obtained from FEM model

and ANSYS in Figure 5.11

$x10^6$	Point 1	Point 2	Point 3	Point 4	Point 5
FEM	44971	43563	42002	40497	38999
ANSYS	44954	43557	42004	40497	38999
ERR	0.04%	0.01%	0%	0%	0%

$x10^6$	Point 6	Point 7	Point 8	Point 9	Point 10	Point 11
FEM	37501	35997	34509	32982	31564	31388
ANSYS	37500	36001	34495	33034	31376	30869
ERR	0%	0.01%	0.04%	0.1%	0.6%	2%

5.3 Comparison between FEM model results and Experimental data

As stated by Cowin (1993), there is significant lack of quantitative data on the relationship between the strain history a bone tissue experiences and the resulting bone tissue modeling. The strain history data should extend over a time period on the order of a year since the time required to complete a major bone modeling may be this long or longer. Even for some famous experiments done by Lanyon et al.(1982), the extent of the data base is not sufficient to select among the various proposed modeling rate equations and bone stimuli. Most modeling experiments are qualitative rather than quantitative. These qualitative studies do not give much help to quantitatively oriented modeling theories.

Due to limits of quantitative experimental data available, the comparison between FEM model results and the experiments in this section is only qualitative rather than quantitative and the comparison is also relatively loose.

A study was conducted by Hoshaw (1992) to investigate the hypothesis that mechanical loading of implants and the consequent stress and strain fields influence bone modeling and remodeling at the bone-implant interface. Two implants were placed in each of 20 canine tibiae, allowed to heal for one year, and then subjected to a controlled loading protocol. Implants in the left limb were loaded in axial tension and implants in the right limb served as unloaded control (Figure 5.13)
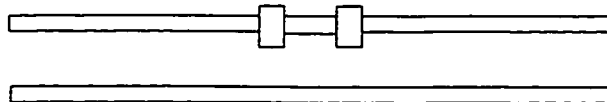
Figure 5.13 Schematic diagram of two implants placed in the bone

A single implant FEM model is shown in Figure 5.14. The fixed end boundary condition was adopted to account for "missing bone" and a couple was introduced which equaled the applied bending moment.
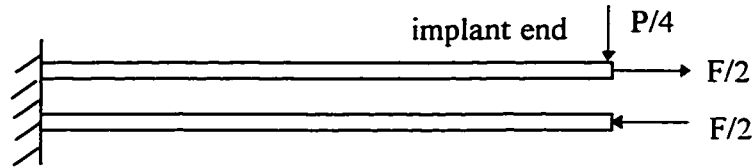
Figure 5.14 Schematic diagram of single implant finite element model.

Figure 5.15 shows scanning electron micrographs of the bone-implant interface and the schematic diagram of bone-implant interface indicating regions of interest for modeling measurements

The bone modeling pattern shown in Figure 5.15 is qualitatively similar to the FEM model results in Figure 5.10 and Figure 5.12. Figure 5.15 shows the bone resorbed around the implant neck while the new bone was added to the endosteal surface around the bottom of the implant. Assuming the boundary condition of the beam end at which the implant is located were fixed, it is equal to the case that the load would be applied at the other end which would become the free end and the load would reverse in direction. This loading pattern is similar to those shown in Figure 5.9 and Figure 5.11 and the modeling pattern in Figure 5.15 is therefore similar to the cases shown in Figure 5.10 and 5.12. This similarity proves that qualitatively the modified modeling theory can more or less be used to explain the experimental results although the much work should be done to exactly match the bone geometry and loading environment.

5.4 Summary

In this chapter, the FEM model was developed to validate the modified modeling theory. Several examples are studied to show the capabilities of new theory when different loading conditions are considered while under those loading environment, the Cowin's modeling theory failed to explain the bone modeling patterns of those examples.

Proximal Control

3S212

Proximal Loaded
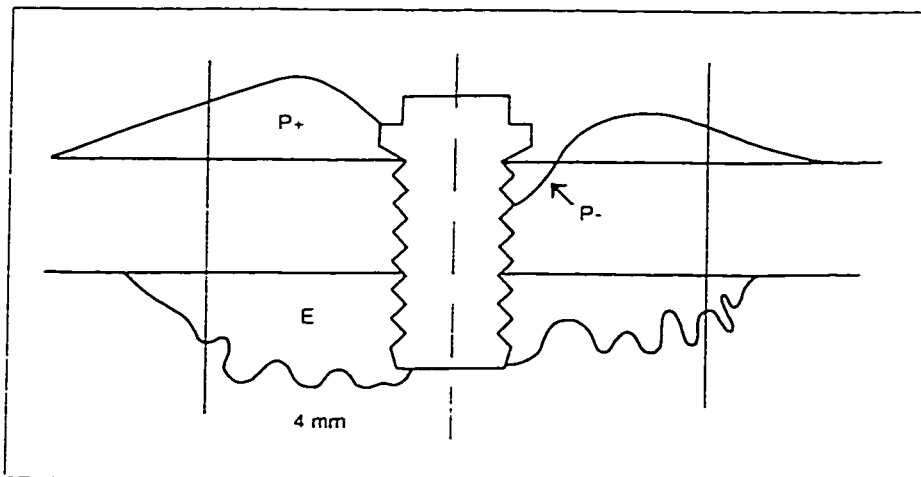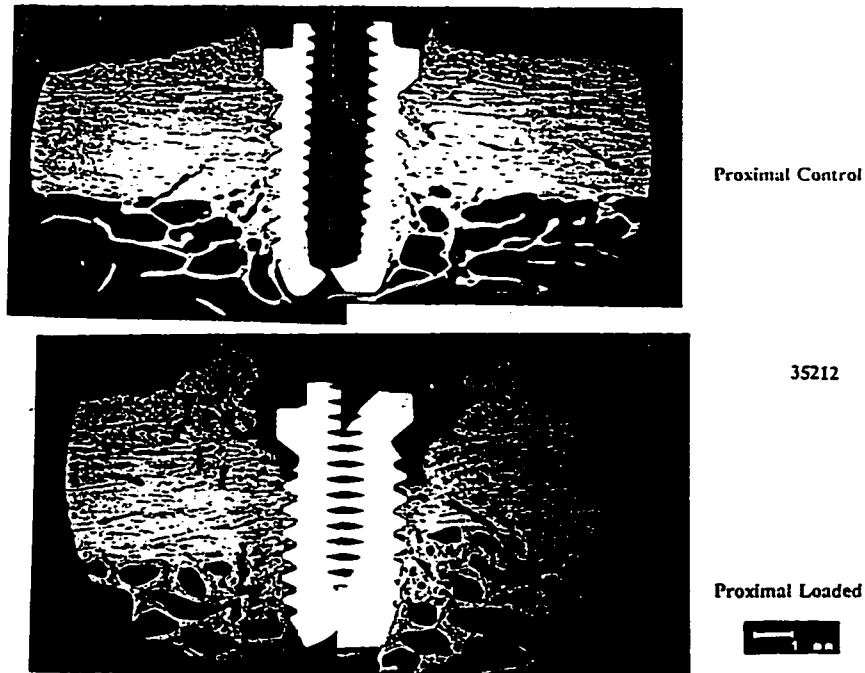
Figure 5.15 Schematic diagram of bone implant interface indicating regions of interest for modeling measurements. P+ means periosteal bone increase and P- indicates that periosteal bone resorption. E means endocortical surfaces (Hoshaw, 1992)

The FEM model results are also compared with the experiment results. The similarities between those results indicates that the new modeling theory can qualitatively be used to explain certain modeling phenomenon.

Chapter 6

Discussion and Conclusion

The investigation of bone as a material that can adapt its architecture as a consequence of its functional requirement was initiated over a century ago. And yet, the solutions to practical clinical problems in orthopedics and orthodontics still await an understanding of the functional adaptation of bone.

Progress toward the solution of these clinical problems will come from the development of theoretical models which fall in two categories: biological and mathematical. Traditionally two kinds of theory are developed separately. Biological ones focus on explaining the bone adaptive behavior qualitatively while the mathematical models try to provide the quantitative solution to those clinical problems with little consideration of the biologic basis.

The mathematical models can be also divided into remodeling theories, which describe the internal modeling of bone, and modeling theories which are used to explain the external modeling of bone. The research described in the previous five chapters put emphasis on the mathematical model and modeling theory specifically but integration of the biological basis with the theory is also considered.

The reason why only modeling theory is studied is that the remodeling theory which focuses on the cancellous bone is much more complicated due to the lack of understanding of adaptive behavior of cancellous bone and associated nonlinear elasticity. Up to now, there has been little success with the internal remodeling models.

In this work a new modified modeling model is developed. The new theory is based on Cowin's modeling theory and adopts the strain tensor as a mechanical sensor which is demonstrated to be a rational choice. By association of the new model with various numerical techniques, several computer

simulation models are presented to validate the new model and simulate some interesting idealized clinical problems.

The difference between the new theory and Cowin's one is that the new theory introduces weighting factors to reflect the different effects of different strain components on adaptation while Cowin's theory intrinsically assumes that tensile strains and compressive strains play the same role in bone modeling and does not have experimental support.

The new theory has its advantages and drawbacks. Since weighting factors are introduced to the model, the unknowns have increased due to the lack of data from the experiments. But as long as the manner in which the internal transducer signal affects cellular activity and recruitment is identified, the values of weighting factors will become available. At this stage, the new theory can be in a relatively simple form which requires only one or two weight factors to be assumed because of very regular nature of loading pattern on long bones.

The new model presented is shown to have some advantages including:

- overcomes the flaw in the existing modeling theories
- has flexibility over existing theories
- reflects biological factors in the model which are not considered by the existing theory

The new model is very capable of handling bone modeling with different bone geometries and complicated loading environment. All examples presented in Chapter 4 and Chapter 5 show an excellent agreement to the analytical solutions or qualitatively to the experimental facts. The results obtained in those examples are very close to real bone modeling situation and provide very promising information on the method to simulate the bone modeling in the real clinical practice. Most of examples can not be solved by Cowin's or other existing theories.

The difficulty with the current study is that there are no enough quantitative animal studies which can be used to determine the bone strain history. In many animal model studies a statement like "the animals were placed

on a treadmill for one hour each day for six months" is the extent of the documentation of the bone tissue history (Cowin, 1993). The need of quantitative experimental data is crucial to the development of new modeling theories which also requires the thorough understanding the mechanism of bone modeling signal transducer. These are proved to be roadblocks to the current study.

The stability of numerical methods adopted over the iterative modeling process is another crucial fact to apply the modeling theory to the real clinical problems. In the current study, only one dimensional modeling (the modeling only happens on the surfaces parallel to axis of long bone) are modeled. When two dimensional modeling (modeling occurs on all surfaces as shown in Figure 6.1) are considered, the FEM can not guarantee the convergence of the time stepping.
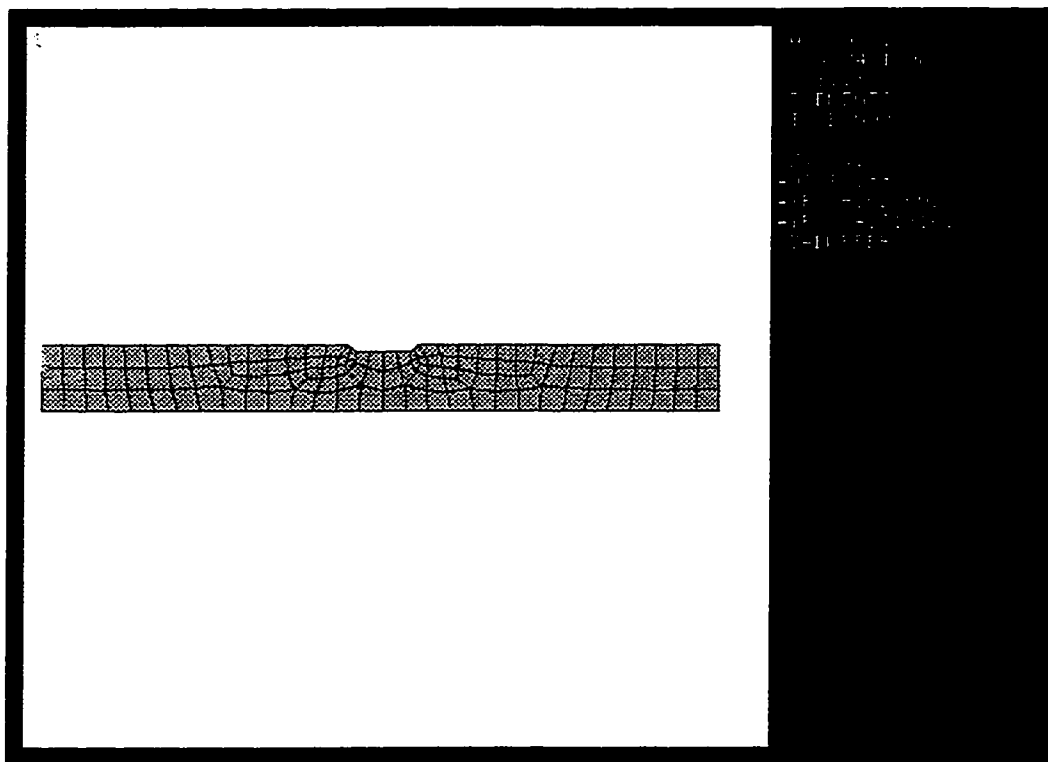

Figure 6.1 Double modelings (in slot area, three surfaces) example.

The quantitative animal modeling studies such as implants put in the dog leg and stability of FEM on double modeling problems are the further work to be done.

References

Ahlberg, J.H., Nilson, E.N., Walsh, J.L. The theory of spline and their application, 1967, Academic press.

Akeson, W. H., Woo, S. L-Y and Rutherford, L. (1976) The effects of rigity of internal fixation plates on long bone remodeling. Acta Orthop. Scand. Vol. 47. 241-249.

Ascenzi, A. , Boyde, A. , Barbos, M. P. and Carando, S. (1987) Micro-biomechanics vs macro-biomechanics in cortical bone. a micromechanical investigation of femurs deformed by bending. J. of Biomechanics. Vol. 20, No. 11/12. 1045-1053.

Ascenzi, A. , Baschier, P. and Benvenuti, A. (1994) The torsional properties of single selected osteons. J. of Biomechanics. Vol. 27, No. 7. 875-884.

Ashman, R. B. , Cowin, S. C. , Buskirk, W. C. Van and Rice, J. C. (1984) A continuous wave technique for the measurement of the elastic properties of cortical bone. J. of Biomechanics. Vol. 17, No. 5. 349-361.

Ashman, R. B. and Buskirk, W. C. Van (1987) The elastic properties of a human mandible. Advances in Dental Research. Vol. 1. 64-67.

Beaupre, G. S. and Hayes, W. C. (1985) Finite element analysis of a three-dimensional open-celled model for trabecular bone. J. of Biomechanical Engineering. Vol. 107, August. 249-256.

Bowman, S. M. , Keaveny, T. M. , Gibson, L. J. , Hayes, W. C. and McMahon, T. M. (1994) J. of Biomechanics. Vol. 27, No. 3. 301-310.

Burger, E. H. , Klein-Nulend J. and Veldhulizen, J. P. (1991) Modulation of osteogenesis in fetal bone rudiments by mechanical stress in vitro. J. of Biomechanics. Vol.24, Suppl. 1. 101-109.

Burr, D. B. (1993) Remodeling and repair of fatigue damage. Calcified Tissue. Vol 53, S75-81.

Buskirk, W. C. Van and Ashman, R. B. (1981) The elastic moduli of bone. Mechanical Properties of Bone, Cowin, S. C. Ed., American Society of Mechanical Engineers, New York. 131-143.

Burkirk, W. C. Van , Cowin, S. C. and Ward, R. N. (1981b) Altrsonic measurement of orthotropic elastic constants of bovine femoral bone. J. of Biomechanical Engineering. Vol. 103. 67-81.

Carter. D. R. , Hayes, W. C. and Schurman, D. J. (1976) Fatigue life of compact bone-II. Effects of Microstructure and density. J. of Biomechanics. Vol. 9. 211-218.

Carter, D. R. and Hayes, W. C. (1976) Bone compressive strength: the influence of density and strain rate. Science. Vol. 94. 1174-1181.

Carter, D. R. and Hayes, W. C. (1977) The compressive behavior of bone as a two-phase porous structure. The Journal of Bone and Joint Surgery. Vol. 59-A, No. 7, October. 954-962.

Carter, D. R., Vasu, Spengler, D. M. and Dueland, R. T.(1979) Stress fields in the unplated and plated canine femur calculatyed from in vivo strain measurements. J. of Biomechanics. Vol. 14, 63-70.

Carter, D. R., Smith, D. J., Spengler, D. M., Daly, C. H. and Frankel, V. H. (1980) Measure and Analysis of in vivo bone strains on the canine radius and ulna. J. of Biomechancis. Vol. 13. 27-38.

Carter, D. R., Harris, W. H., Vasu, R. and Caler, W. E. (1981) The mechanical and biological response of cortical bone in vivo strain histories. Mechancial Properties of Bone, Ed. Cowin, S. C.

Carter, D. R.(1984) Mechanical loading histories and cortical bone remodeling. Calcified Tissue. Vol. 36. S19-S24.

Carter, D. R., Fyhrie, D. P. and Whalen, R. T. (1987) Trabecular bone density and loading history: regulation of connective tissue biology by mechanical energy. J. of Biomchanics. Vol. 20, No. 8. 785-794.

Carter, D. R., Orr, T. E. and Fyhrie, D. P. (1989) Relationships between loading history and femoral cancellous bone arthitecture. J. of Biomechanics. Vol. 22, No. 3. 231-244.

Chapra Steven C., Canale Raymond P., (1988) Numerical methods for engineers.McGraw-Hill.

Cheal, E. J., Hayes, W. C., White, A. A. and Perren, S. M. (1985) Stress analysis of compression plate fixation and its effects on long bone remodeling. J. of Biomechanics. Vol. 18, No. 2. 141-150.

Choi, K. , Kuhn, J. L. , Ciarelli, M. J. and Goldstein (1990) The elastic moduli of human subchondral, trabecular, and cortical bone tissue and the size-dependency of cortical bone modulus. Vol. 23, No.11. 1103-1113.

Churches, A. E., Howleett, C. R. and Waldron, K. J.(1979) The response of living bone to controlled time-varing loading : method and preliminary results. J. of Biomechanics. Vol. 12. 35-45.

Churchies, A. E., Howlett, C. R. and Ward, G. W. (1980) Bone reaction to surgical drilling and pinning. J. of Biomechanics. Vol. 13, 203-209.

Cowin, S. C. and Hegedus, D. H. (1976) Bone remodeling I: theory of adaptive elasticity. J. of Elasticity. Vol. 6, No. 3, July. 313-326.

Cowin, S. C. and Nachlinger, R. R. (1978) Bone remodeling III: uniqueness and stability in adaptive elasticity theory. J. of Elasticity. Vol. 8, No. 3, July. 285-295.

Cowin, S. C. and Buskirk W. C. Van (1978) Internal bone remodeling induced by a medullary pin. J. of Biomechanics. Vol. 11. 269-275.

Cowin, S. C. and Buskirk, W. C. Van (1979) Surface bone remodeling induced by a medullary pin. J. of Biomechanics. Vol. 12. 269-276.

Cowin, S. C. and Firoozbakhsh, K. (1981a) Bone remodeling of diaphysial surfaces under constant load: theoretical predictions. J. of Biomechanics. Vol. No. 7. 471-484.

Cowin, S. C. (1981b) Continuum models of the adaption of bone to stress, Mechanical Properties of Bone, Cowin, S. C. Ed., American Society of Mechanical Engineers, New Yorks, 193-210.

Cowin, S. C. (1984) Mechanical modeling of the stress adaptation process in bone. Calcified Tissue. Vol. 36, S98-103.

Cowin, S. C. (1985) The relationship between the elasticity tensor and the fabric tensor. Mechnaics of Materials. 4. 17-147.

Cowin, S. C. and Hart R. T. (1985) Functional adaptation in long bones: establishing in vivo values for surface remodeling rate coeffecients. J. of Biomechanics. Vol. 18, No. 9. 665-684.

Cowin, S. C. (1986) Wolff's law trabecular architecture at remodeling equlibrium. J. of Biomechanical Engineering. Vol. 108, Februry. 83-88.

Cowin, S. C. (1987) Bone remodeling of diaphyseal surfaces by torsional loads: the theoretical predictions. J. of Biomechanics. Vol 20, No. 11/12. 1111-1120.

Cowin, S. C. and Mehrabadi, M. M. (1989a) Identification of the elastic symmetry of bone and other materials. J. of Biomechanics. Vol. 22, No. 6/7. 503-515.

Cowin, S. C. (1989b) Bone mechanics. CRC Press, Boac Raton, Florida.

Cowin, S. C. , Moss-Salentijn, L. and Moss, M. L. (1991) Candidates for the mechanosensory system in bone. J. of Biomechanical Engineering. Vol. 113, May. 191-197.

Cowin, S. C. , Sadegh, A. M. and Luo G. M. (1992) An evolutionary Wolff's law for trabecular architecture. J. of Biomechanical Engineering. Vol. 114, February. 129-136.

Cowin, S. C. (1992) Nature's structural engineering of bone on a daily basis. Proceedings of the XVIIIth International Congress of Theoretical and Applied Mechanics. 145-158.

Cowin, S. C. , Arramon Y. P. , Luo, G. M. and Sadegh A. M. (1993) Chaos in the discrete-time algorithm for bone-density remodeling rate equations. J. of bIomechanics. Vol. 26, No. 9. 1077-1089.

Cowin, S. C. (1993) Bone stress adaptation models. J. of Biomechanical Engineering. Vol. 115, November. 528-533.

Crolet, J. M. , Aoubiza, B. and Meunier, A. (1993) Compact bone: numberical simulation of mechanical characteristics. J. of Biomechanics. Vol. 26, No. 6. 677-687.

Curry, J. D. (1959) Fifference in tensile strength of bone of different histological types. J. of Anat. Vol. 93, 87-97.

Curry, J. D. (1984a) What should bones be designed to do? Calcified Tissue. Vol. 36, S7-S10.

Curry, J. D. (1984b) Can strain give adequate information for adaptive bone remodeling? Calcified Tissue. Vol. 36, S118-122.

Currey, J. (1984c) The mechanical adaptations of bones. Princeton University Press.

Dalstra, M. , Huiskes, R., Odgaard, A. and Erning, L. Van (1993) Mechanical and textural properties of pelvic trabecular bone. J. of Biomechnaics. Vol. 26, No. 4/5. 523-535.

Danielsen, C. C., Mosekilde, L. and Svenstrup, B. (1993) Cortical bone mass, composition, and mechanical properties in female rates in relation to age, long-term ovariectomy, and estrogen substitution. Calcifid Tissue. Vol. 52, 26-33.

Deligianni, D. D., Maris, A. and Missirlis, Y. F. (1994) Stress relaxation behaviour of trabecular bone specimens. J. of Biomechanics. Vol.27, No. 12. 1469-1476.

Firoozbakhsh, K. and Cowin, S. C. (1980) Devolution of inhomogeneities in bone structure--predictions of adaptive elasticity theory. J. of Biomechnaical Engineering. Vol. 102, November. 287-293.

Frost, H. M. (1963) Bone remodeling dynamics. Charles C thomas Publisher, Spingfield, Illinois.

Frost, H. M. (1986) Intermediary organization of the skeleton, Volume I. CRC Press, Inc. Boca Raton, Florida.

Frost, H. M. (1983) A determinant of bone architecture. Clinical Orthopaedics and Related Research. Vol. 175, May. 287-292.

Frost, H. M. (1986) Intermediary organization of the skeleton, Volume II. CRC Press, Inc. Boca Raton, Florida.

Frost, H. M. (1987) Osteogenesis imperfecta. Clinical Orthopaedics and Related Research. Vol. 216, March. 281-297.

Frost, H. M. (1987) The mechanostat: a proposed pathogenic mechanism of osteoporoses and the bone mass effects of mechanical and nonmechanical agents. Bone and Mineral. Vol. 12, 1987. 73-85.

Fung, Y. C. (1990) Biomechanics, motion, flow, stress, and growth, Spinger-Verlag New York, Inc.

Fung, Y. C. (1993) Biomechanics, mechanical properties of living tissues. Second Ed., Spinger-Verlag New York, Inc.

Fyhrie, D. P. and Carter, D. R. (1986) A unifying principle relating stress to trabecular bone morphology. J. of Orthopaedic Research. Vol. 4, No.3. 304-317.

Geesink, R. G. T. (1990) Hydroxyapatite-coated total hip protheses. Clinical Orthopaedics and Related Research. No. 261, December. 39-58.

Gies, A. A. and Carter, D. R. (1982) Experimental determination of whole long bone sectional properties. J. of Biomechanics. Vol.15. No.4. 297-303.

Goldstein, S. A. , Matthews, L. S. , Janet, M. D. , and Hollster, S. J. (1991) Trabecular bone remodeling: an experimental model. J. of Biomechanics. Vol. 24, Suppl. 1, 135-150.

Goldstein, S. A., Goulet, R., and McCubbrey, D. (1993) Measurement and significance of three-dimensional architecture to the mechanical integrity of trabecular bone. Calcified Tissue. Vol. 53, S127-133.

Goodship, A. E., Lanyon, L. E. and Mcfic, H. (1989) Functional adaptation of bone to increased stress. J. of bone and joint surgery. Vol. 61A, 539-546.

Goulet, R. W. , Goldstein , S. A. , Ciarelli, M. J. , Kuhn, J. L. , Brown, M. B. and Feldkamp, L.A (1994) The relationship between the structural and orthogonal compressive properties of trabecular bone. J. of Biomechanics. Vol.27, No. 4. 375-389.

Harrigan, T. P. and Hamilton, J. J. (1992) An analytical and numberical study of the stability of bone remodeling theories: dependence on microstructural stimulus. J. of Biomechanics. Vol. 25, No. 5. 477-488.

Harrigan, T. P. and Hamilton, J. J. (1993) Finite element simulation of adaptive bone remodeling: a stability criterion and a time stepping method. Internal Journal for Numberical Methods in Engineering. Vol. 36, 837-854.

Harrigan, T. P. and Hamilton, J. J (1994) Necessary and sufficient conditions for global stability and uniqueness in finite element simulations of adaptive bone remodeling. Int. J. Solids structures. Vol. 31, No. 1. 97-107.

Hart, Richard Trapnell (1983) Quantitative response of bone to mechanical stress. Ph. D. Thesis, Case Western Reserve University.

Hart, R. T. , Davy, D. T. and Heiple, K. G. (1984a) A computational method for stress analysis of adaptive elastic materials with a view toward applications in strain-induced bone remodeling. J. of Biomechanical Engineering. Vol. 106, November. 342-350.

Hart, R. T., Davy. D. T. and Heiple, K. G. (1984b) Mathematicla modeling and numerical solution for functionally dependent bone remodeling. Calcified Tissue. S104-109.

Hart, R. T. (1990) A theoretical study of the influence of bone maturation rate on surface remodeling prediction : idealized models. J. of Biomechanics. Vol. 23, No.3. 241-257.

Hasegawa, K., Turner, C. H., Burr, D. B. (1994) Contribution of collagen and mineral to the anisotropy of bone. Calcified Tissue. Vol. 55, 381-386.

Hastings, G. W. and Ducheyne, P. (1984) Natural and living biomaterials. CRC Press, Boca Raton, Florida.

Hegedus, D. H. and Cowin, S. C. (1976) Bone remodeling II: small adaptive elasticity. J. of Elasticity. Vol. 6, No. 4, October. 337-352.

Heiner, J. P., Manley, P., Kohles, S., Ulm, M., Bogart, L., Vanderby, R.(1994) Ingrowth reduces implant-to-bone relative displacements in cranine acebular protheses. J. of Orthopaedic Research. Vol. 12, No. 5, 657-664.

Henry, H. Jones, James, D. Priest, Wilson, C. Hayes, Carol, C. T. and Donald, A. Nagel (1977) Humeral Hypertrophy in response to exercise. J. of Bone and Joint surgery. Vol. 59-A, No.2. March. 204-208.

Hert, J., KuCera, P. Vavra, M. and Volenik, V. (1965) Compression of the mechanical properties of both the primary and Haversian bone tissue. Acta. Anat. Vol. 61, 412-423.

Hert, J., Pribycova, E. and Liskova, M. (1972) Reaction of bone to mechanical stimuli, part 3, microstructure of compact bone of rabbit tibia after intermittent loading. Acta anat, Vol. 82, 218-230.

Hert, J. (1994) A new attempt at the interpretation of the functional architecture of the cancellous none. J. of Biomechanics. Vol. 27, No. 2. 239-242.

Hollister, S. J. , Fyhrie, D. P. , Jepsen, K. J. and Goldstein, S. A. (1991) Application of homogenization theory to the study of trabecular bone mechanics. J. of Biomechanics. Vol. 24, No. 9. 825-839.

Hollister, S. J. , Kikuchi and Goldstein (1993) Do bone ingrowth processes produce a globally optimized structure. J. of Biomechanics. Vol. 26, No. 4/5. 391-407.

Hoshaw, Suan Joy (1992) Investigation of bone modeling and remodeling at a loaded bone-implant interface. Ph. D. thesis. Rensselaer Polytechnic Institute, Troy, New York.

Hoshaw, S. J. , Brunski, J. B. and Cochran, G. V.B. (1994) Mechanical loading of Branemark implants affects interfacial bone modeling and remodeling. The International Journal of Oral & Maxillofacial Implants. Vol. 9, No. 3. 345-359.

Hrudey, Jerry, Privte note.

Huiskes, R. (1982) On the modeling of long bone in structureal analysis. J. of Biomechanics. Vol. 15. 65-69.

Huiskes, R. and Nunamaker, D. (1984) Local stresses and bone adaptation orthopedic implants. Calcified Tissue. S110-117.

Huiskes, R., Weinans, H. , Grootenboer, H. J. , Dalstra, M. , Fudala, B. and SLooff T. (1987) Adaptive bone-remodleing theory applied to prothetic-design analysis. J. of Biomechanics. Vol. 20, No. 11/12. 1135-1150.

Huiskes, R., Weinans, H. and Dalstra, M. (1989) Adaptive bone remodeling and biomechanical design considerations for noncemented total hip arthroplasty. Orthopedics. Vol. 12, No. 9. 1255-1267.

Huiskes, R. (1990) The various stress patterns of press-fit, ingrown, and cemented femoral stems. Clinical Orthopaedics and Related Research. No. 261, December. 27-38.

Janes, G. C., Collopy, D. M., Price, R., Sikorski, J. M. (1993) Bone density after rigid plate fixation of tibial fractures. *J. of Bone and Joint Surgery.* Vol. 75-B, No. 6, November. 915-917.

Jaworski, Z. F. G., Liskova-Kiar, M. and Uhthoff, H. K. (1980) Effect of long - term immobilisation on the pattern of bone loss in older dogs. *J. of Bone and Joint Surgery.* Vol. 62-B, No. 1, February. 104-110.

Jaworski, Z. F. G.(1984) Lamellar bone turnover system and its effector organ. *Calcified Tissue.* Vol 36. S46-55.

Katz, J. L. (1980) Anisotropy of Young's modulus of bone. *Nature.* Vol. 283. 106-107.

Katz, J. L., Yoon, H. S., Lipson, S. and Maharidge, R.(1984) The effects of remodeling on the elastic properties of bone. *Calcified Tissue.* Vol. 36. S31-36.

Katz, J. L. and Meunier, A. (1987) The elastic anisotropy of bone. *J. of Biomechanics.* Vol. 20, No. 11/12. 1063-1070.

Keaveny, T. M. , Borchers, R. E. , Gibson, L. J. and Hayes, W. C. (1993) Trabecular bone modulus and strength can depend on specimen geometry. *J. of Biomechanics.* Vol. 26, No. 8. 991-1000.

Keaveny, T. M. and Bartel D. L. (1993) Effects of porous coating and collar support on early load transfer for a cementless hip prothesis. *J. of Biomechanics.* Vol. 26, No. 10. 1205-1216.

Keaveny, T. M. and Bartel. D. L. (1993) Effects of pouous coating, with and without collar support, on early relative motion for a cementless hip prothesis. *J. of Biomechanics.* Vol. 26, No. 12. 1355-1368.

Keaveny, T. M. and Guo, X. E. , Wachtel, E. F. , McMahon, T. A. and Hayes, W. C. (1994) Trabecular bone exhibits fully linear elastic behavior and yields at low strains. *J. of Biomechanics.* Vol. 27, No. 9. 1127-1136.

Keaveny, T. M. , Wachtel, E. F. , Guo, X. E. and Hayes, W. C. (1994) Mechanical behavior of damaged trabecular bone. J. of Biomechanics. Vol. 27, No. 11. 1309-1318.

Keller, T. S. , Mao, Z. and Spengler, D. M. (1990) Young's modulus, bending strength, and tissue physical properties of human compact bone. J. of Orthopaedic Research. Vol. 8, No. 4. 592-603.

Kohles, S. S. , Vanderby Jr. , Ashman, R. B. , Manley, P. A. , Markel, M. D. and Heiner, J. P. (1994) Ultrasonically determined elasticity and cortical density in canine femora after hip arthroplasty. J. of Biomechanics. Vol. 27, No. 2. 137-144.

Lanyon, L. E.(1973) Analysis of surface bone strains in the calcaneous of sheep during normal locomotion. J.of Biomechancis. Vol. 6, 41-49.

Lanyon, L. E. and Baggoff, D. G. (1976) Mechanical function as an influence on the structure and form of bone. J. of Bone and Joint Surgery. Vol. 58B. 436-443.

Lanyon, L. E. and Bourn, S. (1979a) The influence of mechanical function on the development and remodeling of the tibia. J. of Bone and Joint Surgery. Vol. 61A. 263-273.

Lanyon, L. E., Magee, P. T. and Baggott, D. G. (1979b) The relationship of functional stress and strain to the process of bone remodeling, an experimental study on the sheep radius. J. of Biomechanics. Vol. 12, 593-600.

Lanyon, L. E.(1981) The measurement and biological significance of bone strain in vivo. Mechanicla Properties of Bone, ED., Cowin. S. C..

Lanyon, L. E. , Goodship, A. E. , Pye, C. J. and MacFie, J. H. (1982) Mechanically adaptive bone remodeling. J. of Biomechanics. Vol. 15, No. 3. 141-151.

Lanyon, L. E. (1984a) Functional strain as a determinant for bone remodeling. Calcified Tissue. S56-61.

Lanyon, L. E. and Rubin, C. T. (1984b) Static vs dynamic loads as an influence on bone remodeling. J. of Biomechanics. VOl. 17, NO. 12. 897-905.

Lanyon, L. E. (1987) Functional strain in bone tissue as an objective, and controlling stimulus for adaptive bone remodeling. J. of Biomechanics. Vol. 20, No. 11/12. 1083-1093.

Lanyon, L. E. (1993) Osteocytes, strain detection, bone modeling and remodleling. Calcified Tissue. Vol 53. S102-107.

Linde, F. and Sorensen, H. C. F. (1993) The effect of different storage methods on the mechanical properties of trabecular bone. J. of Biomechnics. Vol. 26, No.10. 1249-1252.

MacGinite L. A. , Seiz, K. G. , Otter, M. W. and Cochran, G. V. B. (1994) Streaming potential measurements at low ionic concentrations reflect bone microstructure. J. of Biomechanics. Vol. 27, No. 7. 969-978.

Marotti, G. (1993) A new theory of bone lamellation. Calcified Tissue. Vol.53, S47-56.

Martin, R. B. and Burr, D. B. (1989) Structure, function and adaptation of compact bone. Raven Press, New York.

Martin, B. (1992) A theory of fatigue damage accumulation and repair in cortical bone. J. of Orthopaedic Research. Vol. 10, No. 6. 818-825.

Martin, R. B. and Boardman, D. L. (1993a) The effects of collagen fiber orientation, porosity, density, and mineralization on bovine cortical bone bending properties. J. of Biomechanics. Vol. 26, No. 9. 1047-1054.

Martin, B. (1993b) Aging and strength of bone as a structural material. Calcified Tissue. Vol. 53, S34-40.

Martin, B. (1994) Mathematical Model for the mineralization of bone. J. of Orthopaedic Research. Vol. 12, NO. 3, 375-383.

McLean, F. C. and Urist, M. R. (1961) Bone, an introduction to the physiology of skeletal tissue. Second Ed., The University of Chicago Press.

Meade, J. B., Cowin, S. C., Klawitter, J. J., Buskirk, Van W. C. and Skinner, H. B. (1984) Bone remodlling due to continuous applied loads. Calcified Tissue. Vol. 36, S25-30.

Moreland, M. S. (1980) Morphological effects of torsion applied to growthing bone: an vivo study in rabbits. The journal of Bone and Joint Surgery. Vol. 62-B, No. 2, May. 230-237.

Mosekilde, L. (1993) Vertebral structure and strength in vivo and in vitro. Calcified Tissue. Vol. 53, S121-126.

Mow, Van C. and Hayes, W. C. (1991) Basic orthopaedic biomechanics. Raven Press, New York.

Mullender, M. G. , Huiskes, R. and Weinans, H. (1994) A physiological approach to the simulation of bone remodeling as a self-organizational control process. J. of Biomechanics. Vol. 27, No. 11. 189-1394.

Nagurka, M. L. and Hayes, W. C. (1980) An interactive graphics package for calculating cross-sectional properties of complex shapes. J. of Biomechanics. Vol. 13. 59-64.

Nordsletten, L., Kaastad, T. S., Madsen, J. E., Reikeras, O., Ovstebo, R, Stromme, J. H. and Falch, J. (1994) The development of femoral osteopenia in ovariectomozed rates is not reduced by high intensity trademill training: a mechanical and densitometric study. Calcified Tissue. Vol. 55, 436-442.

O'counor, J. A. and Lanyon, L. E. (1982) The influence of strain rate on adaptive bone remodeling. J. of Biomechanics. Vol. 15, No.10. 767-781.

Oxnard C. E. (1993) Bone and bones, architecture and stress, fossils and osteoporosis. J. of Biomechanics. Vol. 26, Suppl. 1. 63-79.

Parfitt, A. M. (1993) Bone age, mineral density, and fatigue damage. Calcified Tissue. Vol. 53, S82-86.

Prendergast, P. J. and Taylor, D. (1994) Prediction of bone adaptation using damage accumulation. J. of Biomechanics. Vol. 27, No. 8. 1067-1076.

Rakotomanana, R. L., Leyvraz, P. F. , Curnier, A. , Heegaard, J. H. and Rubin , P. J. (1992) A finite element model for evaluation of tibial prosthesis-bone interface in total knee replacement. J. of Biomechanics. Vol. 25, No. 12. 1413-1424.

Ray, D. R., Ledbetter, W. B., Bynums, D. and Boyd, C. L. (1971) A parametric analysis of bone fixation plates on fractures equine third metacarpal. J. of Biomechanics. Vol.4, 163-174.

Rietbergen B. Van, Huiskes, R., Weinans, H. , Summer, D. R. , Turner, T. M. and Galante, J. O. (1992) J. of Biomechanics. Vol. 26, No. 4/5. 369-382.

Rho, J. Y., Ashman, R. B. , and Turner, C. H. (1993) Young's modulus of trabecular and cortical bone material: ultrasonic and microtensile measurements. J. of Biomechancis. Vol. 26, No. 2. 111-119.

Rice, J. C., Cowin, S. C. and Bowman, J. A. (1988) On the dependence of the elasticity and strength of cancellous bone on apparent density. J. of Biomechanics. Vol. 21, No. 2. 155-168.

Rico, H. Gonzalez-Riola, J., Revilla, M., Villa, L. F., Gomez-Castresana, F., Escribano, J.(1994) Calcified Tissue . Vol 54. 470-472.

Roberts W. E. (1988) Bone tissue interface. J. of Dental Education. Vol. 52, No. 12. 804-809.

Robertson, D. D., Mintzer, C. M., Weissman, B. N. Ewald, F. C., LeBoff, M. and Spector, M. (1994) Distal loss of femoral bone following total knee arthroplasty. J. of Bone and Joint Surgery.
Vol. 76-A, No. 1. 66-76.

Rockborn, P. and Olsson, S. S. (1993) Loosening and bone resorption in exeter hip arthroplasties. J. of Bone and Joint Surgery. Vol. 75-B, No. 6, Novermber. 865-868.

Rosenberg, A. (1989) Cementless total hip arthroplasty: femoral remodeling and clinical experience. Orthopaedics. Vol. 12, No. 9, September. 1223-1233.

Rubin, C. T. and Lanyon, L. E. (1984a) Regulation of bone formation, by applied dynamic loads. J. of Bone and Joint Surgery. Vol. 66A. 397-412.

Rubin, C. T.(1984b) Skeletal strain and the functional significance of bone architecture. Calcified Tissue. Vol 36, S11-S18.

Rubin, C. T. and Lanyon, L. E. (1987) Osteoregulatory nature of mechanical stimuli: function as a determinant for adaptive remodeling in bone. J. of Orthopaedic Research. Vol. 5, No. 2. 300-310.

Sadegh, A. M., Luo, G. M. and Cowin, S. C. (1993) Bone ingrowth: an application of the boundary element method to bone remodeling at the implant interface. J. of Biomechanics. Vol. 26, No. 2. 167-182.

Skinner, H. B., Kim, A. S., Kim, A. S., Keyak, J. h. and Mote, C. D. (1993) Femoral prosthesis implantation induces changes in bone stress that depend on the extent of porous coating. J. of Orthopaedic Research. Vol. 12, No. 4. 553-563.

Snyder, B. D., Piazza, S. Edwards, W. T. and Hayes. W. C. (1993) Role of trabecular morphology in the etiology of age-related vertebral fractures. Calcified Tissue. Vol. 53, S14-22.

Spadaro, J. A., Werner, F. W., Brenner, R. A., Fortino, M. D., Fay, L. A. and Edwards, W. T. (1994) Cortical and Trabecular bone contribute strength to the osteopenic distal radius. J. of Orthopaedic Research. Vol. 12, No. 2, 211-218.

Sumner, D. R. , Willke, T. L., Berzins, W. A. and Turner, T. M. (1994) Distribution of Young's modulus in the cancellous bone of the proximal canine tibia. J. of Biomechanics. Vol. 27, No. 8. 1095-1099.

Szivek, J. A., Weatherly, G. C., Pilliar, R. M. and Cameron, H. U. (1981) A study of bone remodeling using metal-polymer laminates. J. of Biomedical Materials Research. Vol. 15, 853-865.

Timoshenko, S., Goodier, J.N., Theory of elasticity, Pola, Alto, 1951.

Turner, C. H. (1992) On Wolff's law of trabecular architecture. J. of Biomechanics. Vol. 25, No. 1. 1-9.

Turner, T. M., Urban, R. M., Sumner, D. R. and Galante, J. O. (1993) Revision, without cement, of aseptically loose, cemented total hip protheses. J. of Bone and Joint Surgery. Vol. 75-A, No.6, June. 845-862.

Uhthoff, H. K. and Jaworski. I. F. G. (1978) Bone loss in response to long term immobililation . J. of Bone and Joint Surgery. Vol. 60B. 420-429.

Uhthoff, H. K, Boisvert, D. and Finnegan, M. (1994) Cortical porosis under plates. J. of Bone and Joint Surgery. Vol. 76-A, No. 10, October. 1507-1512.

Uklejewski, R. (1994) Initial piezoelectric polarization of cortical bone matrix as a determinant of the electrokinetic potential zeta of that bone osteonic lamella as mechanoelectret. J. of Biomechanics. Vol. 27, No. 7. 991-992.

Wagner, H. D. and Weiner, S. (1992) On the relationship between the microstructure of bone and its mechanical stiffness. J. of Biomechanics. Vol. 25, No. 11. 1311-1320.

Weinans, H. , Huiskes, R. and Grootenboer, H. J. (1990) Trands of mechanical consequences and modeling of a fibrous membrane around femoral hip prostheses. J. of Biomechanics. Vol. 23, No. 10. 991-1000.

Weinans, H. , Huiskes, R. and Grootenboer, H. J. (1992) The behavior of adaptive bone-remodeling simulation models. J. of Biomechanics. Vol. 25, No. 12. 1425-1441.

Weinans, H. , Huiskes, R. and Grootenboer, H. J. (1993) Quantitative analysis of bone reactions to relative motions at implant-bone interfaces. J. of Biomechanics. Vol. 26, No. 11. 1271-1281.

Welch, R. D., Johnston, C. E., Waldron, M. J. and Poteet, B. P. (1993) Bone changes associated with intraosseous hypertension in the caprine tibia. J. of Bone and Joint Surgery. Vol. 75-A, No. 1, January. 53-60.

Widera, G. E. O. , Tesk, J. A. and Privitzer, E. (1976) Interaction effects among cortical bone, cancellous bone, and periodontal membrane of natural teeth and implants. J. of Biomed. Mater. Res. Symposium. No. 7. 613-623.

Wiel, H. E. Van Der, Lips, P., Nauta, J. and Patka, P (1994) Loss of bone in the proximal part of the femur following unstable fracture of the leg. J. of Bone and Joint Surgery. VOl. 76-A, No. 2. 230-236.

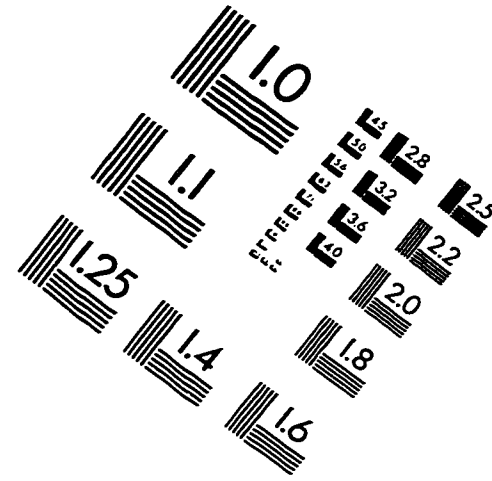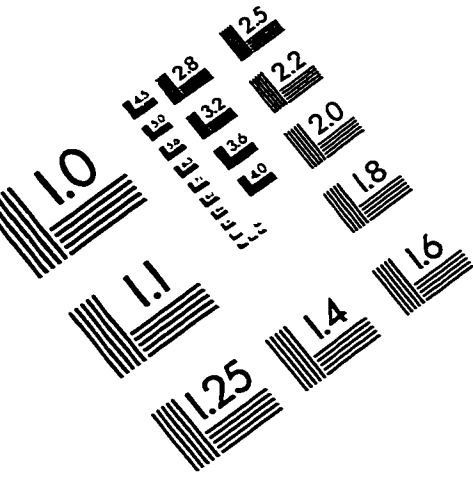Wojciechowski, F. (1976) Properties of plane cross-sections. Machine Design. 48. 105-109.

Woo, S. L., Kuei, S. C., Amiel, D., Gomez, M. A., Hayes, W. C., White, F. C. and Akeson, W. H. (1981) The effects of prolonged physical training on the properties of long bone: a study of Wolff's law. J. of Bone and Joint Surgery. Vol. 63-A, No. 5, June. 780-786.

Yoon, H. S. and Katz, J. L. (1976a) Ultrasonic wave propagation in human cortical bone-I: theoretical consideration for hexagonal symmetry. J. of Biomechanics. Vol. 9. 407-411.

Yoon, H. S. and Katz, J. L. (1976b) Ultrasonic wave propagation in human cortical bone-II: measurements of elastic properties and microhardness. J. of Biomechanics. Vol. 9. 459-464.

Yoon, H. S. and Katz, J. L. (1979) Temperature dependence of the ultrasonic velocities in bone. 1979 IEEE ultrasonic symposium proceedings. 395-398.

IMAGE EVALUATION
TEST TARGET (QA–3)

150mm

6"